MEANDER LOOP MIGRATION AND LIQUEFACTION SUSCEPTIBILITY: LIQUEFACTION ALONG THE HEATHCOTE RIVER DURING THE 2010-11 CANTERBURY EARTHQUAKE SEQUENCE

A thesis submitted in partial fulfilment of

the requirements for the degree of

Master of Science in Geology

at the

University of Canterbury

by

KIERAN THOMAS GRACE

2015

ABSTRACT

Spatial variations in river facies exerted a strong influence on the distribution of liquefaction features observed in Christchurch during the 2010-11 Canterbury Earthquake Sequence (CES). Liquefaction and liquefaction-induced ground deformation was primarily concentrated near modern waterways and areas underlain by Holocene fluvial deposits with shallow water tables (< 1 to 2 m). In southern Christchurch, spatial variations of liquefaction and subsidence were documented in the suburbs within inner meander loops of the Heathcote River. Newly acquired geospatial data, geotechnical reports and eye-witness discussions are compiled to provide a detailed account of the surficial effects of CES liquefaction and ground deformation adjacent to the Heathcote River. LiDAR data and aerial photography are used to produce a new series of original figures which reveal the locations of recurrent liquefaction and subsidence. To investigate why variable liquefaction patterns occurred, the distribution of surface ejecta and associated ground damage is compared with near-surface sedimentologic, topographic, and geomorphic variability to seek relationships between the near-surface properties and observed ground damages.

The most severe liquefaction was concentrated within a topographic low in the suburb of St Martins, an inner meander loop of the Heathcote River, with liquefaction only minor or absent in the surrounding areas. Subsurface investigations at two sites in St Martins enable documentation of fluvial stratigraphy, the expressions of liquefaction, and identification of pre-CES liquefaction features. Excavation to water table depths (~1.5 m below the surface) across sand boils reveals multiple generations of CES liquefaction dikes and sills that cross-cut Holocene fluvial and anthropogenic stratigraphy. Based on in situ geotechnical tests (CPT) indicating sediment with a factor of safety < 1, the majority of surface ejecta was sourced from well-sorted fine to medium sand at < 5 m depth, with the most damaging liquefaction corresponding with the location of a low-lying sandy paleochannel, a remnant river channel from the Holocene migration of the meander in St Martins. In the adjacent suburb of Beckenham, where migration of the Heathcote River has been laterally confined by topography associated with the volcanic lithologies of Banks Peninsula, severe liquefaction was absent with only minor sand boils occurring closest to the modern river channel. Auger sampling across the suburb revealed thick (>1 m) clay-rich overbank and back swamp sediments that produced a stratigraphy which likely confined the units susceptible to liquefaction and prevented widespread ejection of liquefied material.

This analysis suggests river migration promotes the formation and preservation of fluvial deposits prone to liquefaction. Trenching revealed the strongest CES earthquakes with large vertical accelerations favoured sill formation and severe subsidence at highly susceptible locations corresponding with an abandoned channel. Less vulnerable sites containing deeper and thinner sand bodies only liquefied in the strongest and most proximal earthquakes forming minor localised liquefaction features. Liquefaction was less prominent and severe subsidence was absent where lateral confinement of a Heathcote meander has promoted the formation of fluvial stratum resistant to liquefaction.

Correlating CES liquefaction with geomorphic interpretations of Christchurch's Heathcote River highlights methods in which the performance of liquefaction susceptibility models can be improved. These include developing a reliable proxy for estimating soil conditions in meandering fluvial systems by interpreting the geology and geomorphology, derived from LiDAR data and modern river morphology, to improve the methods of accounting for the susceptibility of an area. Combining geomorphic interpretations with geotechnical data can be applied elsewhere to identify regional liquefaction susceptibilities, improve existing liquefaction susceptibility datasets, and predict future earthquake damage.

Table of Contents

CHAPTER 4 SUBSURFACE INVESTIGATIONS

List of Figures

List of Tables

ACKNOWLEDGEMENTS

Throughout this thesis, I have to receive ongoing support from my helpful supervisors for which I am very grateful. Thank you to Kari Bassett for presenting me with this interesting topic and providing me with valuable feedback throughout my study. Thank you to Mark Quigley for the discussion in the field and helpful comments and insights into earthquake processes, and to Matthew Hughes for the helpful guidance with spatial analysis. Thank you also to David Bell and Stefan Winkler for the helpful discussion among others.

I would like to offer thanks to the University of Canterbury Geological Sciences Department technical and administrative staff for all their help, in particular Chris Grimshaw for his assistance with sediment analysis. Thank you also to the UC Mason Trust for funding.

I wish to thank Peter Greening who allowed me to use his property for my research which has provided this thesis with a great amount of detail. Thank you also to Paul Garrett for the use of his excellent photos and discussion in the field, and to Ken Reece for his expert skills on the digger.

Finally, thanks to my family and friends who have helped me greatly in your own way.

For my father, Russell

Your endless support and encouragement will always be felt

CHAPTER 1 INTRODUCTION

1.1 INTRODUCTION

1.1.1 Study background

Recent events such as the 2010 Port-au-Prince Haiti earthquake, the 2010-11 Canterbury Earthquake Sequence (CES), and the 2011 Tohoku Japan earthquake have highlighted the significant hazards earthquakes pose to urban areas. The spatial distribution of seismically-induced damage is influenced by local site conditions and the causative earthquake characteristics (Idriss and Boulanger, 2008). In Christchurch, New Zealand, a significant liquefaction hazard was identified based on geotechnical soil conditions, hydrological conditions, and from the compilation of existing knowledge derived from international earthquake-generated liquefaction events (i.e.1964 Niigata earthquake; 1990 Luzon earthquake; 1995 Kobe earthquake). Historic liquefaction had also been reported in the Christchurch region in localised areas following the 1901 M_w 6.9 Cheviot earthquake (Berrill et al., 1994; Pettinga et al., 2001; Downes and Yetton, 2012). A series of detailed liquefaction susceptibility and hazard maps had been compiled to assess regional vulnerabilities to earthquake-induced damage in Christchurch and identify areas that were most at risk (e.g. Elder et al., 1991; Brown & Weeber, 1992; Christchurch Engineering Lifelines Group, 1997; Clough, 2005). The liquefaction susceptibility maps were based on a review of the near-surface geology and hydrogeology or calculations of liquefaction potential based on geotechnical data and assumed earthquake characteristics (Brackley, 2012). The liquefaction potential in Christchurch was dramatically confirmed by the widespread ejection of liquefied material and ground deformation following the 2010-11 CES (Cubrinovski et al., 2012; Villamor et al., 2012; Quigley et al., 2013).

The CES caused widespread liquefaction across the city of Christchurch, with extensive damage to residential buildings and lifeline systems (Cubrinovski and Green, 2010; van Ballegooy et al., 2014). The majority of liquefaction was focused in eastern Christchurch and in suburbs adjacent to the city's Avon and Heathcote Rivers, especially within modern inner meander loops (Cubrinovski et al., 2012). Previous liquefaction susceptibility studies correctly identified the severe liquefaction potential of eastern Christchurch, where the majority of damage occurred. However, a number of smaller areas revealed differences between observed and predicted liquefaction distributions recorded as significant

underestimations, where substantial liquefaction occurred, or overestimations where areas predicted to be vulnerable to liquefaction showed little or no ground damage.

The CES liquefaction distributions provide an opportunity to assess the quality of previously constructed susceptibility maps and the spatial variability of earthquake-induced ground deformations across a range of seismic shaking. A direct approach to understanding what factors influenced the distribution of liquefaction is to identify the geologic and geotechnical properties of the affected areas. This information can be combined to understand the geomorphic influences on contemporary and paleoliquefaction manifestations adjacent to major urban river systems where the most severe damage in Christchurch occurred (Idriss and Boulanger, 2008; Wotherspoon et al., 2012; Bastin et al., 2015). Delineating areas vulnerable to earthquake environmental impacts therefore requires an understanding of geomorphic influences and paleoseismic events combined with relevant geotechnical assessments. This approach in Christchurch requires knowledge of meandering river systems and point bar formation which creates spatial variations in lithologies and depositional morphologies.

Widespread distributions of sand-dominant facies at shallow depths produced a substrate susceptible to ground failure and the formation of sand boils, lateral spreading, and subsidence across Christchurch (Brown and Weeber, 1992). The spatial distribution of susceptible sedimentary units that caused the most extensive damage are directly related to the coevolution of Christchurch's late Holocene alluvial environment and prograding coastal plain (Hughes et al., 2015; Quigley et al., in review). Critical mixtures of sands and silts required for liquefaction result from unique depositional environments, reflecting specific water velocities and particular geomorphic conditions (e.g. Bridge, 1992; Hooke, 2008; Ghinassi et al., 2013). The geometry of accumulated facies preserved in alluvial landscapes is dependent on the flow regime, lateral migration rates and associated changes in grain size distributions (Hooke, 2007; Willis and Tang, 2010).

Historic geologic conditions and geomorphic changes in river channels influence the distribution of liquefiable layers (Wotherspoon et al., 2012), while the age of the sediments, thickness, and the amount of compaction also affect the likelihood of these layers to liquefy in a seismic event (Ishihara, 1985; Ishihara et al., 1993; Youd et al., 2001; Idriss and Boulanger, 2008). The formation of point bar deposits comprised of loose sand and silt in

meandering river systems thus have a critical control on liquefaction susceptibility in seismically active areas. Migrating fluvial systems and changing channel morphologies form heterogeneous stratigraphy within meander loops, which influences the distribution of liquefaction-induced ground deformations during earthquake shaking (Fig. 1.1) (Idriss and Boulanger, 2008). Linking the deposition of successive fluvial deposits and liquefaction susceptibility requires an understanding of facies associations in meandering rivers.

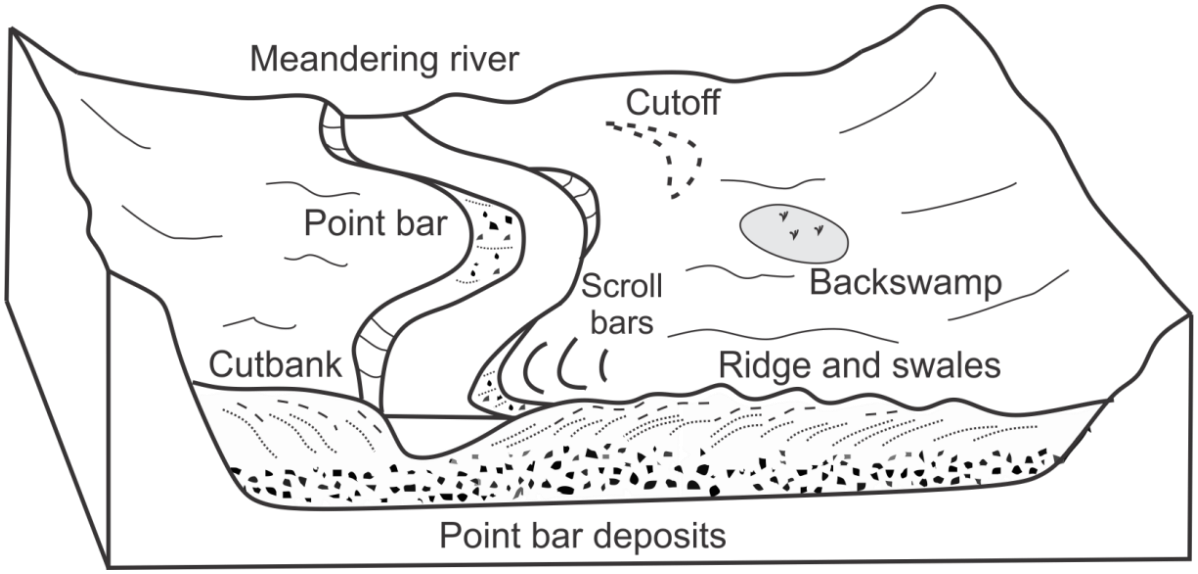

Figure 1.1: Schematic cross-section view of the heterogeneity of alluvial lithofacies at the apex of a meander bend in a migrating river system. Dynamic flow regimes produce heterolithic stratigraphy of sand (dotted lines) and silt (dashed lines) deposits underlain by coarser sediments. The channel moves laterally across the valley floor as the meandering river migrates from erosion and subsequent deposition. Modified from Brierley and Fryirs, (2005).

Widespread liquefaction distributions and extensive liquefaction-induced lateral spreading was observed in the suburbs in eastern Christchurch through the CES (i.e. Avonside, Burwood, Dallington, Avondale, Bexley) (Cubrinovski and Green, 2010; Jacka and Murahidy, 2011; Cubrinovski et al., 2012; Bowen et al., 2012; van Ballegooy et al., 2014). The extensive ground deformations prompted the abandonment of >7000 residential properties in the residential Red Zone in eastern Christchurch (CERA, 2012). As a result, substantial amounts of literature has been published following the CES regarding the soil geotechnical properties, liquefaction distributions, and ground deformation patterns near to the Avon River (e.g. Robinson et al., 2012; Quigley et al., 2013; Bastin et al., 2013; 2015; 2015b). Significantly less literature has been published regarding the Heathcote River in

southern Christchurch, although both rivers are located in a similar setting, share similar morphologies, and are next to densely populated areas. Tonkin and Taylor liquefaction reports and high resolution aerial photography was commissioned by the New Zealand Earthquake Commission (EQC) and the Ministry of Civil Defence and Emergency Management following each major earthquake event (Canterbury Geotechnical Database, 2012; 2013). The data shows the southern Christchurch suburb of St Martins (Fig. 1.2), an inner meander loop adjacent to the Heathcote River, experienced moderate quantities of liquefaction with more severe liquefaction-induced ground deformation occurring within the interior of the suburb. Conversely, little liquefaction was observed within the opposite suburb of Beckenham, within the corresponding southward meander loop of the Heathcote River (Fig. 1.2). These spatial variations of liquefaction and associated subsidence patterns in southern Christchurch adjacent to the Heathcote River are therefore the principal focus of this thesis.

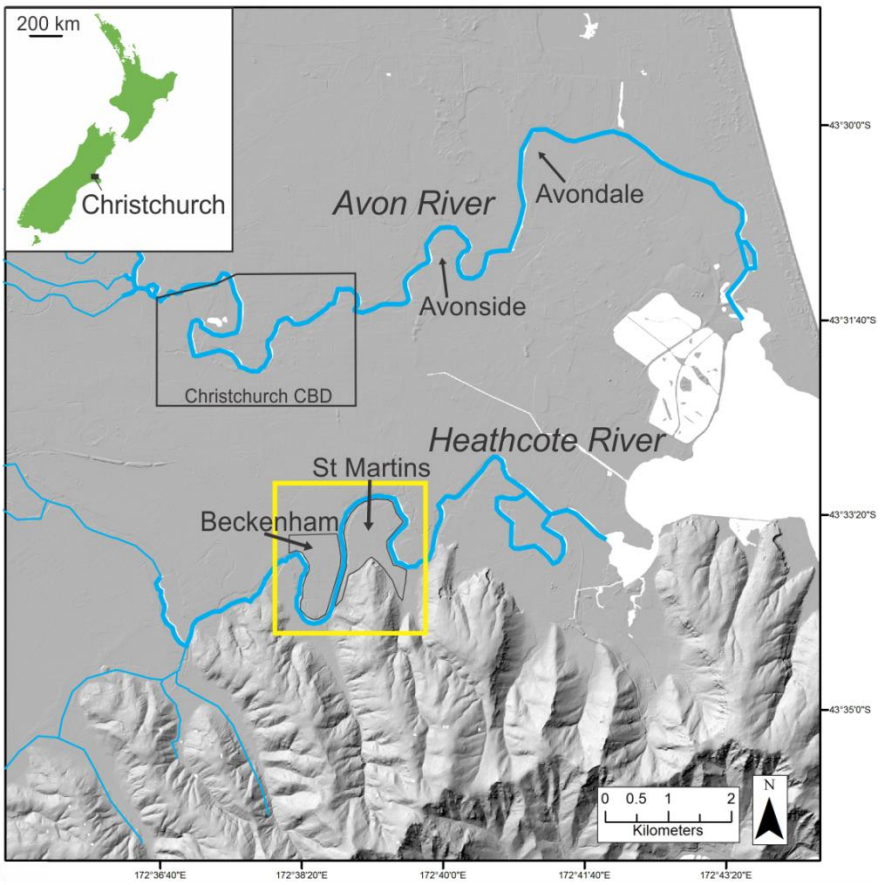

Figure 1.2: Central Christchurch with the locations of the meandering river systems in blue, and the study area in yellow. Note Beckenham and St Martins in opposite inner meander loops of the Heathcote River. Also shown are the locations of the Avonside and Avondale suburbs adjacent to the Avon River. Inset map of New Zealand showing the location of the study region.

1.1.2 Geotechnical data

Substantial geotechnical investigations throughout Christchurch has been undertaken, chiefly by EQC, private insurers, property owners and their consultants, incorporating over 16,000 cone penetration tests (CPT) (Maurer et al., 2014b). The in situ test apparatus penetrates the ground and the sensors within the cone generate continuous data revealing the subsurface geotechnical engineering properties of the soil stratigraphy based on cone resistance and friction ratios (Idriss and Boulanger, 2008). The relative resistance of the sediments act as a proxy for the subsurface soil properties. CPT have become the most common method for site-specific liquefaction assessments in Christchurch due to rapid testing times, continuous recording, and the repeatability of the test (van Ballegooy et al., 2014). The depths of layers prone to liquefaction identified from the CPT are used to derive parameters representing liquefaction vulnerability (i.e. Liquefaction Potential Index and Factor of Safety) (Maurer et al., 2014b). The Liquefaction Potential Index (LPI) defined by Iwasaki et al. (1982), measures the vulnerability of a site to liquefaction effects based on the summation of liquefaction severity of each layer in the soil profile (Maurer et al., 2014; van Ballegooy et al., 2014). Liquefaction triggering analysis includes the calculation of a Factor of Safety against liquefaction (FS) at different points within the subsurface related to the potential development of significant strains and excess pore water pressures (Idriss and Boulanger, 2008). The likelihood a soil will liquefy is considered probable if $FS < 1$. As a result of extensive geotechnical testing in Christchurch, residential land considered safe for redevelopment by CERA is categorised by the Ministry of Building, Innovation and Employment (MBIE) into three technical categories (TC) to assist with new construction and foundation design in areas vulnerable to liquefaction (Canterbury Geotechnical Database, 2012). Other locations that encompass areas most severely affected by liquefaction in Christchurch, and are deemed impractical or uneconomic for rebuilding, are categorised as the residential Red Zone.

As the CES has illustrated, there is a critical need to predict the occurrence and severity of soil liquefaction for engineering design, hazard mapping, urban planning, and regulatory purposes (Maurer et al., 2014). The distributions of CES liquefaction show notable discrepancies between measured and estimated deformation from geotechnical liquefaction vulnerability assessments as a result of significant soil heterogeneity (van Ballegooy et al., 2014). The development of analytical procedures for assessing liquefaction triggering has relied on empirical data to identify soil resistance from various in situ test indices, but

susceptibility analysis needs to also consider land surface properties to identify local-scale differences that affect the severity of liquefaction a site will likely experience during earthquake shaking (Idriss and Boulanger, 2008).

1.1.3 Study focus

This thesis presents the first spatial analysis of recurrent liquefaction and surface deformations adjacent to the Heathcote River in southern Christchurch following the CES. High-resolution aerial photography and geospatial data are combined with detailed subsurface investigations to document CES effects for the purpose of (1) identifying the geologic conditions under which liquefaction in southern Christchurch was induced, (2) determining the geomorphic and environmental evolution which influenced the severity of earthquake-induced damages, (3) assessing the morphology and characteristics of subsurface liquefaction features preserved in the geologic record, and (4) consider the potential application of geomorphic mapping to determine the likely distribution of potentially liquefiable sediments within fluvial settings. The distribution of liquefaction features along the Heathcote River during the CES provides an opportunity to study in detail the surface morphology and subsurface material properties to characterise the geomorphic evolution of this sinuous river, and identify the causes for the variability of damage experienced. By recognising evolutionary processes in curved channel segments, and how migration affects spatial variations in fluvial facies, the impact of meander loop migration on liquefaction distributions in the suburbs adjacent to Christchurch's rivers in can be explored.

The liquefaction observed in Christchurch throughout the CES also provides an opportunity to compare the localised distributions identified adjacent to the Heathcote River, with the wide-spread ground deformations observed along the Avon River (Fig. 1.2). Comparisons of surface deformations between the two meandering rivers can provide valuable insights into determining the evolution, paleogeography and depositional regimes of these similar river systems, and the susceptibility of river deposits depending on the geomorphic setting. Knowledge gained from this study will improve our understanding of the emplacement mechanisms of liquefiable material, the role of channel migration on liquefaction susceptibility, and the accuracy of geotechnical methods for predicting liquefaction susceptibility of sediments deposited by a migrating river.

1.2 CHRISTCHURCH AND THE CANTERBURY EARTHQUAKE SEQUENCE

1.2.1 Regional setting

Christchurch, New Zealand's second largest city with a population of ~340,000 (Statistics New Zealand), is located on the eastern coast of the South Island of New Zealand (Fig. 1.3). The South Island is astride the boundary between the Pacific and Indo-Australian tectonic plates (Fig. 1.3). Oblique collision of the Pacific and Indo-Australian plates has uplifted the Southern Alps mountain range and formed numerous crustal faults including the 650 km long Alpine Fault inferred to accommodate c. 70 % of the 48–39 mm/yr total relative plate motion (Wallace et al., 2007). The Alpine Fault has long been recognized as a significant earthquake hazard for Christchurch, capable of creating a moment magnitude (M_w) ≥ 8 earthquake, with further significant earthquake hazards from other regional fault systems capable of M_w ≥ 7.0 earthquakes (Pettinga et al., 2001; Litchfield et al., 2014).

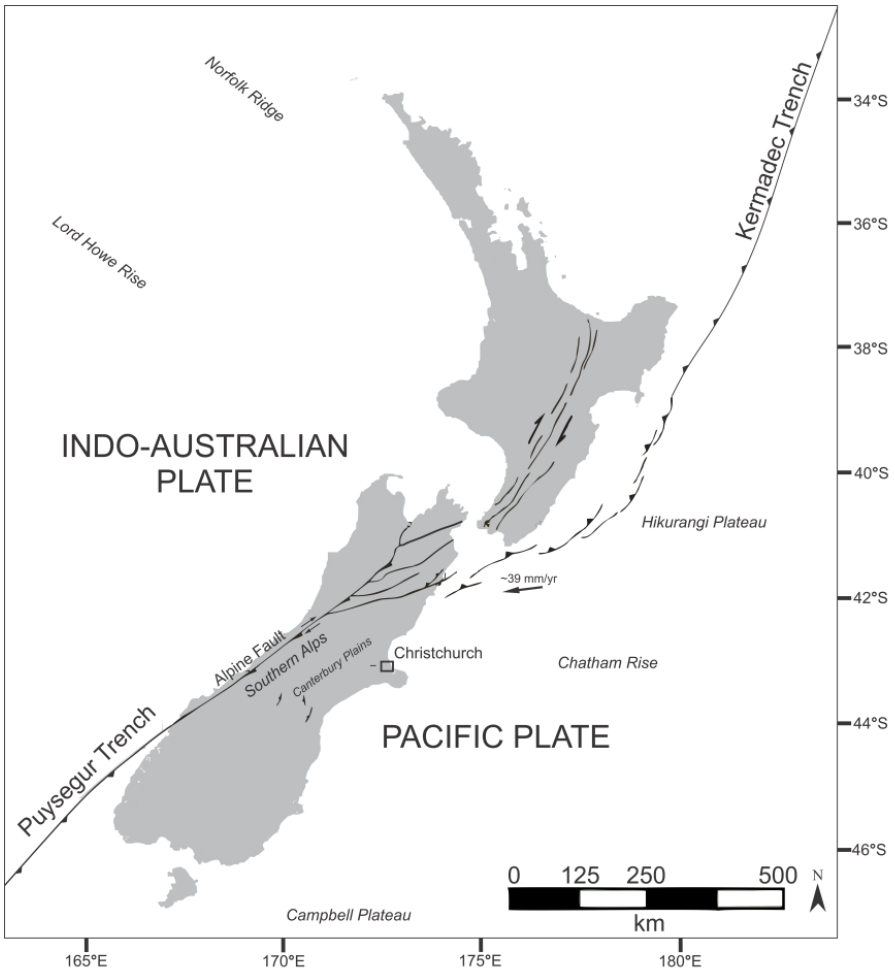

Figure 1.3: The New Zealand tectonic setting with major active structural features and relative convergence vectors (Wallace et al., 2007) at the plate boundary. Modified from Pettinga et al. (1998).

Christchurch lies in a region with relatively low strain rates at the periphery of the plate boundary deformation zone (Howard et al., 2005; Wallace et al., 2007). The underlying basement rock is comprised of the Paleozoic to Mesozoic sedimentary and metamorphic sequences, known as the Torlesse Composite Terrane, of dominantly greywacke and argillite rock (Forsythe et al., 2008). The basement rocks are overlain by 1-2 km of Late Cretaceous to Neogene sedimentary and volcanic rocks beneath the unconsolidated Quaternary sediments of the Canterbury Plains to the west of Christchurch (Forsythe et al., 2008). The Canterbury Plains consist of complex sequences of coalescing fans and abandoned braided-river floodplains, deposited as outwash by eastward-flowing rivers emerging from the foot hills of the Southern Alps (Fig. 1.4) (Brown and Weeber, 1992). The plains comprise unconsolidated to weakly lithified Quaternary cover sediments and sedimentary rocks ~240 m - 1 km thick (Jongens et al., 2012; Hornblow et al., 2014). The latest aggradation of outwash sediments is thought to have occurred during the Last Glacial Cold Period (LGCP) (~28,000 to ~18,000 years ago) followed by Holocene incision of the braided river systems extending up to 50 km toward the current coastline to the east (Forsythe et al., 2008).

Christchurch city, located on the eastern coastal margin of the Canterbury Plains, is primarily situated on Late Quaternary sediments in a low-lying alluvial landscape (Fig. 1.4). Prior to European settlement (~1850) Christchurch mainly consisted of swamps, sand dunes, estuaries and lagoons before subsequent draining and reclamation for residential and commercial development (Brown and Weeber, 1992). Sedimentation has been influenced by glacial and interglacial climate fluctuations and associated eustatic changes (Forsythe et al., 2008). The Late Quaternary alluvial deposits interfinger with estuarine and shallow marine deposits making Christchurch soils extremely variable over short distances both horizontally and vertically (Brown and Weeber, 1992).

The hillslope suburbs of the Port Hills, to the south of Christchurch City, are located on sloping Miocene volcanic rocks and draping loess deposits of Banks Peninsula, the eroded remnants of the two large overlapping Lyttleton and Akaroa volcanoes consisting of predominantly basaltic and trachytic lithology (Fig. 1.4) (Forsythe et al., 2008). Quaternary loess and colluvially-reworked loess deposits mantle the underlying volcanic topography. Aeolian silty-clay deposits are widespread on slopes and ridges on Banks Peninsula and are commonly up to several metres thick (Bell and Trangmar, 1987).

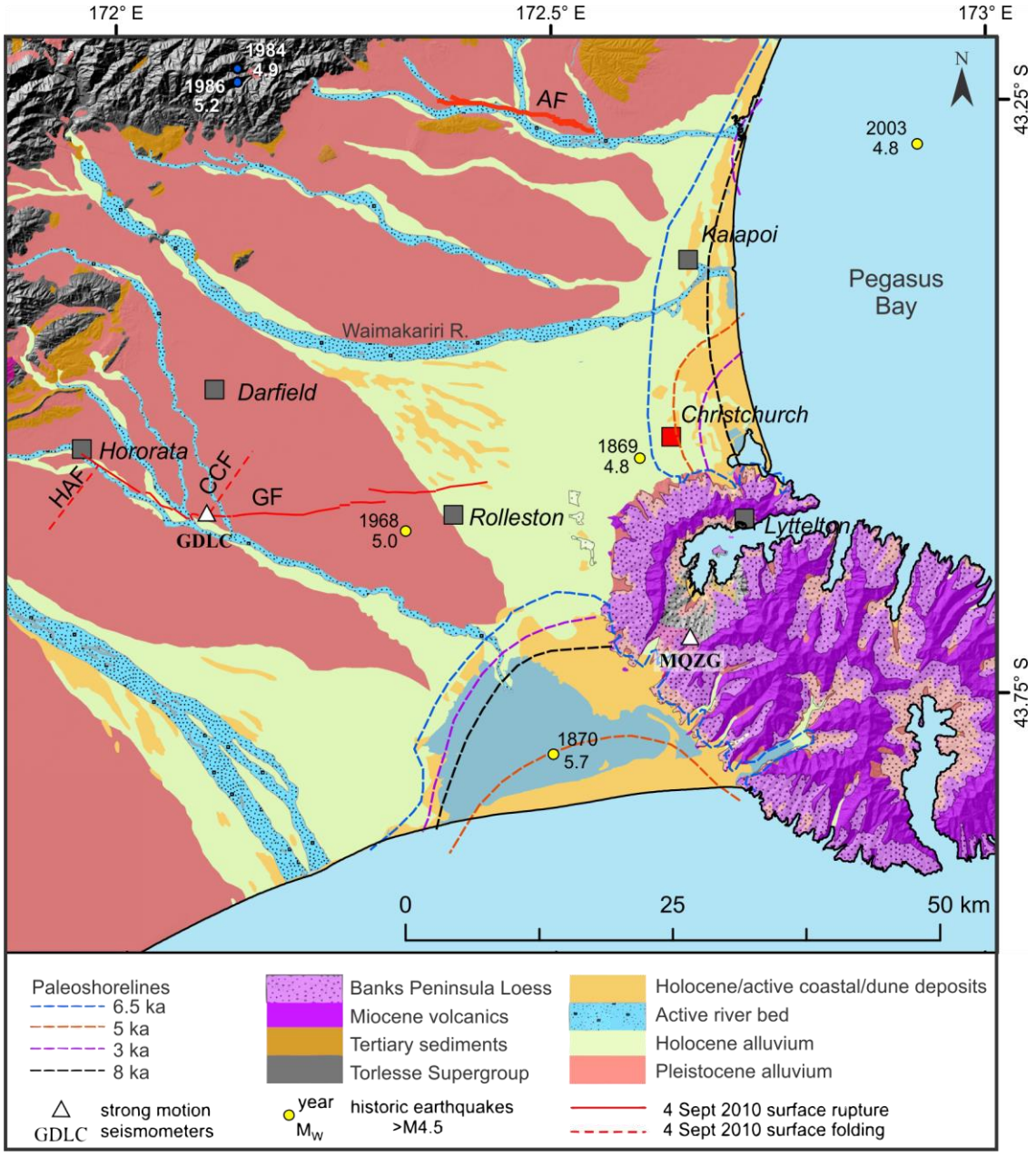

Figure 1.4: Geology of the Canterbury region and the location of surface rupture and folding during the 4 September 2010 earthquake. Notable urban centres and pre-CES earthquakes are shown, along with the Holocene shorelines in the Christchurch area (Brown and Weeber, 1992). Note the position of the 6.5 ka shoreline some 10 km inland from the present shoreline. Modified from Quigley et al. (in review).

The most recent phase of cyclic climate fluctuation at the coastal margin has produced interfingering of river gravels with sand, silt, clay and peat in the area where Christchurch city is located (Brown and Weeber, 1992). At its glacial minimum ~18 ka, sea level was ~125 m below its current level and progressively rose following the last glacial period; until 6.5 ka where the coast line transgressed to its maximum inland extent approximately 10 km west of the modern coastline (Fig. 1.4) (Brown and Weeber, 1992). Following the mid-Holocene

highstand, the coastline prograded forming the uppermost alluvial sediments of the Springston Formation, in western and central Christchurch, and the coastal and shallow marine sediments of the Christchurch Formation to the east. These fluvial deposits have been redistributed by the meandering Avon and Heathcote Rivers and overlie the Riccarton Gravel, the uppermost glacial outwash gravel (Fig. 1.5) (Brown and Weeber, 1992).

The Springston Formation contains channel and overbank sediments of well-sorted gravel, sand, silt, clay and peat deposits forming the composite surface underlying Christchurch city with a maximum thickness of 20 m (Fig. 1.5) (Brown and Weeber, 1992). The accumulation of gravels in the uppermost several meters is typically attributed to incursions from the Waimakariri River that has intermittedly avulsed across the city (Fig. 1.4) (Brown and Weeber, 1992). East of the Springston Formation lies the Christchurch Formation comprising beach, estuarine, lagoonal, dune, and coastal swamp deposits of gravel, sand , silt, clay, and peat (Fig. 1.5) (Brown and Weeber, 1992). The thickness of the formation along the eastern Christchurch coast is approximately 40 m thinning inland (Forsyth et al., 2008). These units are derived from material eroded from the Southern Alps and transported by the Waimakariri River north of the city.

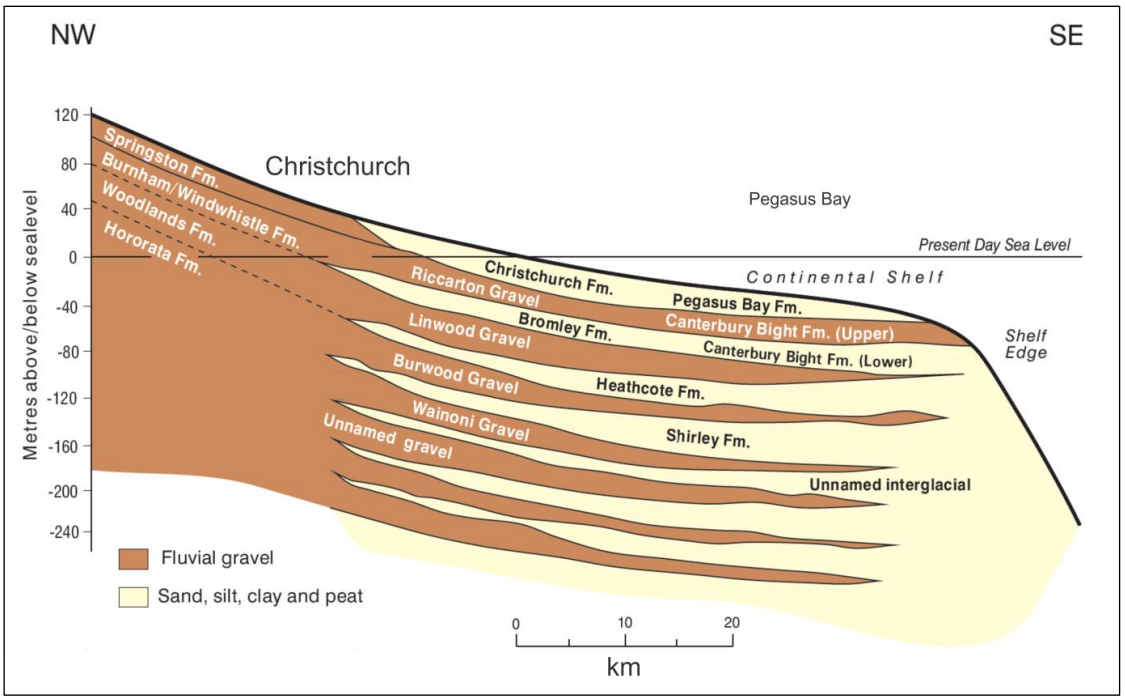

Figure 1.5: Geologic cross-section through interfingered glacial and intergacial Quaternary deposits underlying Christchurch to the continental shelf. From Brown and Weeber, (1992).

1.2.2 Pre-CES earthquake history in Christchurch

At least five historic >M_w 6.0 earthquakes within 150 km of Christchurch have been recorded between 1869 and 1988 causing minor building damages including the 1869 M_w 4.7-4.9 Christchurch and 1870 M_w 5.6-5.8 Lake Ellesmere earthquakes (Downes and Yetton, 2012). The 1869 Christchurch earthquake was felt throughout the city causing widespread damage to chimneys and the contents of many properties (Elder et al., 1991; Pettinga et al., 2001; Downes and Yetton, 2012). The 1901 M_w 6.9 Cheviot earthquake caused extensive damage to the Christchurch Cathedral spire, with localised liquefaction observed in Kaiapoi 15 km north of Christchurch City (Fig. 1.4) (Berrill et al., 1994; Wotherspoon et al., 2012). Subsequent regional earthquakes of $M_w \geq 6.0$ have generated shaking of Mercalli Intensity (MMI) >5 in Christchurch including the 1881 M_w ~6 Castle Hill, 1888 M_w 7.1-7.3 North Canterbury, 1922 M_w 6.4 Motunau, and 1929 M_w 7.1 Arthur's Pass earthquakes (Cowan, 1991; Pettinga et al., 2001)

1.2.3 Seismicity and epicentre migration

The 2010 M_w 7.1 Darfield earthquake and subsequent aftershock sequence (collectively referred to as the Canterbury Earthquake Sequence) caused liquefaction to more than one third of the Christchurch urban area (Bradley and Hughes, 2013; van Ballegooy et al., 2014). The majority of damage was attributed to the differential settlement of buildings and pipework caused by the ejection of sediment, subsidence and lateral spreading initiated by liquefaction (Cubrinovski and Green, 2010; Beavan et al., 2012). Between September 2010 and September 2012, the CES had 12 $M_w \geq 5.0$ and 3 $M_w \geq 6.0$ events (Table 1.1) (Bannister and Gledhill, 2012; Quigley et al., in review). The direct cost of CES damage is estimated to be ~NZ$ 40 B (*https://www.tvnz.co.nz/one-news/new-zealand/christchurch-counts-the-cost-four-years-on-from-earthquake-6239375*). The major earthquake events are identified in Table 1.1 and the location of the epicentres are displayed in Figure 1.6.

Table 1.1: Significant CES events and $M_w \geq 5.0$ aftershocks (data from www.geonet.org.nz).

Date	Time	M_w	Depth (km)	Distance from Christchurch CBD
4 Sep 2010	4:35am	7.1	11	37.8 km
	4:37am	5.5	11.9	27.8 km
	4:37am	5.2	7.8	24.7 km
	4:37am	5.9	10	25.4 km
	4:38am	5.2	10.2	42.0 km
	4:38am	5.4	6.3	37.0 km
	4:39am	5.3	17.6	43.6 km
	4:41am	5.0	5	27.7 km
	4:42am	5.0	9.4	19.9 km
	4:43am	5.1	9.5	38.8 km
	4:44am	5.9	5	45.9 km
	4:52am	5.5	7.5	20.3 km
	4:55pm	5.4	5	54.1 km
	4:56am	5.6	9.1	34.5 km
	4:59am	5.5	8.1	35.6 km
	5:18am	5.1	5	35.9 km
	7:56am	5.1	8.7	19.8 km
	7:56am	5.1	5	20.4 km
	11:12am	5.1	8.7	37.3 km
	11:12am	5.1	8.7	37.4 km
	11:12am	5.3	8.5	35.9 km
	11:14am	5.2	7.7	37.1 km
	11:14am	5.3	6.8	37.8 km
22 Feb 2011	12:51pm	6.2	6	6.7 km
	1:04pm	5.8	5.9	6.7 km
	2:50pm	5.9	6.6	6.6 km
	2:51pm	5.1	7.3	6.5 km
	4:04pm	5.0	12	3.8 km
13 Jun 2011	1:01pm	5.3	8.9	10.4 km
	2:21pm	6.0	6.9	9.2 km
23 Dec 2011	1:58pm	5.8	9.6	13.8 km
	2:00pm	5.2	7.7	15.5 km
	2:06pm	5.3	10.1	17.7 km
	3:18pm	5.9	7	8.5 km
	4:50pm	5.1	11.2	11.7 km

The CES commenced with the M_w 7.1 Darfield earthquake at 4:35 am on September 4, with the epicentre approximately 40 km west of Christchurch at a depth of ~11 km (Fig. 1.6) (Gledhill et al., 2011). The earthquake produced a ~29.5 km-long ground surface rupture with maximum displacements of up to ~5 m horizontally and ~1.5 m vertically (Quigley et al. 2010; 2012; Villamor et al, 2012). The fault rupture was complex, involving multiple failure planes, with the majority of earthquake generated displacement being released through the right lateral rupture of the EW-striking Greendale Fault (Quigley et al., 2010). Extensive

damage occurred to residential properties and underground lifelines, especially un-reinforced masonry buildings and within areas closest to Christchurch's rivers and streams (Cubrinovski and Green, 2010; Cubrinovski et al., 2011)

The 22 February 2011 M_w 6.2 Christchurch earthquake occurred at 12:51 pm with an epicentre ~6 km SE of the central business district (CBD) at a depth of approximately 6 km (Fig. 1.6) (Beavan et al., 2012). The devastating earthquake event occurred on a previously unknown steeply dipping blind fault striking NE. The proximity of the epicentre, steeply dipping nature, and the up-dip component of slip of the fault contributed to large vertical ground accelerations across Christchurch of significantly higher amplitude compared to the M_w 7.1 September event (Bradley and Cubrinovski, 2011; Bannister and Gledhill, 2012). The violent ground movement resulted in multiple building collapses and a total of 185 fatalities (*http://www.nzhistory.net.nz/page/christchurch-earthquake-kills-185*).

The 13 June 2011 earthquakes of M_w 5.3 and M_w 6.0 ruptured on blind faults in eastern Christchurch, epicentres 10 km SE of the CBD on a NNW-striking left lateral fault and ENE-striking reverse-right lateral fault respectively (Fig. 1.6) (Beavan et al., 2012; Bannister and Gledhill, 2012). The 23 December 2011 M_w 5.8 and M_w 5.9 earthquakes ruptured offshore in Pegasus Bay with epicentres 15 km east of the CBD on NE-striking reverse-right lateral blind faults at depths of ~2-5 km (Fig. 1.6) (Bannister and Gledhill, 2012).

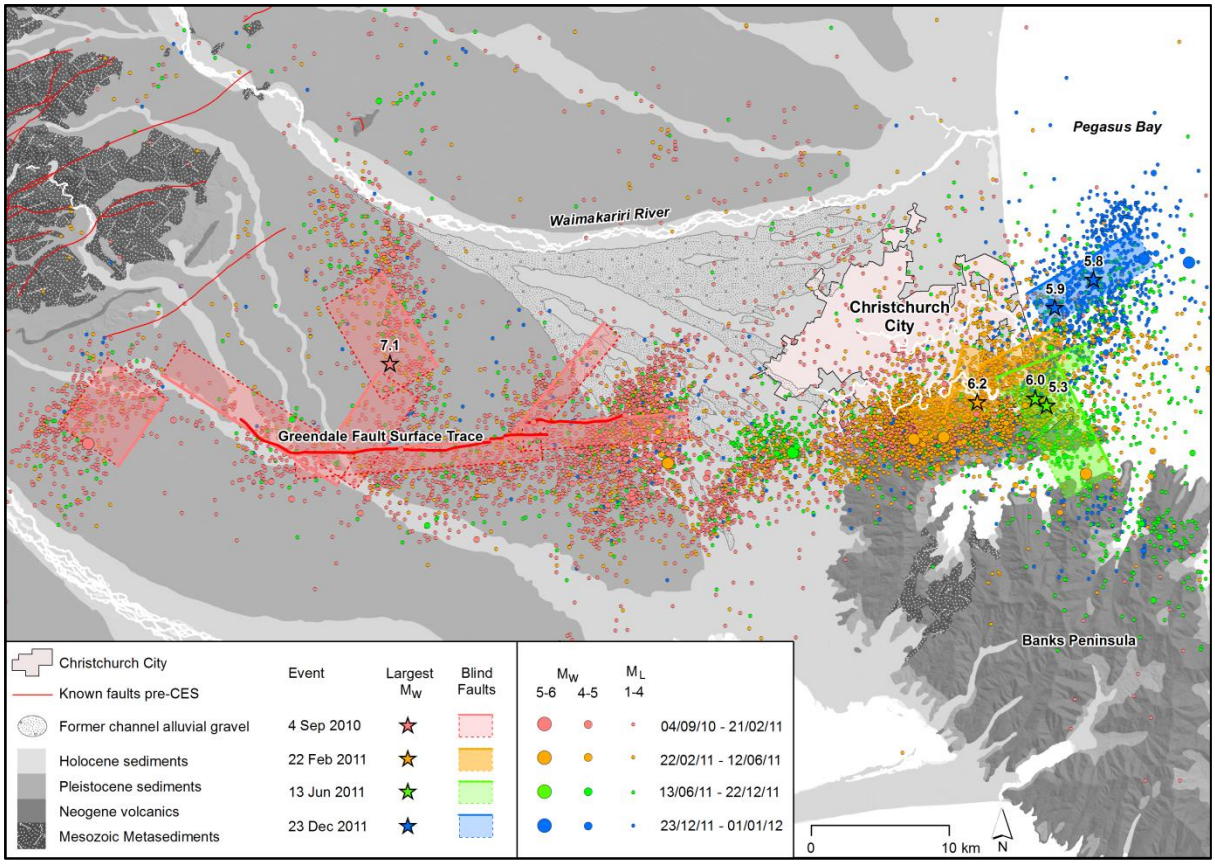

Figure 1.6: Regional surficial geology, seismicity and fault location map of the Canterbury region affected by the CES. Epicentre locations for local magnitude (M_L) ≥3.0 events from 4 September 2010 to 10 February 2013 (data from www.geonet.org.nz). Projected surface locations of major blind faults in bold, projected base of all major faults shown by dotted lines (from Beavan et al. 2012). Earthquakes colour-coded by time as indicated by legend. Location of mapped Greendale Fault surface ruptures in red (from Quigley et al. 2012). Epicentres of most significant earthquakes are indicated with stars for 4 September 2010 (pink), 22 February 2011 (orange), 13 June 2011 (green) and 23 December 2011 (blue). From Quigley et al. (in review).

1.3 LIQUEFACTION RESEARCH

Historic examples of surface liquefaction have been useful in assessing the relationship between liquefaction distributions and material susceptibility for engineering purposes. Significant ground deformation resulted in dramatic bearing failures of infrastructure during the 1964 Niigata Japan earthquake, which helped identify liquefaction as a major earthquake engineering issue (Idriss and Boulanger, 2008). Further observations of liquefaction-induced ground deformations have assisted in categorising the materials most susceptible, including the 1990 Luzon Philippines earthquake (Ishihara et al., 1993), the 1995 Kobe earthquake in Japan (Yasuda et al., 1996), the 1999 Kocaeli earthquake in Turkey (Bardet et al., 2000), the

1999 Chi-Chi earthquake in Taiwan (Chu et al., 2004) and the 2011 Van earthquake in Turkey (Akin et al., 2013). As a result of these earthquakes, the triggering mechanisms and the destructive effects are generally well known for major seismic events.

1.3.1 Review of Christchurch liquefaction susceptibility estimated prior to the CES

As mentioned previously, prior to the CES there was a long-standing awareness of highly susceptible sediments in the Christchurch area and proximal faults capable of producing liquefaction-inducing earthquakes. Previous liquefaction susceptibility maps in Christchurch were based on near-surface geology and hydrogeology, or calculations of liquefaction potential from geotechnical data (Brown and Weeber, 1992). Below is a synthesis of studies published prior to the CES documenting the likely environmental effects of a liquefaction-inducing earthquake in Christchurch.

In an assessment of the earthquake hazard in Christchurch, Elder et al. (1991) produced a map of soils susceptible to liquefaction based on available subsurface data (Fig. 1.7). Elder et al. (1991) concluded a substantial area of Christchurch was underlain with sand that would be susceptible to liquefaction if sufficiently loose. Much of the recorded liquefaction distributions during the CES occurred in areas predicted by Elder et al. (1991) to be highly susceptible. The resulting magnitudes of liquefaction, however, were mostly underestimated in the areas northwest of the CBD and in southern Christchurch where severe liquefaction occurred.

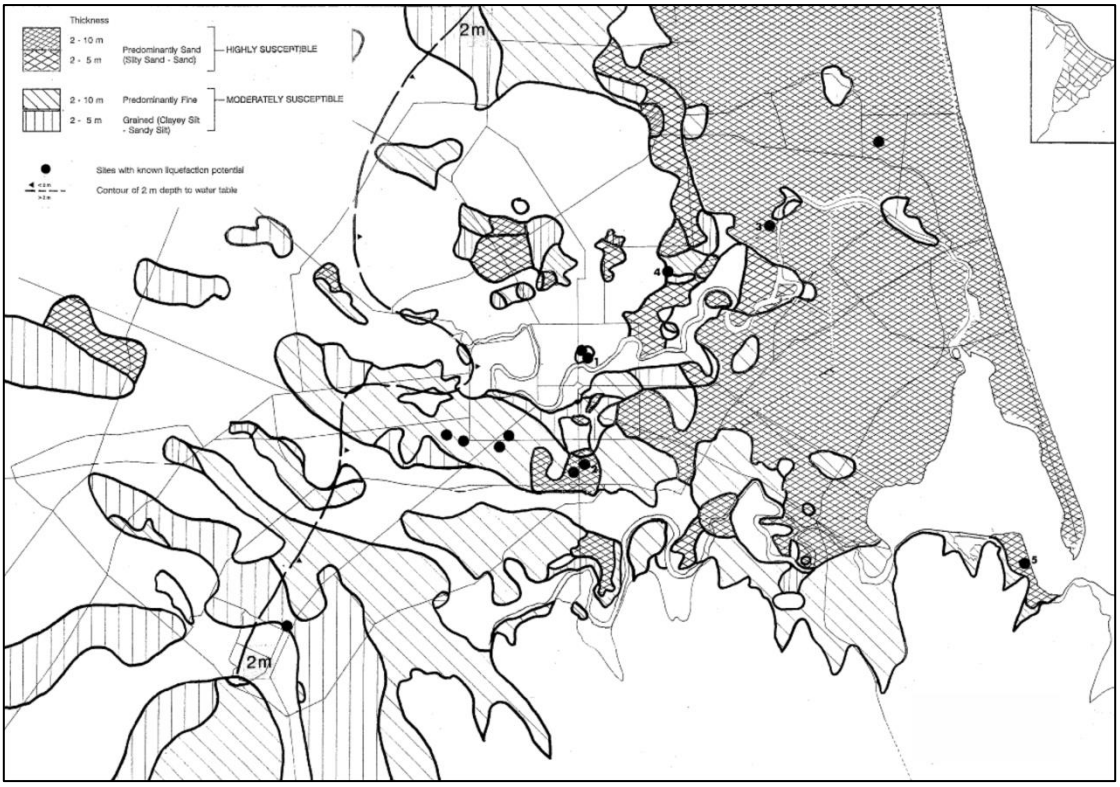

Figure 1.7: Christchurch map of soil types susceptible to liquefaction from Elder et al. (1991).

Brown and Weeber (1992) produced a liquefaction susceptibility map based on the dominant grain size of near-surface strata and likely depth to groundwater as part of a summary publication on the geology of the Christchurch area (Fig. 1.8). They recognised subsurface soils in Christchurch are extremely variable over short distances, and indicated the central and eastern areas of the city are the most susceptible to liquefaction. Due to the variability of subsurface materials, they recommended site-specific foundation investigations for all heavy structures and cautioned against extrapolating conditions from adjacent sites. Following the CES, the Brown and Weeber (1992) liquefaction susceptibility assessment was seen to have correctly predicted eastern parts of the city would experience substantial liquefaction when exposed to strong earthquake shaking. They also correctly predicted the distribution of liquefaction experienced within the suburbs adjacent to the Heathcote River in southern Christchurch. The map however did not recognise the liquefaction-induced ground deformations experienced in the central and eastern CBD which led to damage of many buildings (Cubrinovski et al., 2011).

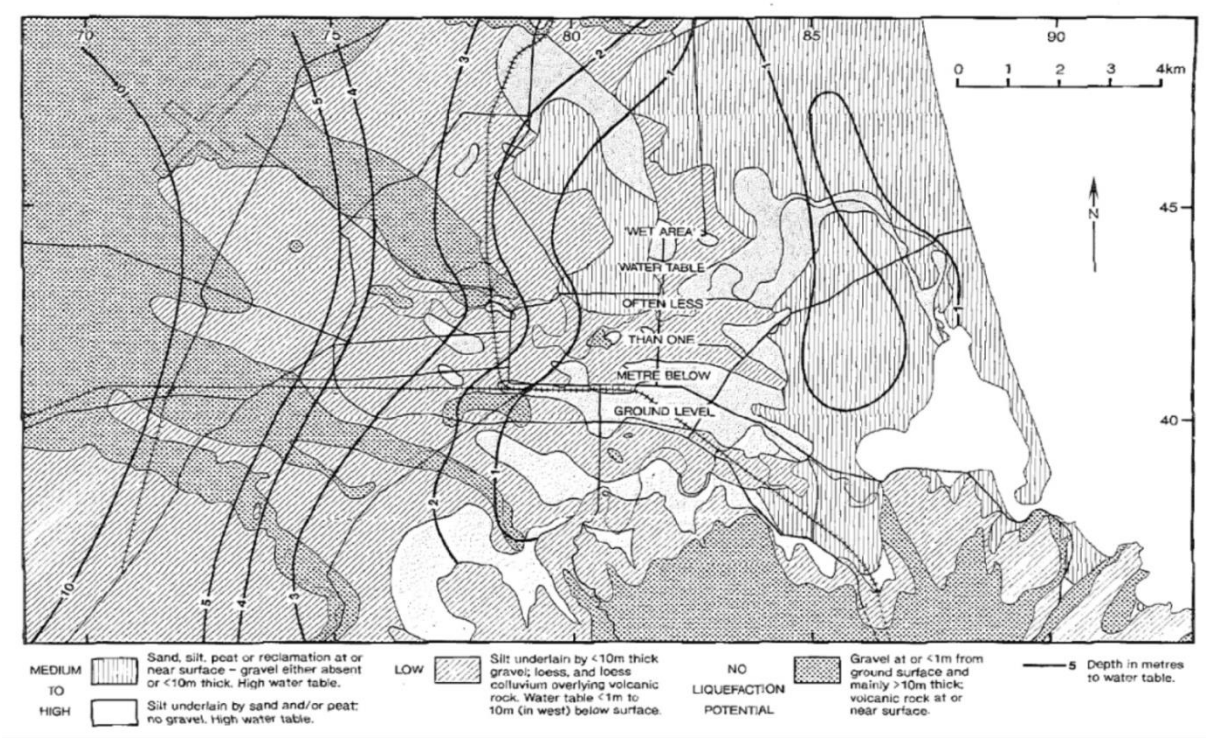

Figure 1.8: Liquefaction susceptibility map of Christchurch from Brown & Weeber (1992).

The Risks and Realities report of the Christchurch Engineering Lifelines Group produced a liquefaction susceptibility map in 1997 (Fig. 1.9). The map combined previous soil studies with ground water data to delineate two zones of susceptibility. Zone A (brown area) was categorised as having high susceptibility as the areas were underlain predominantly by sands with shallow ground water tables (<1.5 m). Zone B (yellow area) was categorised as having moderate susceptibility as the areas were underlain by silts and sandy silts and the depth to groundwater is generally 1-2 m. The map's predictions were consistent with the widespread liquefaction distribution in eastern Christchurch observed during the CES. The map however did not predict the extensive liquefaction distributions across the suburbs of Avonside and St Martins, and overestimated the susceptibility of Beckenham.

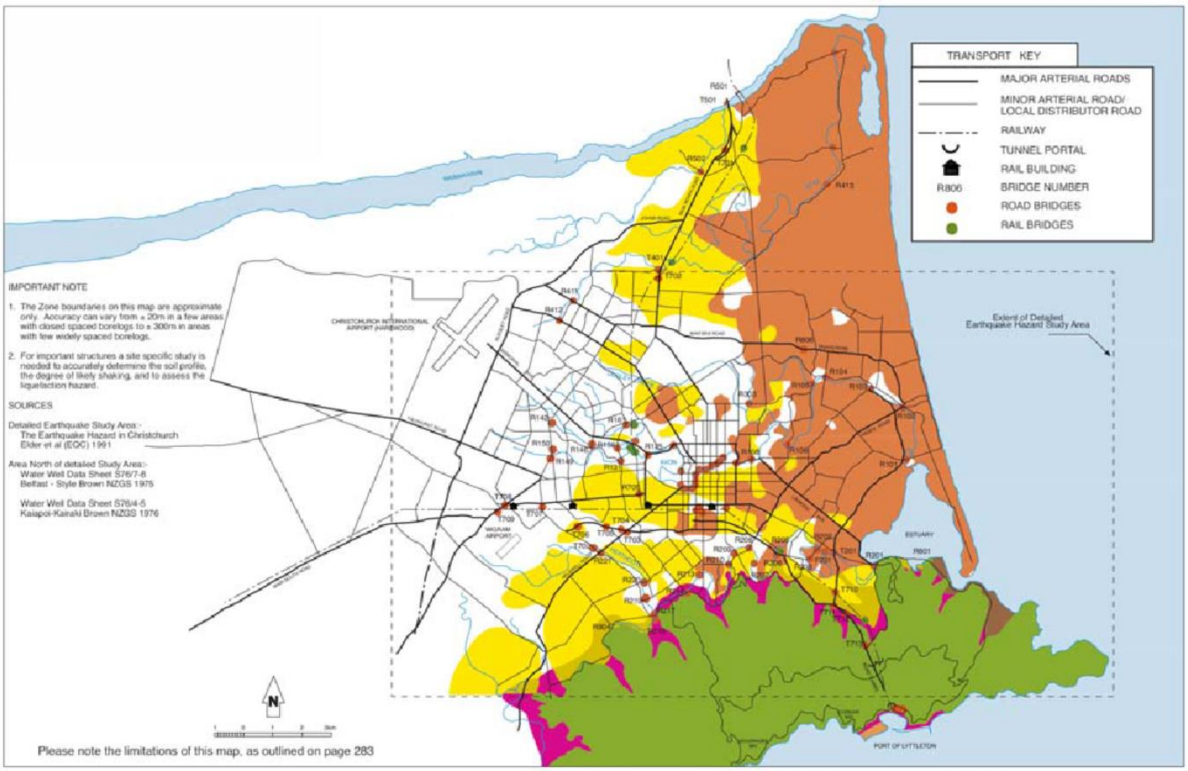

Figure 1.9: Map of liquefaction susceptibility zones from the Christchurch Engineering Lifelines Group (1997).

Environment Canterbury (ECan) contracted the consulting firm Beca in 2001 to improve earlier liquefaction susceptibility maps by incorporating soil strength data into the liquefaction analysis. Revised groundwater levels and adjustments to the liquefaction prediction algorithm were included to produce liquefaction potential and ground damage maps for seasonal ground water levels (Fig. 1.10) (Clough, 2005). The liquefaction hazard map generally predicted the widespread liquefaction well, but the major peak ground accelerations experienced in the CES and insufficient soil information made for certain errors within the mapped areas. The liquefaction potential of areas in eastern Christchurch and the suburbs adjacent to the major urban rivers were generally underestimated based on observations through the CES.

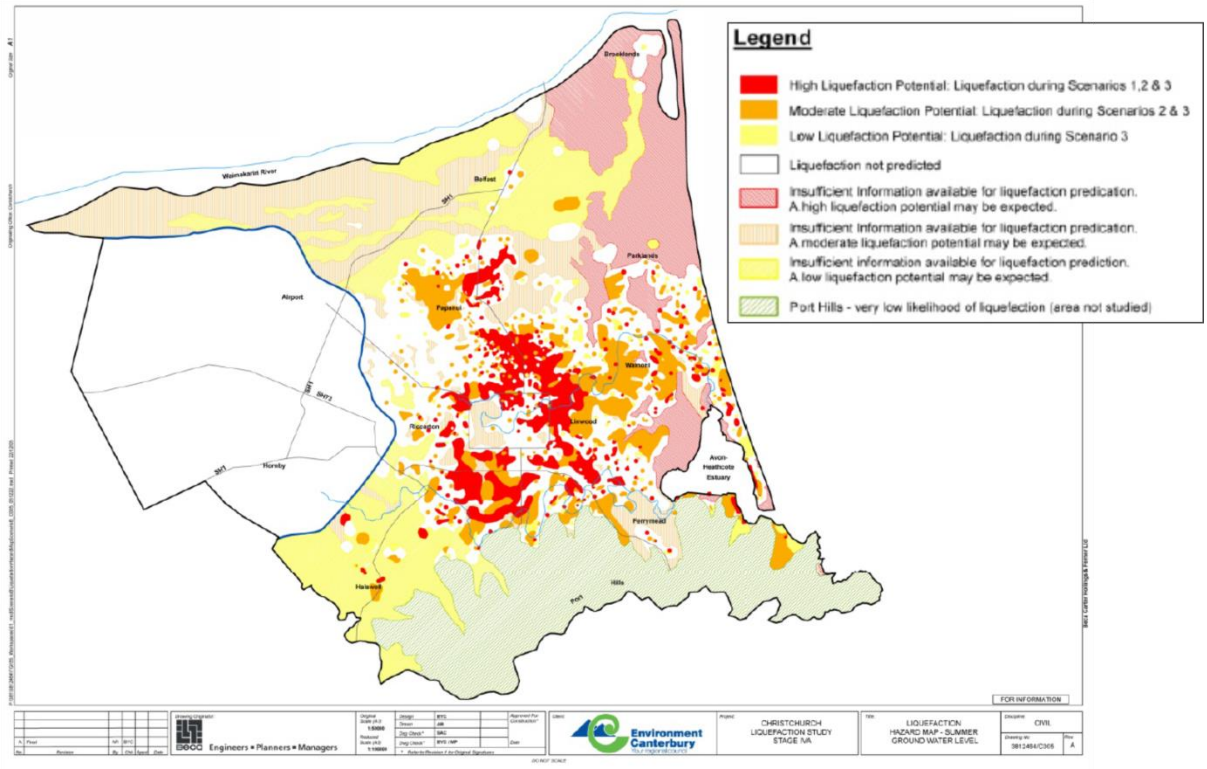

Figure 1.10: Liquefaction susceptibility assessment for the Christchurch urban area for summer ground water levels from Clough (2005).

Surficial liquefaction distributions and localised ground deformations due to earthquake-induced shaking are difficult to quantitatively predict because of the inherent heterogeneity of alluvial deposits, sporadic formation of cracks and sand boils, and the uncertainty of seismic shaking intensity and duration (Idriss and Boulanger, 2008). Areas classified in the above liquefaction susceptibility maps interpreted to contain sediments of 'low' vulnerability to liquefaction, may still be susceptible depending on the causative earthquake characteristics or the temporal effects between aftershocks generating excess pore pressure and water table fluctuations.

Historical records or geologic evidence of previous liquefaction provides the most direct evidence that a soil deposit is susceptible to liquefaction, as soils that have liquefied in prior earthquakes are often observed to liquefy in subsequent events (e.g. Quigley et al., 2013; Bastin et al., 2015). The lack of observed liquefaction from historic earthquakes made predicting liquefaction susceptibilities in Christchurch prior to the CES difficult.

1.3.2 Liquefaction surface manifestation

Intense seismic shaking from the main CES events initiated up to ten episodes of liquefaction in particularly susceptible areas in eastern Christchurch (Quigley et al., 2013). The most severe and widely distributed liquefaction was triggered as a result of the M_w 7.1 September 2010, M_w 6.2 February 2011, M_w 6.0 June 2011 and 5.9 December 2011 earthquakes. Smaller magnitude CES earthquakes (Table 1.1) also initiated surface liquefaction, and subsurface liquefaction not resulting in surface manifestations (Quigley et al., 2013). The effects from liquefaction in Christchurch were often localised and changed substantially over relatively short distances (50 - 100 m) from very severe to low or no surface expression (Cubrinovski and Green, 2010). The ejection of liquefied material formed cone shaped sand boils that were subsequently eroded by waning flows (Fig. 1.11). Ejected sediments consisted of fine sand and coarse silt that commonly became modified by aeolian processes in the days following deposition (Quigley et al., 2013).

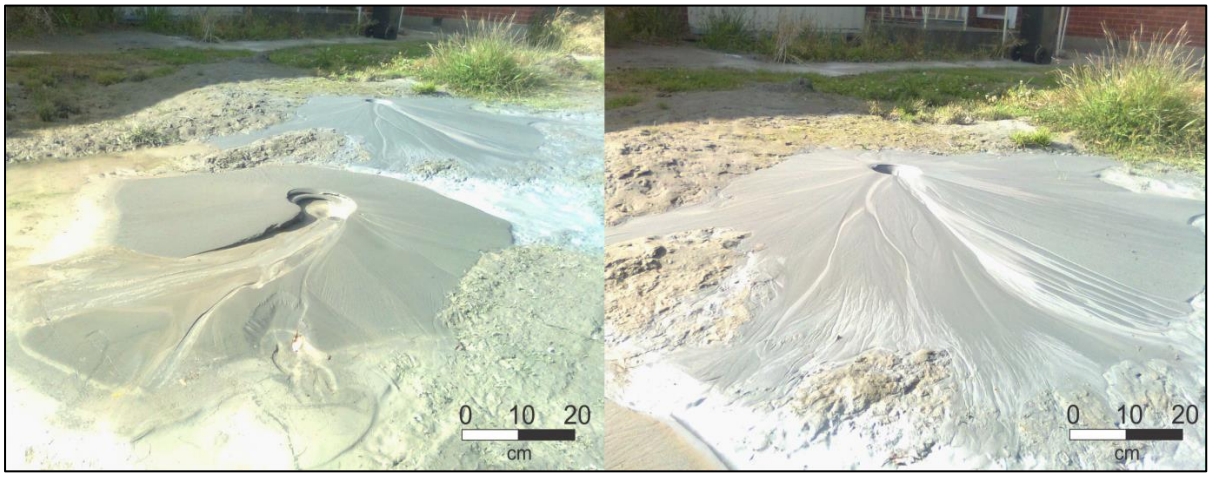

Figure 1.11: Surface manifestations of liquefaction ejecta as sand boils following the 22 February 2011 M_w 6.2 Christchurch earthquake in Cresselly Place, St Martins. Photos by Paul Garrett.

Liquefaction is initiated by the transformation of a fluid saturated and loosely consolidated material from a solid to a liquefied state as a consequence of increased pore water pressure from earthquake-induced cyclic shearing (Youd and Perkins, 1978; Tuttle, 2001; Obermeier et al., 2005, Cubrinovski and Green, 2010). As excess pore water pressures exceed the static confining pressure, the sediment transitions to a liquefied state where it may be ejected to the surface (Fig. 1.12) (Idriss and Boulanger, 2008). The liquefied material containing water, sand and silt is typically injected vertically and laterally through a non-liquefiable crust layer as ‘feeder’ dikes and sills, and deposited at the ground surface as characteristic cone-shaped

sand boils (sand volcanoes) burying upper soil layers (Obermeier, 1996).The combination of shallow loosely compacted sediments, a high water table, and strong seismic shaking facilitates the initiation of liquefaction and the accumulation of ejected material at the ground surface (Obermeier et al., 2005; Idriss and Boulanger, 2008).

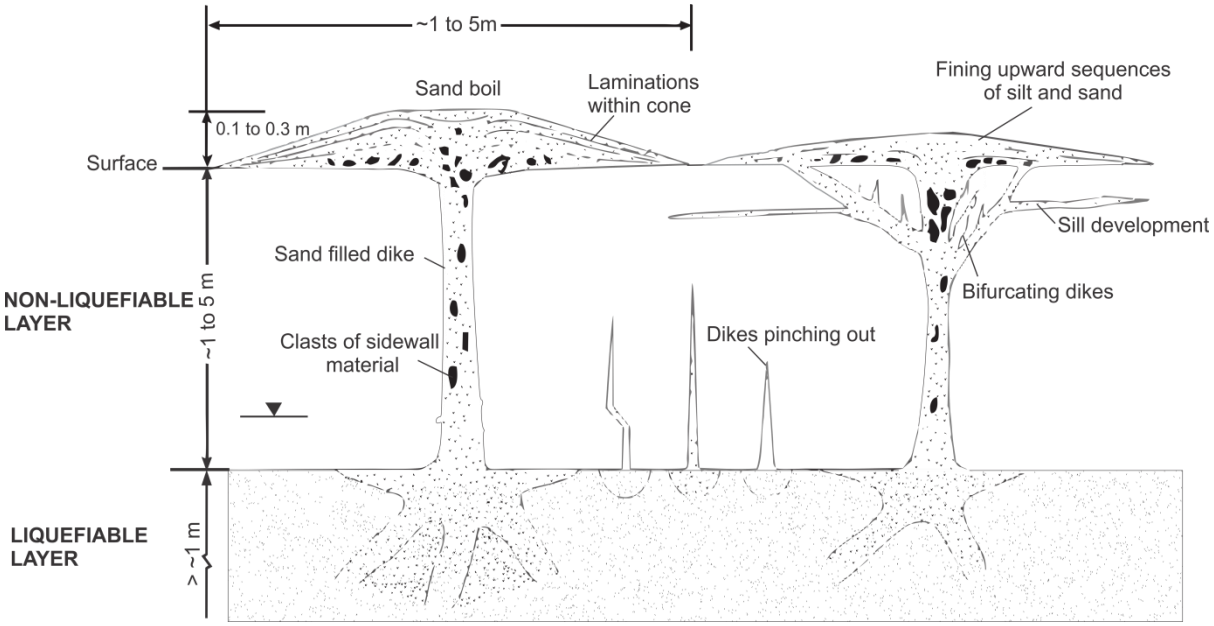

Figure 1.12: Schematic vertical section of subsurface liquefaction features and surface accumulations. Dikes intrude the overlying non-liquefiable 'crust' and consist of silty and sandy liquefied sediment producing cone-shaped sand boils. Modified from Obermeier, (1996).

In addition to surface ejecta, liquefaction produces associated ground deformations forming pressure ridges or blistering of the ground surface from dike and sill injection, and depressions and settlement from sediment withdrawal from the liquefied layer and post-liquefaction volumetric densification leading to bearing capacity failures and significant damage to buildings (Cubrinovski and Green, 2010; Hughes et al, 2015). The amount of surface subsidence is generally dependent on the density of the sand layers and how close the liquefying layers are to the surface (van Ballegooy et al., 2014). Particularly severe damage is induced by lateral spreading where subsurface liquefied sediment allows rafting of the overlying crust by up to several meters down a slight inclination or toward the free face of a river channel (Fig. 1.13) (Cubrinovski et al., 2012). Liquefaction-induced lateral spread typically causes substantial property damage because locations most susceptible to spreading (relatively flat areas adjacent to waterways) are often developed residential areas. Lateral deformations of less than a few meters may occur at many sites over widespread areas in

large earthquakes and cause considerable damage to buried utilities. The deformation of the overlying crust initiated by lateral spreading may also facilitate the ejection of sediment to the surface through spreading cracks (Fig. 1.13) (Raunch, 1997). The expulsion of pressurised water entrains and removes sand and silt grains from the source sediment through permeable pathways opened as a result of the spreading. Post-CES floodplain cross-sections showed floodplain subsidence and river channel narrowing and shallowing resulting from lateral spreading toward the channel and sedimentation from liquefaction ejecta entering waterways (Hughes et al., 2015).

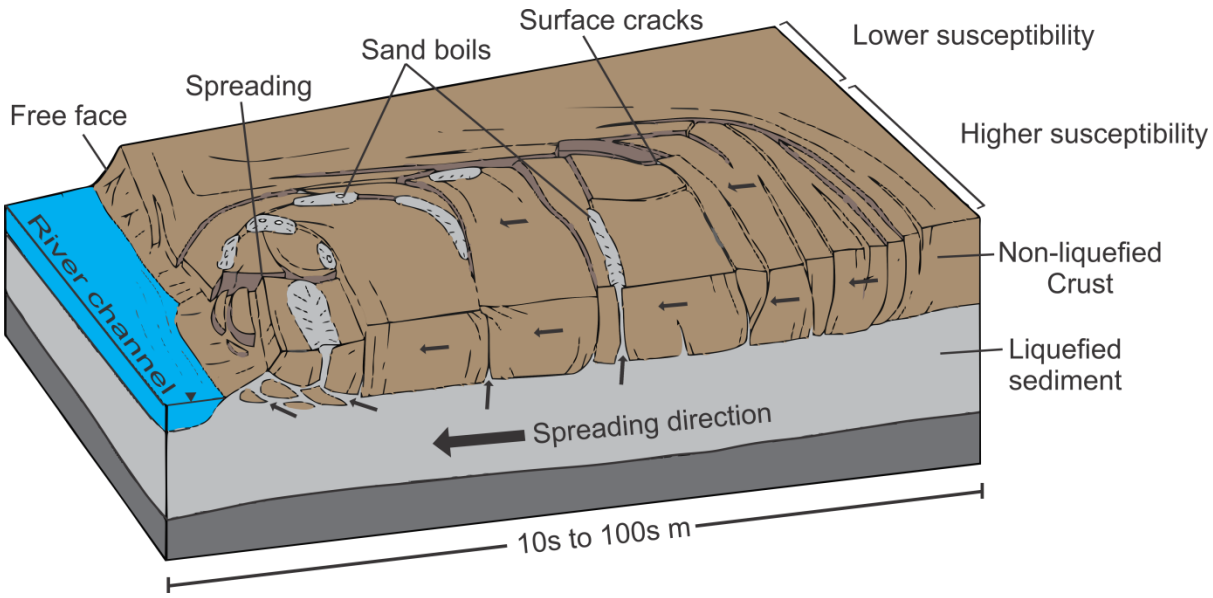

Figure 1.13: Schematic block diagram of complex deformation patterns of lateral spreading from earthquake-induced soil liquefaction showing spreading of the upper crust layer toward the free face of a river channel. Liquefied sediment is also ejected vertically through spreading cracks. Modified from Raunch, (1997).

The removal of liquefied material promotes subsidence as a result of lateral spreading, topographic re-levelling, volume loss due to water expulsion, sediment ejection to the ground surface and post-liquefaction volumetric densification (Villemure et al., 2012). Because liquefiable material in the near-subsurface often occurs in lenses or as irregular forms, associated ground settlements due to compaction and the expulsion of water are generally irregular and uneven (Brown and Weeber, 1992). The effects of this irregular deformation are identified as differential settlements (Cubrinovski et al., 2012; 2014; Robinson et al. 2012). These phenomena are referred to as liquefaction-induced ground deformations in this thesis.

The categories used for defining liquefaction severity are presented in Table 1.2 and include variations in the volume of ejected material and the amount of settlement and cracking.

Table 1.2: Liquefaction severity categories and expected surface observations based on the criteria outlined by Green et al. (2005).

Liquefaction Severity	Surface Observations
Minor	• Small amounts of ejected material (<1 m^2; <100 mm thick) • Settlements 0 to 0.1 m
Moderate	• Large amounts of ejected material (>1 m^2; ~100 to 300 mm thick) • Small ground cracking • Settlement 0.1 to 0.5 m
Severe	• Extensive and frequent amounts of ejected material (>1 m^2; >300 mm thick) blanketing streets and properties • Many ground cracks/ lateral spreading visible • Extensive settlement >0.5 m

1.3.3 Liquefaction susceptibility parameters

Liquefaction is typically influenced by sediment properties (grain size, grain shape, sorting), geotechnical properties (sediment density, ground water depth, pore water pressure, effective confining stress), and earthquake characteristics including peak ground acceleration (PGA), M_w, and distance from seismic source (Brown and Weeber, 1992; Idriss and Boulanger, 2008). Also, topography and distance to the free face of a river channel will influence how an area will respond to seismic shaking, and the generation of surface deformation. Zones with high water tables consisting of young saturated unconsolidated sand with sufficient confining pressures are most prone to liquefy during ground shaking (Youd et al., 2001). The effects from liquefaction (sand boils and flooding) and associated ground deformation (blistering from sill injections, differential settlement and lateral spreading) are expected to be most severe where sandy sediments are of greatest thickness and are relatively young, saturated, loose, well-sorted and where interbedded clayey or gravel deposits are thin or absent (Brown and Weeber, 1992).

The overlying non-liquefiable crust thickness above deposits prone to liquefaction has a profound influence on the development of surface damage (Ishihara, 1985). Crust thickness, cohesiveness and uniformity will either promote or inhibit the surface ejection of sediment.

Thinner and less-consolidated crustal units allow the excess pore water pressures of the underlying liquefied sand to break through the surface capping layer, initiating ground deformations and sand boiling (Idriss and Boulanger, 2008). A thicker surface curst may be strong enough to resist cracking from the forces of excess pore pressure and prevent the surface manifestation of liquefaction.

The controlling factors which initiate liquefaction in uniform clean sand are generally well-known, however liquefaction behaviour of sand with a large fines content (silt and clay) is less understood (Rahman and Lo, 2008). Brown and Weeber (1992) describe the inclusion of fines causes soils to resist the generation of excess pore water pressures, reducing the susceptibility of a soil to liquefy. This understanding of liquefaction resistance has been subject to more recent research by Idriss and Boulanger (2008) who explain the inclusion of fines will increase or decrease the liquefaction tendency of a soil deposit, depending on plasticity.

Liquefaction occurrence in the soil profile is not always associated with surface deformation and damage to structures (Ishihara, 1985). Liquefaction may occur to depths greater than 10 m, with surface manifestation or deformation absent. However, the most significant effects result from the liquefaction of susceptible materials occur typically in the upper 10 m, depending on the location (i.e. near sea level or at high elevations) (Brown and Weeber, 1992). Increasing effective confining stress (density and thickness of overburden) and greater distances to saturated material below the surface require stronger and longer durations of ground motions to induce liquefaction and ground deformations (Brown and Weeber, 1992).

The minimum PGA required to trigger liquefaction of a soil is typically determined by the site-specific geotechnical tests or empirical calculations (Bradley and Hughes, 2013; Maurer et al., 2014; Lunina and Gladkov, 2015). Data gathered from these tests allow the seismic triggering thresholds for initiating liquefaction to be calculated, identifying the susceptibility of a particular site to liquefaction for a given earthquake event (Green et al., 2014).

1.3.4 Meandering river geomorphology and liquefaction susceptibility

An issue with classifying alluvial deposits in sinuous rivers is their heterogeneity, and how this influences liquefaction susceptibility. Current literature suggests the depositional variations caused by meander loop migration produce grain size differences corresponding

with channel deposits, point bar lateral accretion deposits, cut bank and channel abandonment deposits, and internal variations in sorting (Willis and Tang, 2010). Geomorphic studies of modern river systems have provided insights into the nature of these facies (e.g. Willis, 1989; Hooke, 2007; Labrecque et al., 2011; Toonen et al., 2012; Asahi et al., 2013; Fryirs and Brierley, 2012; Ghinassi et al., 2013). It is clear from these studies that the characteristics of point bar deposits are closely associated with specific alluvial settings. For example, point bar deposits in an unconfined setting, that permits channel bend expansion and downstream migration, results in the preservation of sequences that fine both upward and downstream (Bridge et al., 1995). Alternatively, areas where modern floodplains are confined by elevated glacial or volcanic formations, forming obstructions to migrating channels, affect the migratory and accretionary regimes and promote the formation of internal sediment heterogeneities (Fryirs and Brierley, 2012).

The effects of alluvial plain evolution on local liquefaction distributions are less well known. Several studies have identified the influence of channel migration and point bar lateral accretion in sinuous channel segments on the distributions of liquefaction features from large earthquakes. Tuttle (2001) identifies sand boils following scroll patterns of point bar deposits within inner meander loops of the New Madrid seismic zone in the central United States (Fig. 1.14). The distribution of surface ejecta suggests point bar deposits directly influence the distribution of liquefaction, and the geometry of accreted deposits serves as preferred pathways for surface ejecta (Tuttle, 2001).

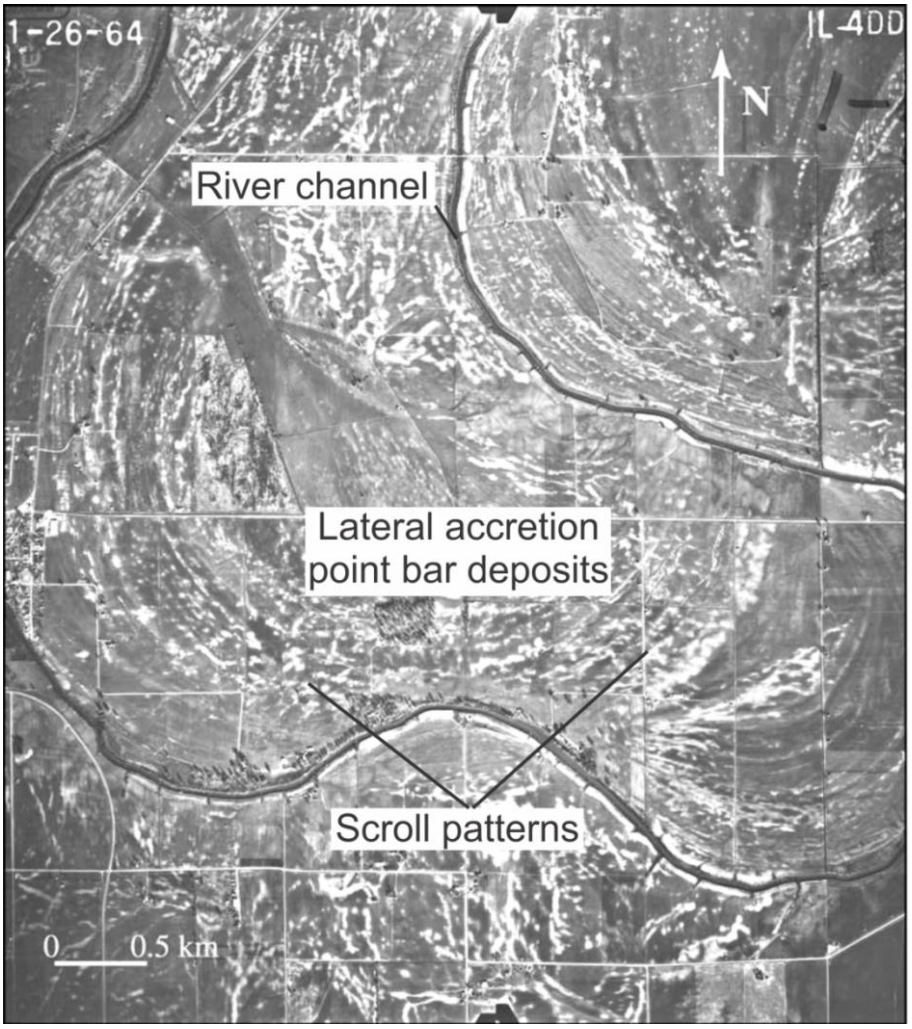

Figure 1.14: Surface ejecta (white areas) following scroll patterns of point bar deposits in the New Madrid seismic zone, showing river migration path has influenced the liquefaction distributions. From Tuttle (2001).

Similarly, Ishihara (1993) identifies a strong correlation with the location of abandoned meanders and point bars with the observed distribution of liquefaction-induced damage in Dagupan City in the Philippines following the 1990 Luzon earthquake (Fig. 1.15). The migration of the Pantal River during flood events formed unconsolidated deposits of sands and silts prone to liquefaction. These were the locations where the most severe liquefaction and lateral spreading were observed following the M_w 7.8 earthquake (Fig. 1.15)

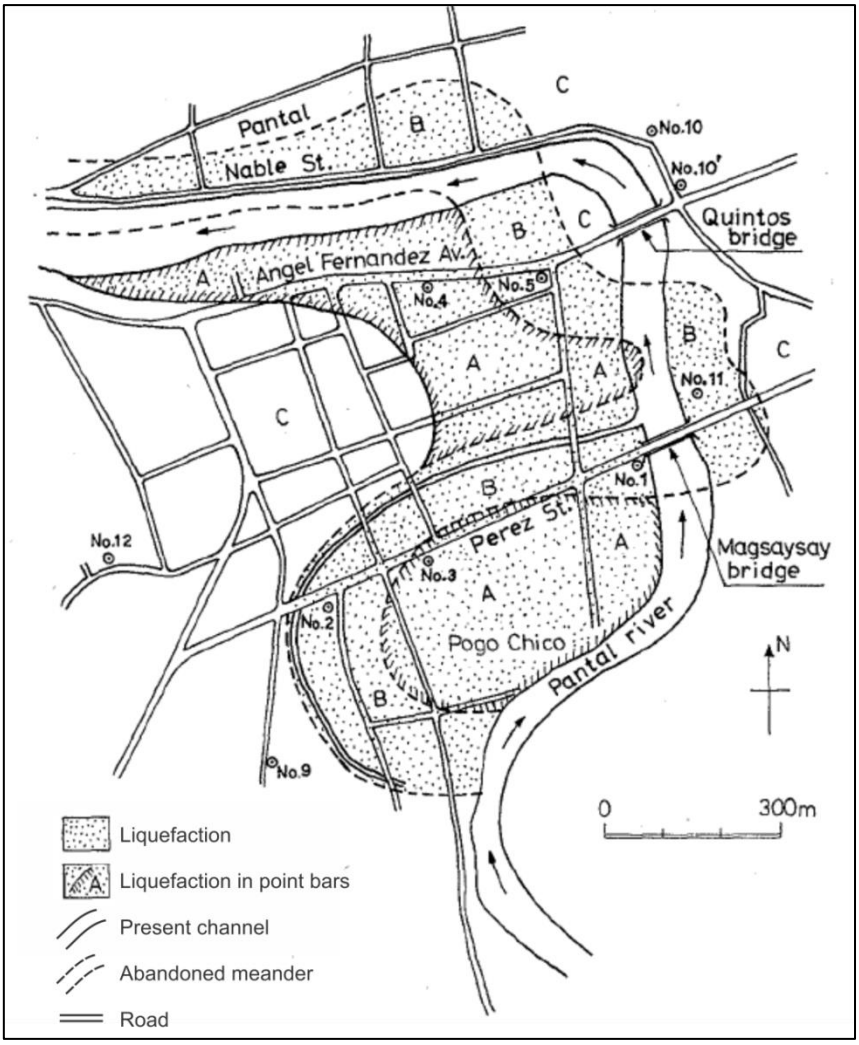

Figure 1.15: Correlation of abandoned meanders and damage distributions in Dagupan City following the 1990 M_w 7.8 Luzon earthquake. From Ishihara (1993).

Investigations by Wotherspoon et al. (2012) of historic maps identify the relationship between observed liquefaction in Kaiapoi and former channels of the Waimakariri River following the 2010 M_w 7.1 Darfield earthquake (Fig. 1.16). The majority of liquefaction in Kaiapoi occurred in areas where river channels had been reclaimed or had their flow diverted. This highlights how areas in former river channels and abandoned meanders consist of unconsolidated deposits of sands and silts which are highly susceptible to liquefaction during earthquakes.

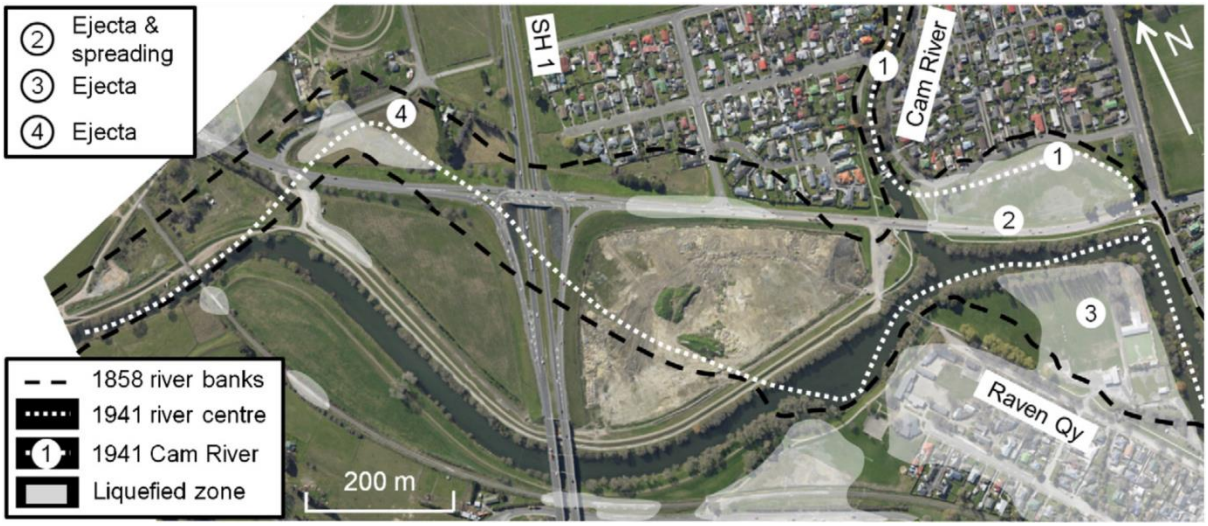

Figure 1.16: Aerial photograph of western Kaiapoi indicating the locations of the former Waimakariri River channels and liquefied zones following the M_w 7.1 Darfield earthquake. From Wotherspoon et al. (2012).

These studies highlight the importance of the fluvial history in seismically active regions, and the high susceptibility of point bar and abandoned or reclaimed river channels to liquefaction. Current liquefaction vulnerability analysis relies on empirical data to provide information on liquefaction resistance using various in situ tests (i.e., CPT), but investigations also need to consider landform evolution to classify local scale differences that effect susceptibility as observed in the above studies (Idriss and Boulanger, 2008).

1.4 THESIS SCOPE

1.4.1 Thesis Objectives

The intentions of this thesis are to build an understanding of migrating river systems and their control on spatial distributions of liquefaction depending on the evolution of sedimentary facies and proximity to geomorphic features. By identifying the distribution of liquefaction features through the CES, and linking these observations with the evolution of Christchurch's migrating rivers, the processes permitting the formation of heterolithic fluvial deposits, which have a critical control on liquefaction susceptibility, may be recognised. Outcomes will include an understanding of river migration and lateral accretion in sinuous channel segments and the role of river migration on sporadic liquefaction distributions observed in southern Christchurch following the CES.

The major objectives of this study are;

- Determine how meander loop migration influences soil susceptibility to liquefaction and how the different morphology, soil characteristics and particle size distributions relate to depositional history of the river system.
- Analyse the sedimentology, penetration resistances from in situ tests (CPT), and the structural characteristics of the sites in question, and identify how these features vary in relation to the river's ability to migrate.
- Assess the presence of paleoliquefaction from historic earthquakes to categorise the susceptibility of individual sites and postulate possible triggering events.
- Define the links between the nature of meander bends and the liquefaction potential of the resulting deposits. Determine if liquefaction distribution during the CES is related to geomorphic and lithological differences between locations adjacent to Christchurch's urban river systems.

Extensive evidence exists about the liquefaction susceptibility of natural deposits and the damaging effects to land and infrastructure in proximity to river channels. However, current engineering and susceptibility studies also need to recognise the importance of geomorphic influences on identifying strata parameters and predicting coseismic ground deformation. Acknowledging geomorphic information is critical to better understanding the scale of possible liquefaction-induced damage, thus potentially reducing the impacts of an earthquake. This thesis hopes to assist land management agencies, engineering companies and hazard planners to make better-informed decisions regarding liquefaction hazard categorisation, engineering design and effective land use planning.

1.4.2 Thesis Organization

Chapter 2: Research Methods

This chapter describes the research methods employed to identify the studied field locations, the field and laboratory methods used, and the collection and analysis of sediment samples and geotechnical data. Firstly, remote sensing techniques are described, and the field sites and reasons for their selection are presented. Secondly, the methods pertaining to field sampling and analysis are presented. Finally, the methods for identifying physical earthquake features are explained.

Chapter 3: Meander Bend Geomorphology and CES Surface Observations

The purpose of this chapter is to provide background information on river migration processes and lateral accretion deposits, the location and characteristics of study area, and present new figures of the surface observations and ground deformation experienced through the CES. Recognition of spatial differences in channel morphology, liquefaction distributions, and the geologic setting are then used to understand how migration of the Heathcote River in southern Christchurch effected CES liquefaction distributions.

Chapter 4: Subsurface investigations

This chapter presents the results from subsurface investigations across the study area and compares the observed liquefaction features to the geomorphic setting, discusses liquefaction emplacement mechanisms, and how the physical material properties effected manifestations from sediment analysis of collected soil samples. The geologic evolution, expressions of liquefaction, site characteristics and geomorphology are then discussed along with paleoseismic implications and the use of liquefaction characteristics as proxies for previous channel locations.

Chapter 5: Conclusions

Chapter 5 summarises the influence of meander migration on liquefaction susceptibility in the context of the study area, and discusses future implications for geotechnical investigations, land use, and liquefaction susceptibility mapping. The benefits of combining geomorphic interpretations with geotechnical data to quantify the surface effects of liquefaction and consequent land damage in future seismic events are then discussed.

CHAPTER 2 RESEARCH METHODS

2.1 INTRODUCTION

Based on the focus and objectives of this thesis, the research methods conducted were split into five main areas; remote sensing techniques; subsurface investigations; sediment analysis; geotechnical data; and a review of the ground shaking experienced across Christchurch. The aim of this chapter is to describe each research method employed in this thesis providing detailed information on each procedure. The combination of these research methods provides a greater understanding of the migration processes of Christchurch's river systems and the geomorphic influence on liquefaction distributions during the CES. Detailed descriptions of the individual research methods are outlined below with additional information in the following chapters.

2.2 REMOTE SENSING TECHNIQUES

2.2.1 Mapping liquefaction distributions by aerial photography

A key method in establishing liquefaction distributions and ground deformation features following an earthquake is through aerial photography. High-resolution aerial photographs were collected following the major CES earthquakes by New Zealand Aerial Mapping for the Christchurch Response Centre (Canterbury Geotechnical Database, 2012). The photographs were examined to identify the distributions and severity of ejected material and combined with observed ground cracks. The aerial extent of surface liquefaction features comprising linear arrays of sand boils and ground cracks were mapped in detail using ArcGIS and are presented in Chapter 3.

2.2.2 Post-earthquake digital elevation analysis

Aircraft-based Light Detection and Ranging (LiDAR) data was collected over Christchurch and the surrounding regions before and following the major CES events. Each LiDAR dataset created 5-m-resolution Digital Elevation Models (DEM) of the bare land surface for interpretation of pre-and post-earthquake ground elevation changes (Hughes et al., 2015). The DEMs form a topographic surface model of the ground surface and are differenced by subtracting ground movements from each earthquake event to provide estimates of vertical ground displacement. The DEMs were added to ArcGIS for spatial analysis.

For surface modelling purposes and assessing elevation changes through earthquake events, the vertical tectonic ground movements (ΔE_{Tec}), inferred from earthquake source data and modelling (Beavan et al., 2012), were subtracted from the total elevation changes (ΔE_{Tot}) to produce elevation changes due to liquefaction (ΔE_{Liq}). The results were corrected for the tectonic component using predicted fault displacement from the geodetic models of Beavan et al. (2012). Surface modelling enabled quantitative elevation differencing and vertical movements between the earthquakes within specific landforms to be identified. Points were assigned at different distances from the modern river channel locations to quantitative identify ground deformation patterns across the study areas.

2.2.3 Geomorphic mapping by digital elevation model

Geomorphology reflects the form and origin of the ground surface by identifying the nature of the surface material and the underlying geologic properties (Schumm and Lichty, 1965). Identifying the geomorphologic characteristics requires and understanding of the landform properties and the formation processes of the surficial material. Characterising a particular site requires the identification of dominant land processes and an interpretation of previous geologic settings. While geotechnical investigative data, including bore holes and geotechnical probes (e.g. CPT) provide in situ physical properties of the subsurface materials, the data gathered may provide incoherent information between isolated sites. An understanding of geomorphological information provides an area-wide indication of subsurface properties, and provides insights into erosion and deposition processes including environmental changes (past or present) that have shaped the ground surface (Brackley, 2012).

Topographic and hillshade images were derived from the DEMs using ArcGIS for geomorphic analysis and are presented in Chapter 3. The images generated of the ground surface identify the nature and origin of the landforms and the underlying geologic materials. When used in conjunction with liquefaction elevation changes, significant landforms can be identified. Recognising differences in channel morphology assists with understanding how river migration affected the distributions of liquefaction. The DEMs are also used to identify the sloping topography of the land surface to identify the susceptibility of an area to lateral spreading. Having combined the surface elevation properties with liquefaction distributions

from ground observations and aerial photo analysis, this data was ultimately used to constrain locations for detailed field research.

2.3 TRENCHING THROUGH LIQUEFACTION FEATURES

2.3.1 Site selection and trench digging

Two adjacent suburbs were selected within inner meander loops of the Heathcote River, in southern Christchurch, to investigate morphological and stratigraphic relationships of the point bar deposits, and the CES liquefaction features. St Martins and Beckenham were selected because of the level of liquefaction severity, distinct liquefaction distribution patterns during the CES, and proximity to the modern Heathcote River channel (Fig. 2.1). In St Martins, two locations where selected for trenching analysis based on allogenic sediments at the surface, ground subsidence patterns, CES liquefaction distributions, and field observations. The locations were also selected for accessibility. Site 1 was located in St Martins Park and Site 2 was located at the former site of a residential property at 68a St Martins Road (Fig. 2.1).

Excavation of the trenches enabled the identification of subsurface features that fed surface vents during the CES that facilitated the substantial ground elevation changes and associated damages. Detailed stratigraphic logs of the soil horizons and liquefaction features were constructed which allowed for textural and compositional properties of the fluvial facies to be identified, and the proportions and spatial distribution of modern liquefaction features. Comparisons with aerial photography permitted the assignment of modern liquefaction features to individual earthquake events.

In Beckenham three sampling locations were selected along the interior of the inner meander loop. The sites include Beckenham Park (Aug 1), the residential property at 70 Corson Ave (Aug 2), and the intersection of Waimea Tce and Eastern Tce (Aug 3) (Fig. 2.1). Hand auger excavation at each site of depths up to 2 m allowed the collection and analysis of the subsurface soils.

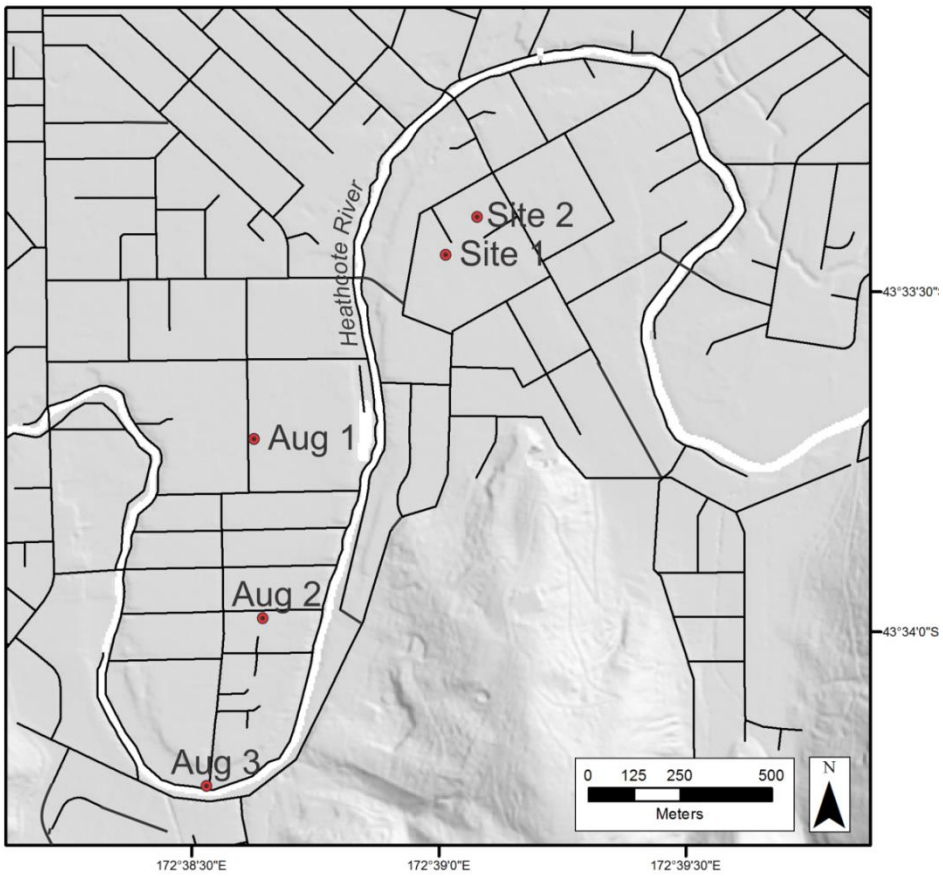

Figure 2.1: Locations of subsurface investigations and major roads across the study area.

Figure 2.2: Excavated trench at Site 2 at the former residential property at 68a St Martins Road, St Martins.

2.3.2 Trench logging

Trenches where dug by excavator to a predetermined depth based on water table elevation data (Fig. 2.2). The trenches were excavated perpendicular to aligned sand blows and the maximum horizontal movement vectors through the earthquakes. At Site 1, the trench was ~1.6 m deep and 7 m long. At Site 2, the trench was ~1.5 m deep and 10 m long. The width and lengths of the trenches were influenced by site area limitations.

The trench walls were cleaned using hand scrapers and divided into 1 m^2 sectors using string and nails which enabled accurate sketches of the liquefaction feature morphology and fluvial stratigraphy. The trench logs were sketched on to graph paper to make accurate scaled versions of the trench wall structure. The trench walls were also recorded by photographs that were stitched together to create a photo mosaic. The liquefaction features identified in the floor at Site 1 were also recorded.

2.3.3 Radiocarbon dating

The geologic ages of stratigraphic horizons and pre-CES liquefaction features were constrained by radiocarbon dating organic fragments collected from various elevations within the walls of the trenches. Dating ^{14}C isotopes relative to other non-radioactive isotopes of carbon allows the measurement of the time elapsed since the organic material was growing. Dating these organic samples from within the fluvial deposits gives a relative age range of when the organic fragment stopped growing, subsequently deducing the age of the stratigraphy in which the organic material was deposited.

Four organic samples collected from trenching were sent to Rafter Radiocarbon Laboratory in Wellington, New Zealand, for Accelerator Mass Spectrometry (AMS). The organic pieces are cleaned and then prepared for chemical pre-treatment by cellulose extraction to remove any contaminants. The sample is then combusted in a sealed quartz tube generating carbon dioxide that is converted to graphite (graphitisation). The carbon isotopes are measured using the AMS dating technique where a particle accelerator is used to count the relative numbers of the different carbon isotopes present in the material. Once the ^{14}C content is known, it is compared to that of a standard material. The difference is attributed to the time that has elapsed since the organic sample was growing before it was deposited in the fluvial sediment. The AMS laboratory reports including sample treatment details are presented in Appendix A.

2.4 SEDIMENT ANALYSIS

2.4.1 Trench and hand auger sampling

To identify the composition and lithological changes of the subsurface, a total of 39 sediment samples were collected for grain size analysis from each stratigraphic unit and liquefaction feature within each trench. The samples were described to identify grain size, sorting, colour, amount of mottling, presence of organic material and relationships to surrounding layers. Changes in surface elevation and depth were recorded while gathering each sample. Colour variations between the identified liquefaction features were classified using the Munsell colour chart.

Samples were also collected by hand auger to gather sediment from below the trench floors, and at locations where trench excavation was unable to be carried out (Fig. 2.3). The hand auger consists of an auger head with an opening to collect unconsolidated sediment, attached to extendable steel rods that are rotated by a handle. The auger is rotated into the ground until the head becomes filled, and then is lifted out of the borehole to be emptied. The samples removed from the auger head are aligned in 1 m rows for comparison and sampling of the sediment.

Two samples were also collected from recent detailed subsurface liquefaction studies in Avonside (Sullivan Park and 11 Bracken Street), within an inner meander bend of the Avon River (Bastin et al, 2015). The samples were used to compare the grain sizes of fluvial stratigraphy adjacent to the Avon River with the samples collected from the study area adjacent to the Heathcote River.

Figure 2.3: Hand auger sample collection from below the floor of the excavated trench at St Martins Park (Site 1).

2.4.2 Laser-Sizer grain size analysis

Laser-Sizer analysis was carried out using the Saturn Digisizer II 5205, provided in the University of Canterbury sedimentology laboratory. Laser-Sizer analysis is useful for identifying the particle size of each stratigraphic unit and correlating liquefaction features with possible source units. To prepare for analysis, small amounts of the sediment samples are mixed with a deflocculant (calgon) before being added to the DigiSizer. The DigiSizer uses a laser in conjunction with a device containing an array of detector elements to measure particle sizes. The detectors measure the intensity of light scattered by the particles at various angles depending on the grains size, shape, refractive index and wavelength of incident light. The particle size distributions are subsequently calculated from the angle distribution of the scattered light intensity collected by the detectors. The raw grain size data is then analysed using a spreadsheet to produce probabilistic grain size distribution curves which allows comparisons between the grain sizes of fluvial stratigraphy and liquefaction features.

2.4.3 Pipette clay analysis

To characterise the total proportion of clay within sediments from the study locations, eight samples (two from Site 1, two from Site 2, St Martins; two from Beckenham; two from Avonside) were analysed using the pipette method (Fig. 2.4). A weighed soil sample (~20 g) is disaggregated using distilled water and is passed through a 4 phi wet-sieve to remove the sand fraction from the sample. The removed sand fraction is dried and weighed. The sieved subsample is added to a litre cylinder where it is topped up to exactly 1L using distilled water and 20 ml of sodium hexametaphosphate (calgon) dispersant to prevent the flocculation of the clay particles. Having left the cylinder overnight to check for flocculation of clays, the column is stirred vigorously using a brass stirrer to distribute all the material uniformly throughout the column, and a timer is started once the stirrer is removed. Specific volumes (20 ml) are extracted from the column using a pipette at specified depths and time intervals over a period of 8 hours. Each subsample is placed into a 50 ml beaker and is dried in an oven to remove the water content. The weight of each dried sample is representative of the proportion of the total clay fraction remaining in suspension. Thus, each subsample removed measures the proportion of total sediment finer than the size that has settled to the specified depth in the specified time giving the distribution of grain sizes (Lewis and McConchie, 1994). For the purposes of this study, the particle size for clay is identified as 9 phi and below.

Figure 2.4: Undertaking the pipette analysis.

2.5 GEOTECHNICAL DATA

2.5.1 CPT

The liquefaction potential of the subsurface fluvial stratigraphy was evaluated from CPT data using the Idriss and Boulanger (2008) method. This method establishes the liquefaction potential by comparing the cyclic stress ratio (CSR), which evaluates loading induced at different depths by an earthquake, with the cyclic resistance ratio (CRR), which represents the ability of the soil to resist liquefaction. The CPT data was accessed using the Canterbury Geotechnical Database (CGD) (https://canterburygeotechnicaldatabase.projectorbit.com). The database was developed for geotechnical and structural engineers to access geotechnical data collected across Christchurch following the CES. Currently, engineers designing foundations in Christchurch use CPT records to assess the ground conditions of a property to specify the most effective foundation design for new buildings (Maurer et al., 2015).

2.5.2 CLiq

The raw CPT data were imported to the liquefaction analysis software CLiq, by GeoLogismiki, which provides calculation plots for basic CPT data interpretation, factor of safety, liquefaction potential index, and post-earthquake displacements. The program uses assessment parameter constants of earthquake and site properties which are able to be adjusted with each CPT to make the susceptibility prediction of a location more accurate. For the purposes of this study, the liquefaction susceptibility of the subsurface strata was assessed using the factor of safety. The likelihood a soil will liquefy is expressed as a factor of safety against liquefaction (FS), where FS < 1 is considered potentially liquefiable. The results of CPT across the study area were correlated with the stratigraphy to ~3.5 m depth, as determined from the trench and hand augers. This enabled the possible depths of the liquefiable source sediment to be recognised.

2.5.3 Hydrological conditions

As greater liquefaction manifestation and subsidence are likely to occur in areas with shallower water tables, the ground water elevations across the study area were assessed from the CGD. A representative median water table elevation was calculated across the study area based on Environment Canterbury (ECan) and Tonkin & Taylor Ltd (T&T) measurements derived from each well. The water table depths were based on surveyed well-head levels prior to each major earthquake event, to account for seasonal variation, and subtracting the

elevations from DEMs of the ground surface. The water table surface models were colour banded using ArcGIS to reflect the water table depths below the surface. The depths to the water table could then be correlated with liquefaction distributions and used to predict the ground water depths at the trenching sites.

2.6 GROUND ACCELERATION DATA

PGA at the study area was estimated using ground motion records following each major CES event. Ground shaking parameters are important when comparing site-specific and regional scale investigations of liquefaction distributions as higher shaking intensities typically facilitated greater amounts of liquefaction (Idriss and Boulanger, 2008). The earthquake intensity measurements (PGA) are used to estimate the level of ground shaking experienced at a particular location in a seismic event using strong-motion accelerographs (Bradley and Hughes, 2013). The accelerographs in Christchurch measured the strong shaking during CES events and the spatial distributions of PGAs were estimated from recorded ground motions. GeoNet, a collaboration between EQC and GNS Science, published the earthquake ground motions and shaking intensity following the significant earthquakes for analysis (*http://info.geonet.org.nz/display/appdata/Strong-Motion+Data*). The recordings for PGA analysis from the individual earthquakes used for this study were obtained from the Cashmere High School strong motion station (CMHS) approximately 2 km from the study area. The station is located adjacent to the Heathcote River and has similar site conditions to study area.

2.7 SUMMARY

A realistic geological interpretation and evolution modelling requires the full use and integration of geological data, including engineering data, to understand how migrating fluvial depositional systems influence liquefaction distributions. Each method has been employed to model the land surface and better recognise subsurface properties of the areas adjacent to the Heathcote River. Initially, remotely generated data was used to obtain surface elevation properties of the study area and identify liquefaction distributions throughout the CES. Geographic Information System (GIS) modelling was employed to identify the direct physical changes from uplift and subsidence across the study areas. The remote sensing techniques and aerial imagery assisted with the identification of geomorphic features which are presented in Chapter 3. Having combined the surface elevation properties with

liquefaction distributions from ground observations and aerial photo analysis, these data were ultimately used to constrain locations for detailed field research. Trenching allowed for the identification of the injection mechanisms and sediment composition analysis of subsurface soils, described in Chapter 4. Qualitative and quantitative results from these methods contribute to the identification of migration patterns of the Heathcote River and implications for future liquefaction hazard assessments, discussed in Chapter 5.

CHAPTER 3 MEANDER BEND GEOMORPHOLOGY AND CES SURFACE OBSERVATIONS

3.1 INTRODUCTION

This chapter introduces the dynamic processes of meandering river systems, examines the geometries and spatial distribution of fluvial architecture in meander bends, and introduces the geology and geomorphology of the study area. A series of original figures using newly acquired geospatial data, geotechnical reports, and discussions with eye-witnesses are presented to provide a detailed account of the liquefaction distributions and ground deformation across the study area throughout the CES. The physical attributes from the figures and spatial analysis are then used to reconstruct the planform evolution of the Heathcote River and investigate how the setting influenced the severity of liquefaction distributions and subsidence experienced during the CES.

3.2 MEANDER MIGRATION AND GEOMORPHOLOGY

3.2.1 Channel migration and lateral accretion

Meandering rivers typically consist of a moderately sloping, medium energy, sinuous, single channel river which optimise their bend curvature through migration processes, or the development of cut-offs to maximise transporting efficiency (Fryirs and Brierley, 2012; Ghinassi et al., 2013). The ability of a meandering channel to migrate is primarily determined by valley floor properties including bank cohesiveness, bank stability, topography and vegetation, as wells as the magnitude and durations of river discharges (Asahi et al., 2013). Migrating river channels form alluvial plains dominated by lateral accretion deposits in the form of point bars capped by vertical accretion levee and overbank deposits of sediment in suspension during floods (Fryirs and Brierley, 2012).

During bankfull conditions, the thalweg in a channel is concentrated at the outside concave bank causing erosion and retreat along one side of a meander bend (Fig. 3.1) (Willis and Tang, 2010). Flow becomes deflected from the thalweg zone developing a helicoidal flow toward the inner convex bank of the channel where eroded sediments are transported (Fryirs and Brierley, 2012; Ghinassi et al., 2013). Bank erosion via fluvial entrainment or undercutting of the concave bank and redeposition and aggradation of material along the

convex bank causes the lateral accretion of sediments and the formation of a point bar promoting the migration of the channel (Willis and Tang, 2010).

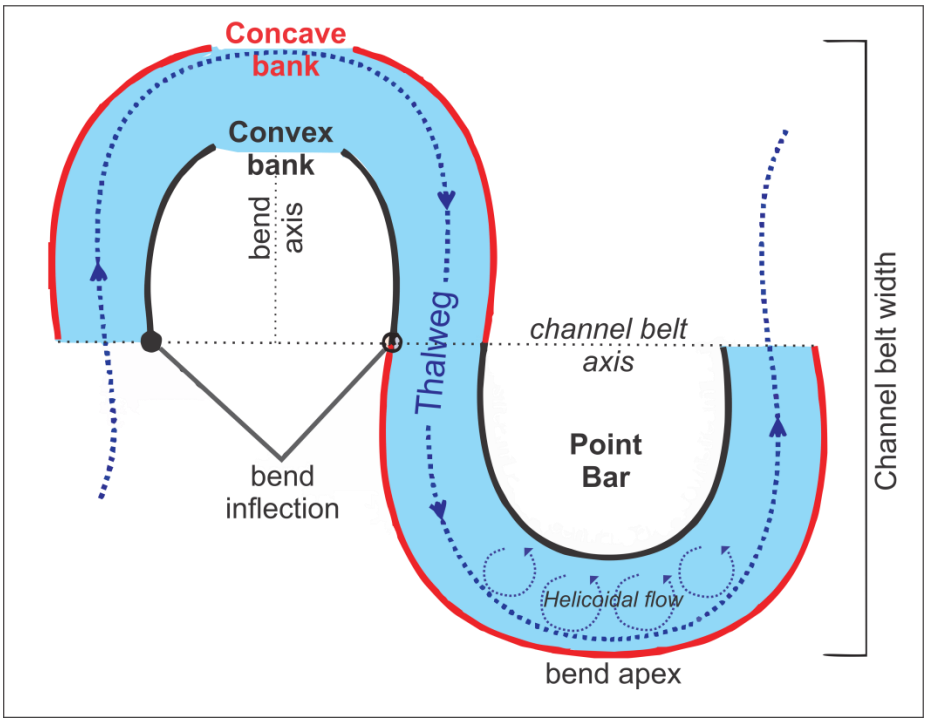

Figure 3.1 Descriptive terminology of meander loops. Concave bank erosion and point bar development from helicoidal flow during bankfull conditions. Modified from Ghinassi et al. (2013).

Several modes of river migration have been identified including expansion (an increase in sinuosity), translation (movement of a meander bend downstream), rotation (development of bend asymmetry) and more complex migration patterns (Fig. 3.2) (Brice, 1974). The relative stability and cohesiveness of the concave banks determine the ease with which the channel is able to adjust laterally (Fryirs and Brierley, 2012). Where a meandering river is confined in a valley setting and lateral expansion is inhibited, the obstructions commonly cause downstream translation of the sinuous channel system as the resistant substrate limits the capacity for lateral channel adjustments (Labrecque et al., 2011; Fryirs and Brierley, 2012).

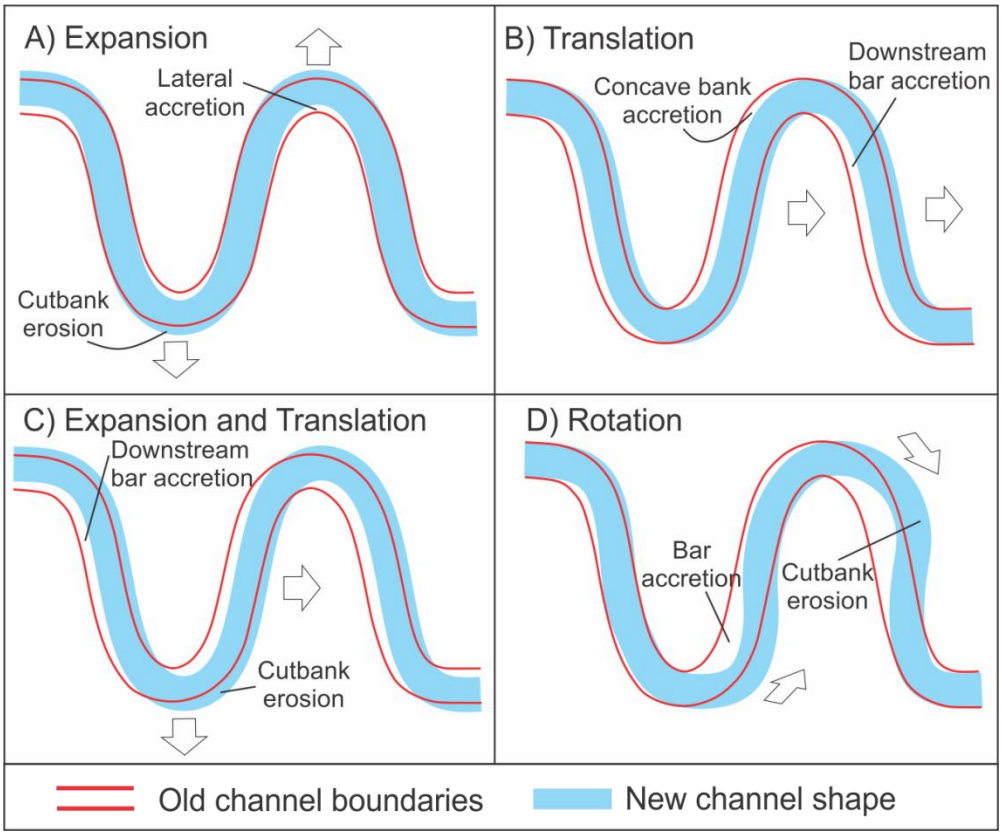

Figure 3.2: Planview of different meander bend migration patterns. (A) Expansion (an increase in sinuosity). (B) Translation (movement of the channel downstream), Expansion and rotation (combination of increasing sinuosity and downstream migration). (D) Rotation (development of bend asymmetry). Flow direction left to right. Arrows indicate total bend movement directions.

3.2.2 Point bar development

Point bar stratigraphy typically consists of upward-fining sequences of sand and fines (silt and clay) inclined toward the centre of the channel, reflecting the asymmetrical channel geometry at the bend apex in response to bend expansion (Fig. 3.3) (Willis, 1989; Bridge et al., 1995; Fryirs and Brierley, 2012). Deposits at the base of the point bar sequence are generally sand-dominated with less energy available to transport the coarser sediment higher up the bar surface (Labrecque et al., 2011). Helicoidal flow, however, deposits coarser sediment over the bar surface as the thalweg shifts to the outside of the bend during flooding events (Fig. 3.3). Coarser sediments record the aggradation of point bars during rising flood stages in channel bends, with fines draping indicating the falling flood and normal flow conditions (Willis and Tang, 2010). Surface expressions of lateral accretion deposits may form ridge and swale topography producing meander scroll patterns indicating lateral migration directions and point bar evolution (Fig. 3.3) (Peakall et al., 2007).

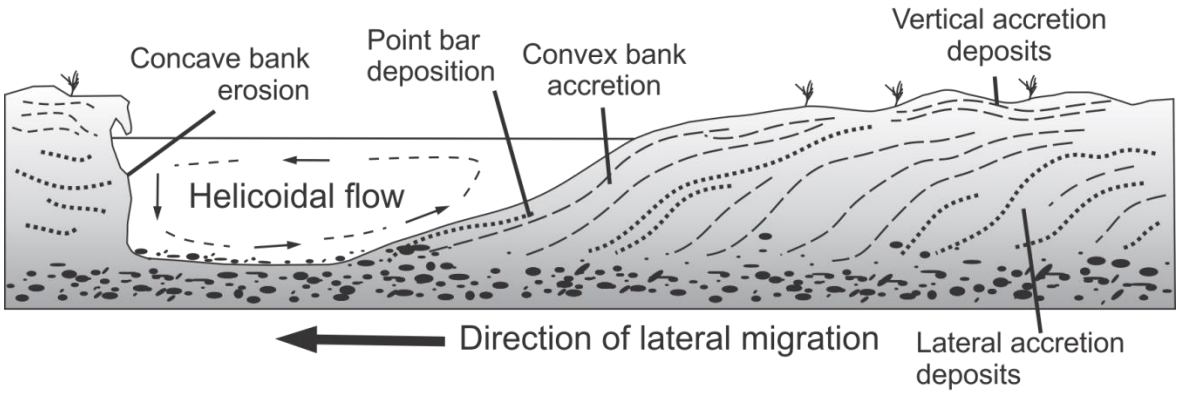

Figure 3.3: Cross-section of point bar development along the convex bank of a meander bend. Bar forms follow the alignment of the channel bend of sand (dotted lines) and fines (dashed lines) underlain by coarser sediments. The channel moves laterally across the valley floor as the meandering river migrates from erosion and subsequent deposition. The bar surface is typically inclined toward the channel bend apex. Modified from Brierley and Fryirs (2005).

Overbank deposition of fine material (silt and clay) during flooding events produces vertical accretion deposits. As a river tops its banks, its carrying capacity greatly decreases and the suspended sediment is deposited as a horizontal surface across the floodplain, forming levees in proximal areas and back swamps in distal areas (Fryirs and Brierley, 2012; Ghinassi et al., 2013). Channel deposits form the basal component of a floodplain overlain by vertical accretion deposits from overbank processes as a channel migrates (Willis and Tang, 2010). Tidal influences and the depositional effects of tidal-fluvial transitions also effect the development of point bar stratigraphy (Dalrymple and Choi, 2007).

3.2.3 Avulsion

Channel avulsion is triggered when a sudden shift in a river course promotes the formation of a new channel geometry (Toonen et al., 2012). The avulsion mechanism is typically associated with aggrading river beds cutting through levees forming a cut-off (e.g. Hooke, 2004) or tectonic deformation relocating the channel in the adjacent floodplain (e.g. Duffy et al., 2013). The location and timing of avulsions are dependent on local conditions (e.g. floodplain elevation, catchments size) and the timing of flood events. Channel abandonment and the formation of a new channel course is recorded in an alluvial basin through the preservation of paleochannels which are subsequently filled with overbank material during and after abandonment as the new channel develops in the adjacent floodplain (Fryirs and

Brierley, 2012). Paleochannels are commonly recognised as depressions in the landscape located at the position of a formerly active channel (Fig. 3.4) (Toonen et al., 2012).

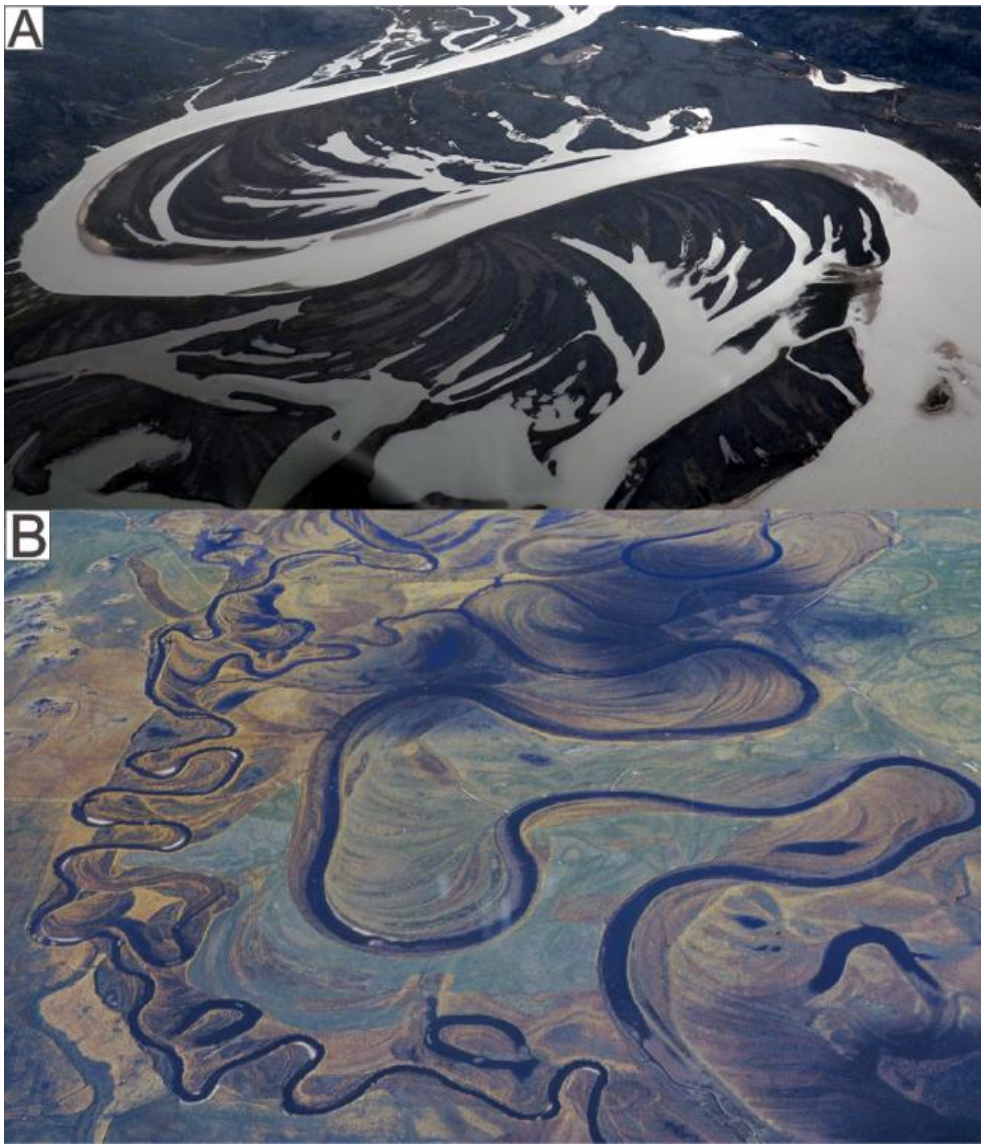

Figure 3.4: (A) Aerial photograph of a migrating river in Auyuittuq National Park, Canada, forming low-lying paleochannels containing standing water within the meander loops. Photo by Mike, S. (B) Aerial photograph of many abandonaned channels and characteristic meander scrolls across point bars in a meandering river in Otago, New Zealand. Photo by Dr. Doug Lewis.

Depending on the rate of abandonment and proximity to the active channel, paleochannels contain sandy bedforms accumulated prior to an avulsion event, overlain with finer channel abandonment sediments (Fig. 3.5) (Willis and Tang, 2010; Toonen et al., 2012). A sudden reduction in flow conditions reduces the transporting capacity making the channel incapable of altering the pre-existing bedform morphology, preserving the sandy channel deposits

(Toonen et al., 2012). The coarser-grained sediments form a sharp boundary with later fill deposits of silt and clay across all portions of the river channel as the flow becomes diverted and a paleochannel is formed (Fig. 3.5). Analysing the geometry and dating channel fill materials from a paleochannel can be used to infer paleoenvironment conditions and abandonment rates of a river system (Toonen et al., 2012).

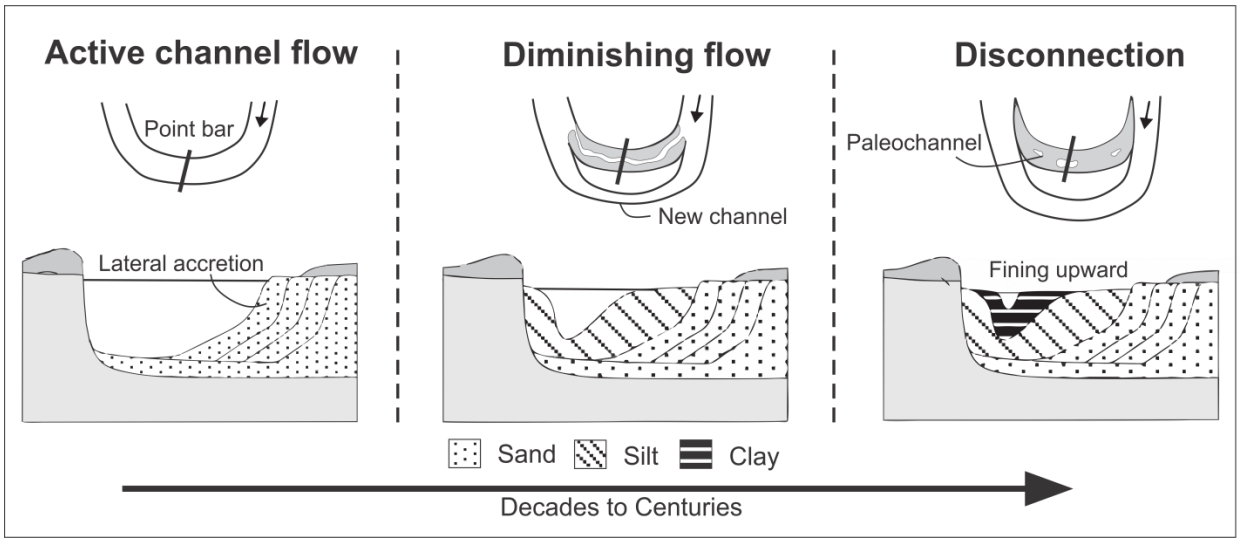

Figure 3.5: Sedimentation model for channel fills of an avulsion abandoned channel. Cross-section of channels show the development of upward-fining sequences as the flow conditions change. Modified from Toonen et al. (2012).

3.2.4 Implications for liquefaction

The scale of liquefaction-induced ground deformation can be dependent on the geometry and extent of the preserved alluvial deposits. Point bar deposits contain sandy materials and therefore are the main suppliers of liquefiable sediments in an alluvial setting (Toonen et al., 2012). Meander bend migration may increase or decrease the continuity of sand bodies, depending on the location and supply of coarser-grained sediments, subsequently influencing the distribution of liquefaction in an earthquake. Grain size variations across channel surfaces within sinuous rivers occur as coarser grains have a tendency to move toward the outside of a channel, where flow velocities are greater (Fryirs and Brierley, 2012). As a channel cuts deeper along the outside of a highly sinuous meander bend and builds up the lateral accretion surfaces on the convex bank, preserved beds successively dip more steeply outward as the deposits thicken (Peakall et al., 2007; Willis and Tang, 2010). Translation of a meander bend downstream will preserve bar deposits with elongate geometries defined by the migration path of the channel (Toonen et al., 2012). The preservation of elongated sand bodies below

finer overbank deposits would expose greater areas to liquefaction-induced ground deformations subject to sufficient ground water and earthquake shaking.

The cohesiveness of crust material influences the propagation of liquefaction surface ejecta. A well-consolidated crust may inhibit the expulsion of pressurised water, regulating the surface manifestation of liquefaction (Idriss and Boulanger, 2008). A cohesive confining layer, overlying a liquefiable body, may however allow greater pore fluid pressures to be generated in the subsurface. An increase in pore fluid pressures may allow more sediment to be liquefied and ejected to the surface once the confining pressure becomes critical and the cohesive crust is deformed.

Erosion, migration or abandonment would allow the formation of significant sediment heterogeneities in a meandering river system. Abandoned channels contain coarser-grained material prone to liquefaction preserved by finer fill deposits creating a crust layer. The typically low-lying elevations of paleochannels also make the deposits prone to liquefaction as the sandy bedforms are likely below the water table (Fig. 3.4). Interbedded lateral accretion deposits and the deposition of vertically accreted overbank material produce further internal heterogeneities in bedding architecture and susceptible grain size distributions in an alluvial plain (Willis and Tang, 2010). Based on the spatial variability and lateral continuity of sand-bodies liquefiable zones are inherently difficult to predict especially when these deposits have been modified or overlain with anthropogenic structures. Because of the stratigraphic complexities, an understanding of depositional processes and surface models are essential for understanding the distribution of liquefaction susceptible sediments in migrating river systems.

3.3 CHRISTCHURCH SETTING

Episodes of flooding by the Waimakariri River and reworking of Holocene sediments by the Avon and Heathcote Rivers have predominantly influenced the geomorphology of present-day soils in Christchurch (Fig. 1.4) (Brown and Weeber, 1992; Forsyth et al., 2008). Alluvial gravels dominate the west of the city with sand and silty coastal sediments in the east overlain by finer fluvial deposits from the migration of the meandering Avon and Heathcote Rivers (Brown and Weeber, 1992; Hughes et al., 2015). The meandering stream beds of these river systems have reworked the surficial sediments creating channel and overbank morphologies

across Christchurch at varying elevations, and have recently incised onto the flood plains following water table lowering from the establishment of wells and recurrent dredging of the river bed (Jacka and Murahidy, 2011). The evolution of the alluvial setting has produced a landscape of significant lateral and vertical variability. The Avon and Heathcote Rivers, fed by springs originating in western Christchurch, occupy former channels of the Waimakariri River (Brown and Weeber, 1992). The rivers meander through the city and empty into the Avon-Heathcote estuary before draining into the Pacific Ocean. The tidally-influenced flow regimes for both of these rivers are dominated by groundwater sourced from the Waimakariri River and the central Canterbury Plains, which flow eastward through highly permeable glacio-fluvial gravel aquifers (Forsyth et al., 2008). Across Christchurch, the average water table depth is typically < 2 m with localised areas near river systems < 1 m (Brown and Weeber, 1992).

3.4 STUDY AREA

The Heathcote River, in southern Christchurch, meanders around the base of the Port Hills from west to east (Fig. 3.6). The highly sinuous river course exhibits distinct meanders of varying morphology. The river has a mean flow rate of 1.28 m^3/s in its non-tidal reaches, and a catchment area of ~103 km^2 including the northern face of the Port Hills (NIWA, 2013). During large storm events, with high runoff from the Port Hills, the river can overwhelm the capacity of the flood detention area and portions of the catchment can substantially flood (*http://www.stuff.co.nz/the-press/news/5812487/Heathcote-River-bursts-banks*). Significant dredging in the past has been undertaken to deepen the channel and reduce the flooding hazard (Hicks, 1993).

3.4.1 Location and geomorphology

The meandering reach investigated in this thesis is located 5 km upstream of the Heathcote River mouth in the adjacent suburbs of St Martins and Beckenham (Fig. 3.6). Both suburbs are point bars encompassed within inner meander loops of the Heathcote River at the boundary of tidal influence (Brackley, 2012). The sediment underlying both St Martins and Beckenham dominantly consists of loose, saturated, interbedded alluvial deposits of sand, silt, clay and peat categorised as the Yaldhurst Member of the Springston Formation (Brown and Weeber, 1992). The sediments are heterogeneous in both vertical and lateral directions due to the depositional characteristics of the meandering river and proximity to runoff

derived from the Port Hills (Brown and Weeber, 1992). Valley fill and slope wash of loess- and volcanic-derived colluvium is contained within the valleys south of the study area at the base of the Port Hills.

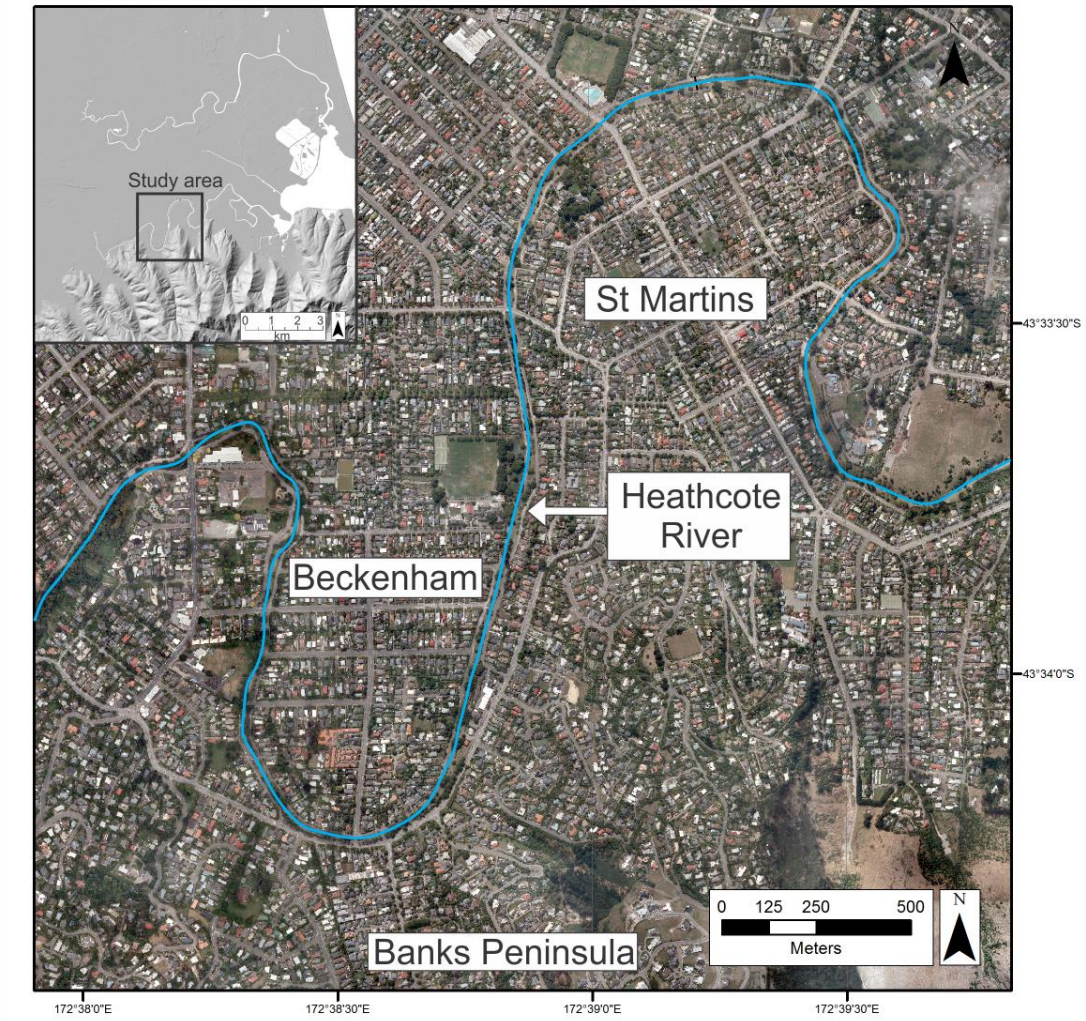

Figure 3.6: Aerial image of the southern Christchurch study area with the location of the Heathcote River (Blue). Inset map shows the study location in relation to other geologic features in Christchurch.

3.4.2 Topography

The topography of the study area consists of flat to gently undulating point bars and floodplains modified by the consolidation of near-surface deposits subsequent to drainage and dewatering. The elevation generally increases in height to the west with the slopes of Banks Peninsula bounding the area to the south. Several point bar topographical elements are observed from the GIS data below (Fig. 3.7).

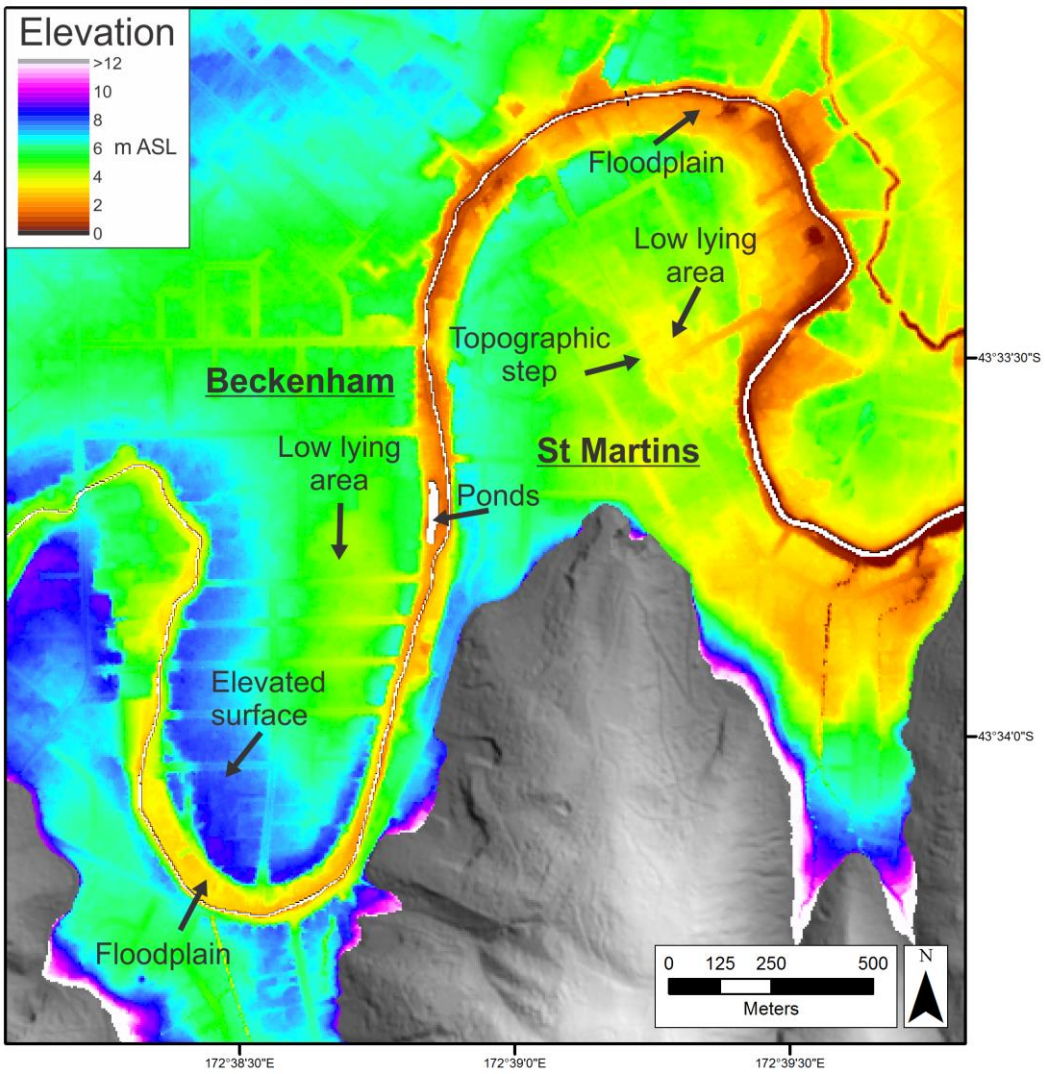

Figure 3.7: Digital elevation model from LiDAR data of the study area showing topographic changes across Beckenham and St Martins. The position of river terraces and low-lying point bar deposits are easily identifiable. Grey areas south of the study area denote the Port Hills of Banks Peninsula. (m ASL = meters above sea level).

The Beckenham point bar is ~550 m wide and ranges in elevation from ~5 to 8 m ASL extending southward to the base of the Port Hills. The point bar elevation increases in the southwest with an elevated surface ~100 m wide nearing the inner meander bend apex (Fig. 3.7). The elevated surface has a significant step (~5 m) down to the modern floodplain surface toward the current river channel. The step between the Beckenham elevated point bar surface and the modern floodplain is a terrace riser where the river that deposited the point bar sediments has subsequently incised forming the modern floodplain and the steep topographic drop. The low-lying floodplain area (10 to 60 m wide) above the banks of the current river channel contains the Beckenham ponds (Fig. 3.7). The eastern and northern

portion of the central Beckenham point bar consists of a lower lying area ~250 m wide, approximately 3 m below the elevated surface to the southwest (Fig. 3.7).

In the adjacent suburb of St Martins, the point bar is ~700 m wide and ranges in elevation from ~3 to 7 m ASL (Fig. 3.7). The southernmost area, at the base of the Port Hills, has relatively flat relief. In the centre of the suburb a curving low-lying area steps down ~1 m. The other side of the depression rises slightly and extends with low relief to the northwest before a steeper drop (~4 m) between the elevated central bar surface and the modern floodplain (Fig. 3.7). Again, the step between the St Martins point bar surface and the modern floodplain is a terrace riser as the river that deposited the point bar sediments has subsequently cut down forming the modern floodplain. The topographic depressions that coincide with two clear meander 'scars' are identifiable across the surface of St Martins in Figure 3.7. The distinctive scars shown in the hillshade image however are notably absent across the surface of Beckenham in the adjacent meander loop (Fig. 3.8). Ridge and swale topography which form meander scrolls indicative of channel migration is also absent across the study area. Other features identified are the location of steep terrace risers, minor streams, and the steep banks of the Port Hills closest to the active channel in southwest St Martins (Fig. 3.8).

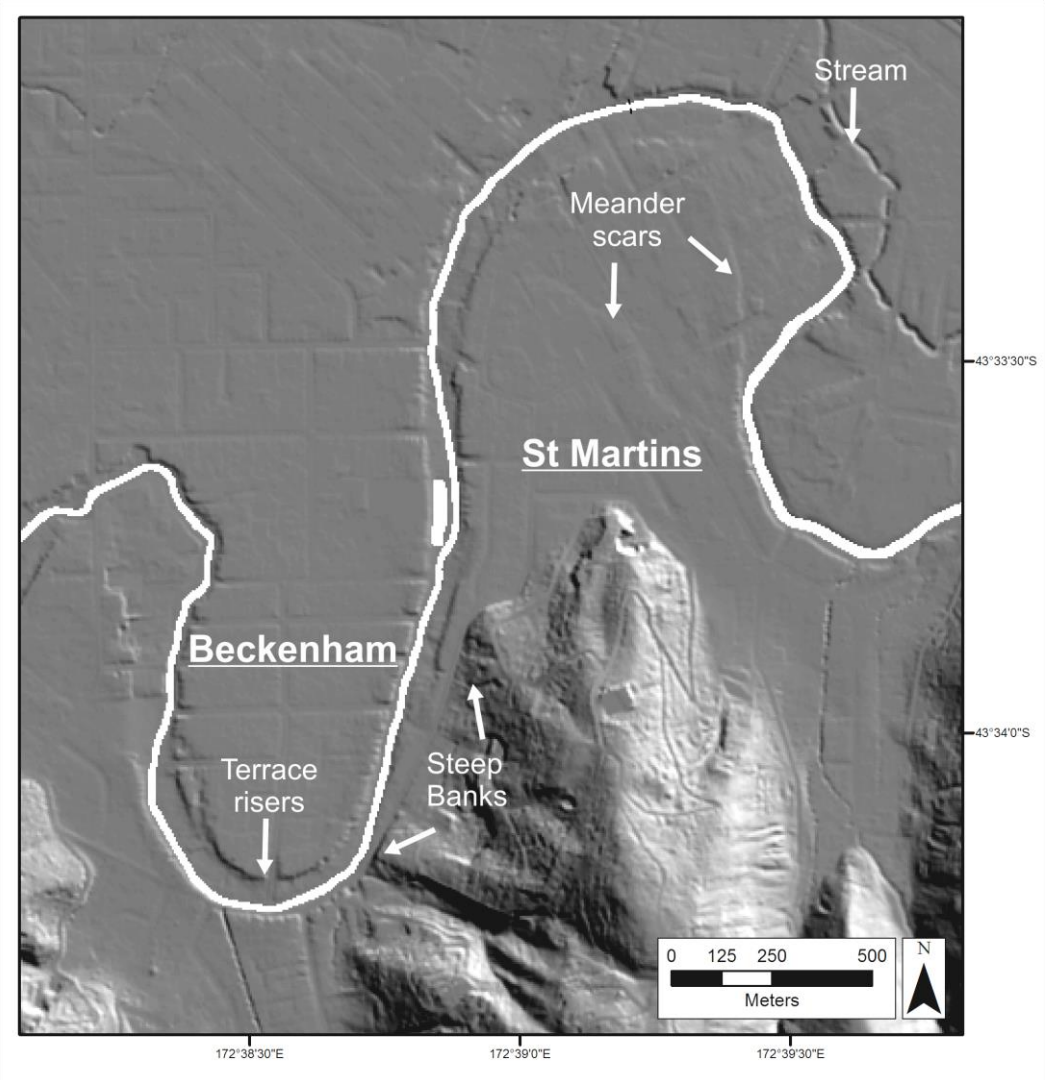

Figure 3.8: Hillshade image generated using ArcGIS from LiDAR data. Major topographic features across study area are highlighted by a prescribed light source angle.

Small-scale topographic variations reflect the inherent complexity of the meandering river system, as revealed in the LiDAR data (Fig. 3.7; 3.8). The subtle topographic changes within the channel belt show the elevated point bar in Beckenham at the bend apex standing slightly higher than the adjacent low area of the point bar to the north east. Prior to European drainage works, the lowest-lying areas had near-permanent standing water (Black Maps, 1856). The material in the lower lying area across the study area is therefore likely to contain considerable clayey and organic material across the point bar surfaces.

3.4.3 Ground water elevations

The depth to ground water shows the water table is closest to the surface adjacent to the active channel, and within the interior of both suburbs (Fig. 3.9). Water table depths of less

than 1 m occur across St Martins within the zones of lowest elevation (Fig. 3.7). Similarly, the region where the water table is closest to the surface in Beckenham is the low-lying centre and eastern portion of the point bar. Greater depths to the water table at the edges of both suburbs may reflect higher topography corresponding with levee deposits (Fig. 3.9).

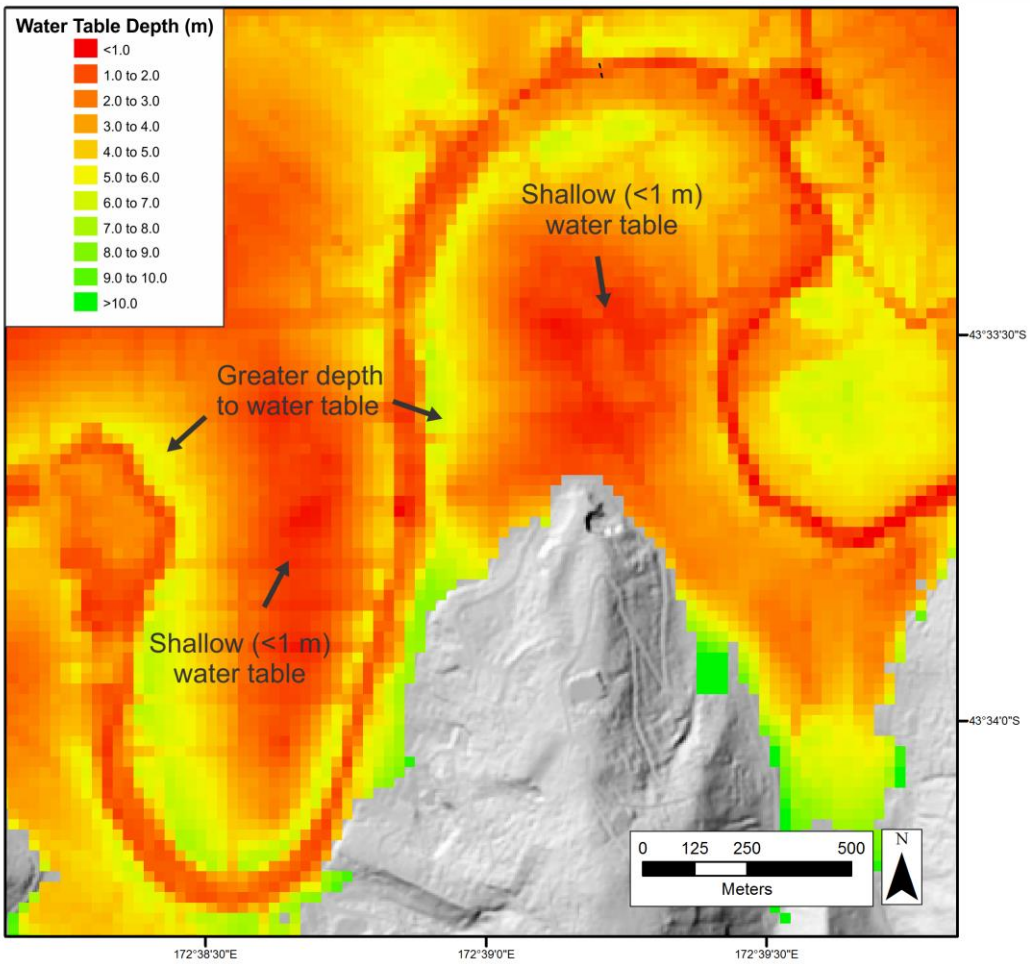

Figure 3.9: Groundwater elevations based on Tonkin & Taylor (2013) measurements from February 2011. Surface models are colour banded using ArcGIS and LiDAR data to show the water table depth below the surface.

The emergence of localised springs following the CES events immediately adjacent to the Port Hills, possibly caused by increased permeability and the development of new fracture-pathways through the Miocene volcanic rock, likely produced a general rise in ground water levels in the areas adjacent to the Port Hills through the CES (Cox et al., 2012).

3.5 CES SURFACE OBSERVATIONS AND GROUND DEFORMATION OF THE STUDY AREA

Four new figures of the study area are presented below, displaying the liquefaction distributions, subsidence patterns and geomorphology. The figures offer new information regarding the spatial variability of liquefaction features and subsidence experienced in southern Christchurch during the CES.

3.5.1 Initial observations following the major CES events

Following the 4th September 2010 M_w 7.1 earthquake, investigations were conducted along the Heathcote River (i.e. Cubrinovski and Green, 2010) specifically targeting areas indicated as being highly susceptible to liquefaction. However, field observations showed little evidence of ground deformation and liquefaction with only minor localised sand boils observed (Cubrinovski and Green, 2010). The small liquefaction manifestations in the study area were generally confined to localised low elevation sites across St Martins (Jacka and Murahidy, 2011).

Following the 22 February 2011M_w 6.2 Christchurch earthquake, significant surface liquefaction and ground deformations in flat areas with high ground water tables were observed in St Martins (Orense et al., 2011). The large distributions of moderate to severe ground deformation damaged a number of residential properties. The St Martins Library partially collapsed as a result of severe differential subsidence of the foundation due to liquefaction (Fig. 3.10). Significant liquefaction also occurred in St Martins following the June and December events.

Figure: 3.10: Damage to the St Martins library following the 22 February earthquakes from intensive shaking and liquefaction-induced ground deformation causing damage to the foundation. Note the tilted power pole due to loss of soil strength in the near-subsurface. From Orense et al, (2011).

3.5.2 Spatial distribution of surface liquefaction features

Aerial photography following each significant CES event is combined with field observations (Cubrinovski and Green, 2010; Orense et al., 2011; Canterbury Geotechnical Database, 2012) of St Martins and Beckenham to produce a new map of the magnitude and extent of surface liquefaction features. The liquefaction features including sand boils and surface cracks were compiled using GIS and overlaid onto a DEM of the study area for interpretation (Fig. 3.11).

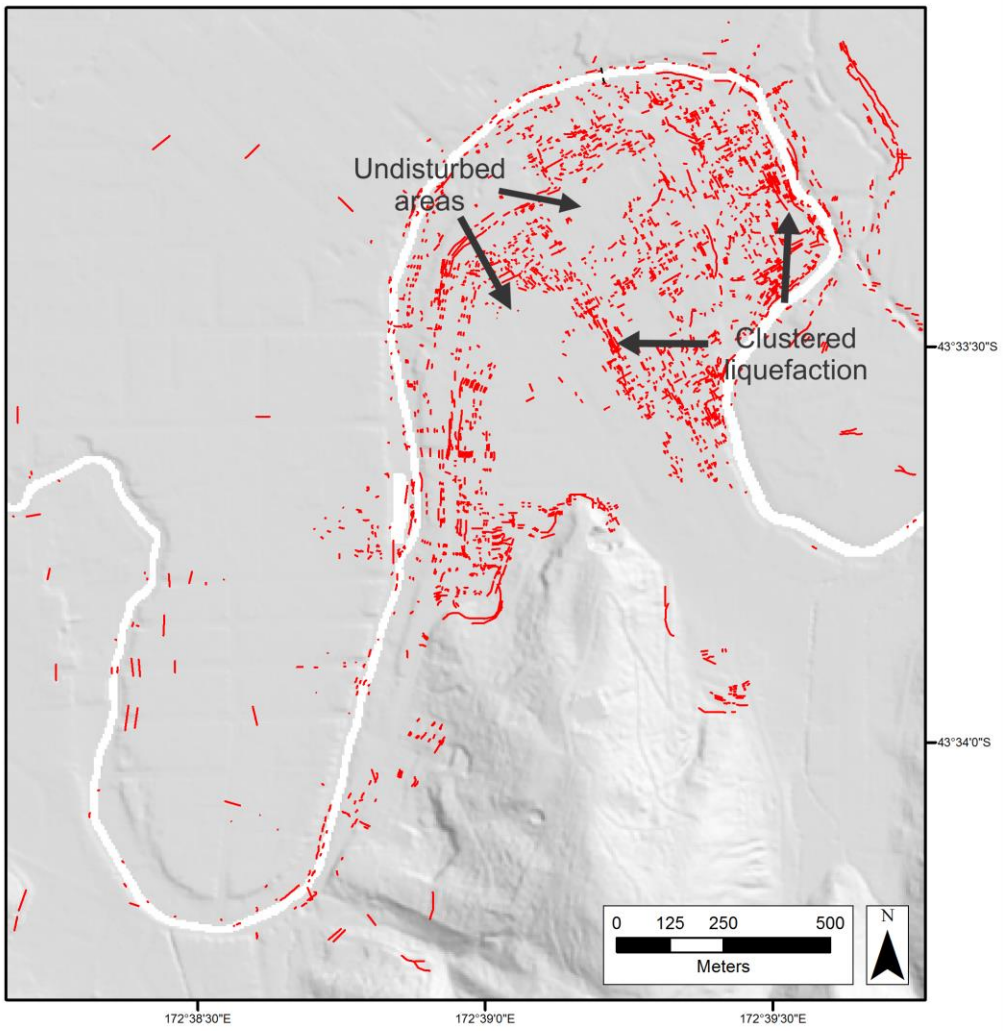

Figure: 3.11: New map of the distributions of surface liquefaction features (red lines) from 4 September 2010, 22 February 2011, 13 June 2011 and 22 December 2011 earthquakes.

A visual comparison between observed liquefaction areas indicates the majority occurred in St Martins (Fig. 3.11). The liquefaction features in St Martins occur both in close proximity to the river and within the interior of the suburb, and are typically elongated parallel to the modern river channel. The most extensive distributions are focused in the central and eastern areas of the suburb, especially in the areas at low elevation (Fig. 3.7) and where the water table is shallowest (Fig. 3.9). Extensive liquefaction also coincides with the location of the meander 'scars' across the suburb (Fig. 3.8). Areas with extensive clusters of liquefaction features are separated by isolated zones (50 to 100 m wide) that were relatively undisturbed throughout the CES (Fig. 3.11). The features mapped on the Port Hills indicate areas of slumping. Surface liquefaction features are generally absent in Beckenham, with only isolated ground cracks and sand boils generally occurring in areas closest to the river channel.

3.5.3 Liquefaction-induced ground deformation

The 22 February 2011 M_w 6.2 Christchurch earthquake caused tectonic surface deformation and vertical elevation changes causing uplift (~0.45 m) to south eastern Christchurch around the Avon-Heathcote Estuary in the hanging wall of the blind reverse-oblique faults (Fig. 3.12) (Beavan et al., 2012; Hughes et al., 2015). The lower reaches of the Heathcote River are located in the region of tectonic uplift while subsidence in the upper river reaches has reduced the river gradient making the waterway more prone to flooding. LiDAR differencing shows the total vertical ground movement in Christchurch through the entire CES showing the distinctive tectonic uplift around the Avon-Heathcote Estuary (Fig. 3.12). Extensive subsidence (>0.5 m) in the suburbs adjacent to the Avon River in eastern Christchurch is also observed.

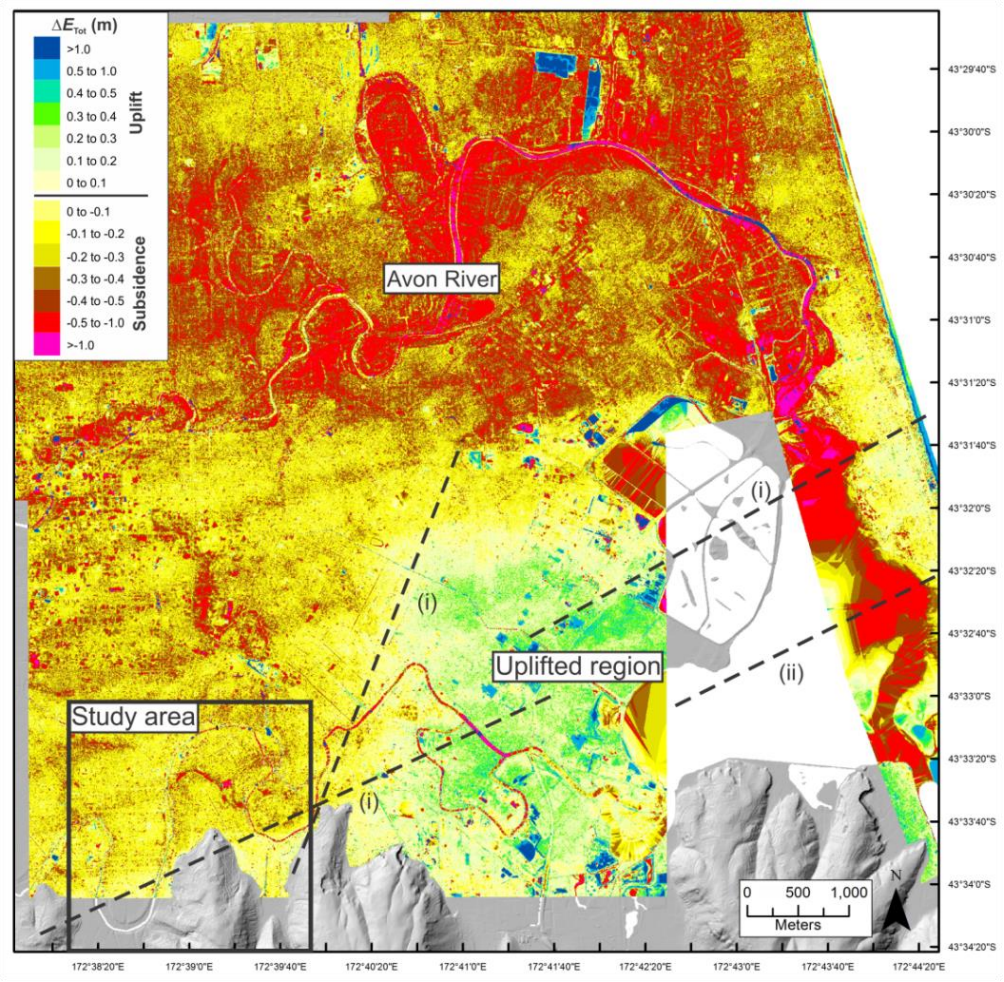

Figure 3.12: Differential LiDAR model of Christchurch illustrating the total vertical ground movement through the entire CES. Blind fault locations (dashed lines) for 22 February 2011 (i) and 13 June 2011 (ii) events (Beavan et al., 2012), and the outline of the study area are shown.

Differential LiDAR models generated using ArcGIS are used to show the liquefaction-induced elevation changes of the study area throughout the CES. For the purposes of this study, vertical tectonic ground movements (ΔE_{Tec}) are subtracted from the total elevation changes (ΔE_{Tot}) (Fig. 3.12) to produce a new model of the elevation changes due to liquefaction (ΔE_{Liq}) across the study area (Fig. 3.13).

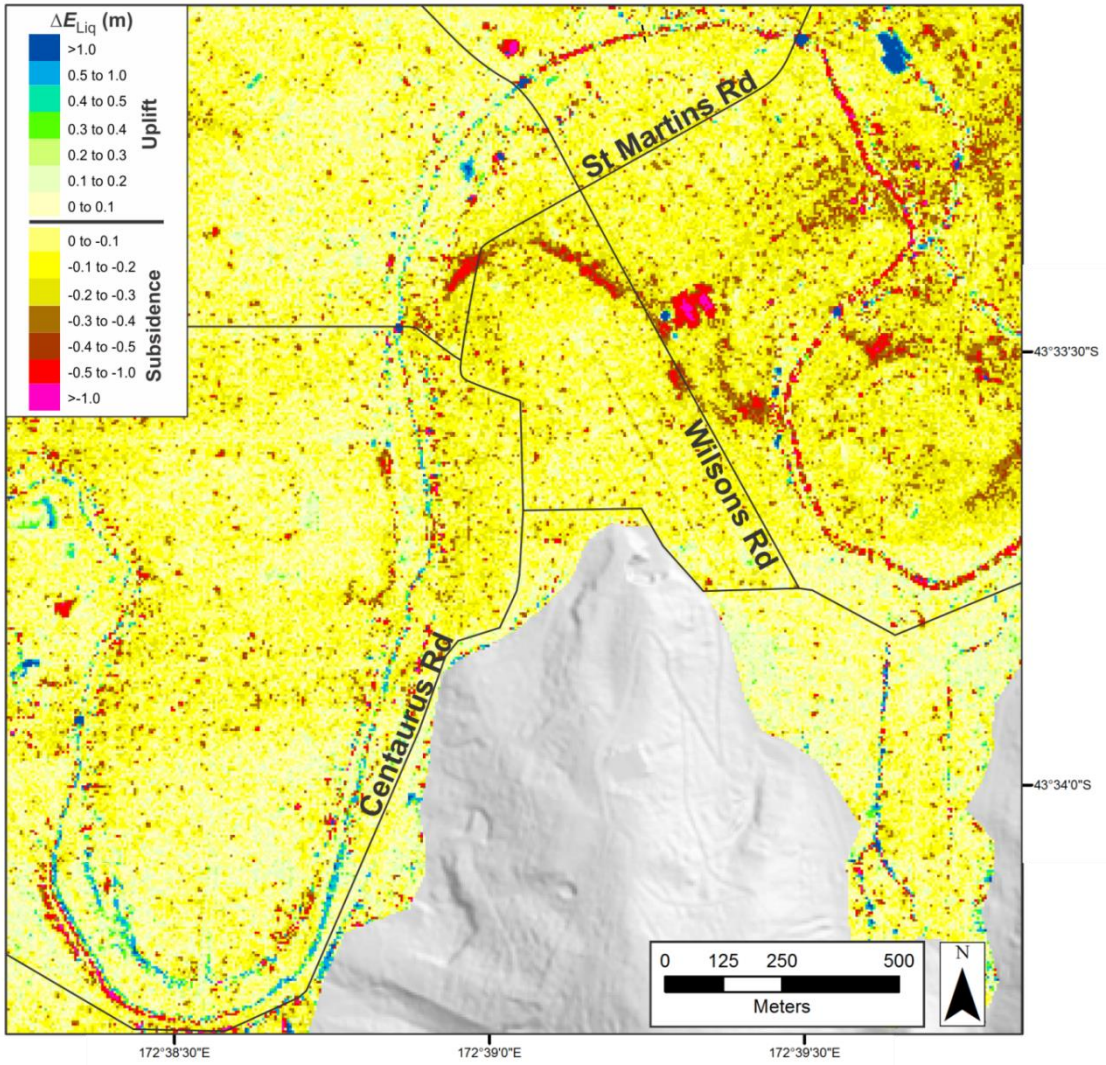

Figure 3.13: New differential LiDAR model illustrating liquefaction-induced surface elevation changes (ΔE_{Liq}) from pre-September 2010 to post-December 2011.

The LiDAR differencing reveals pockets (<1 m^2) of moderate (≥0.3 m) subsidence across St Martins indicating the vertical movement from liquefaction-induced ground deformation (Fig. 3.13). LiDAR differencing also displays localised areas (~0.5 to 1 km^2) in central St Martins where combined vertical movements exceeded 0.5 m signifying areas that experienced the most severe ground deformations (Fig. 3.13). The area of >1 m subsidence in

central St Martins records the removal of the shopping centre on Wilsons Road (Fig. 3.13). Extensive (>0.5 m) surface deformations are absent across Beckenham with smaller localised zones exceeding only ~0.3 m. Various zones of uplift observed across the study area may reflect the horizontal translation of the steep topography and upward-bulging of the river bed (Fig. 3.13).

A histogram was produced from the LiDAR data comparing the amount of surface elevation changes across the surface of the two suburbs from pre-September 2010 to post-December 2011 (Fig. 3.14). The histogram shows Beckenham experienced < 5 % subsidence >0.3 m with the majority of the area subject to ~0.1 m vertical movement (within the error of LiDAR data collection method). St Martins shows ~10 % of the suburb suffered subsidence >0.3 m with ~2 % of the total subsidence >0.5 m. The histogram shows St Martins suffered approximately twice the amount of subsidence greater than 0.2 m compared to Beckenham.

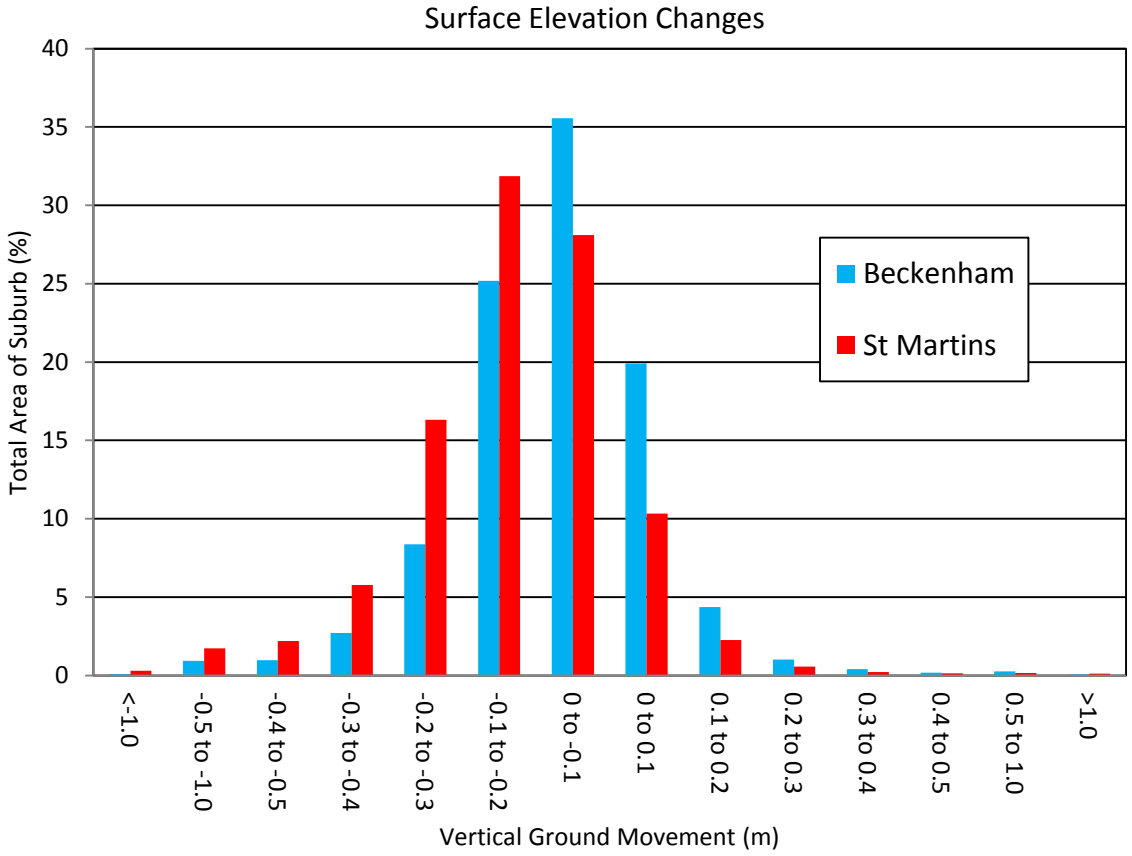

Figure 3.14: Elevation histogram of the study area showing the total area of surface elevation changes in Beckenham and St Martins from pre-September 2010 to post-December 2011.

The severe liquefaction-induced ground deformation (>0.5 m) of central St Martins, identified in the LiDAR data, corresponds with the locations of the previously identified topographic lows (Fig. 3.7), the meander scars (Fig. 3.8), the shallowest water tables (Fig. 3.9), and the distribution of clustered liquefaction features (Fig. 3.11). Despite the occurrence of severe liquefaction, and proximity of the suburbs to the free face of a river channel, extensive lateral spreading was not observed across the study area following the major CES events and no residential properties within the study area were deemed unfit for occupancy by CERA.

3.6 DISCUSSION

3.6.1 Geomorphology and meander migration

The compilation of post-CES surface liquefaction features (Fig. 3.11) and LiDAR differencing (Fig. 3.13) identifies where the majority of surface ejecta and liquefaction-induced settlement was focused across the study area. These data, combined with elevation and surface topography models (Fig. 3.7; 3.8), shows the central point bar surface of St Martins has undergone lateral expansion and downstream translation. The topographic low in central St Martins is interpreted to represent a paleochannel denoting the previous course of the Heathcote River, displaying similar fluvial architecture to the modern meander loop geometry. The identification of a paleochannel suggests the Heathcote River has undergone recent (Holocene) migration at St Martins, promoting the formation of young alluvial deposits. This geomorphology displays typical phases of a channel bend expanding and rotating northeast, shown by the two meander scars (Fig. 3.8), toward the modern river channel. Localised channel adjustments have therefore formed the topographic steps across the point bar surface of St Martins and the distinctive low-lying area representing a paleochannel. Based on the topography, liquefaction and subsidence patterns, I have created a new geomorphic map of the study area displaying the location of the paleochannel and major geomorphic features (Fig. 3.15).

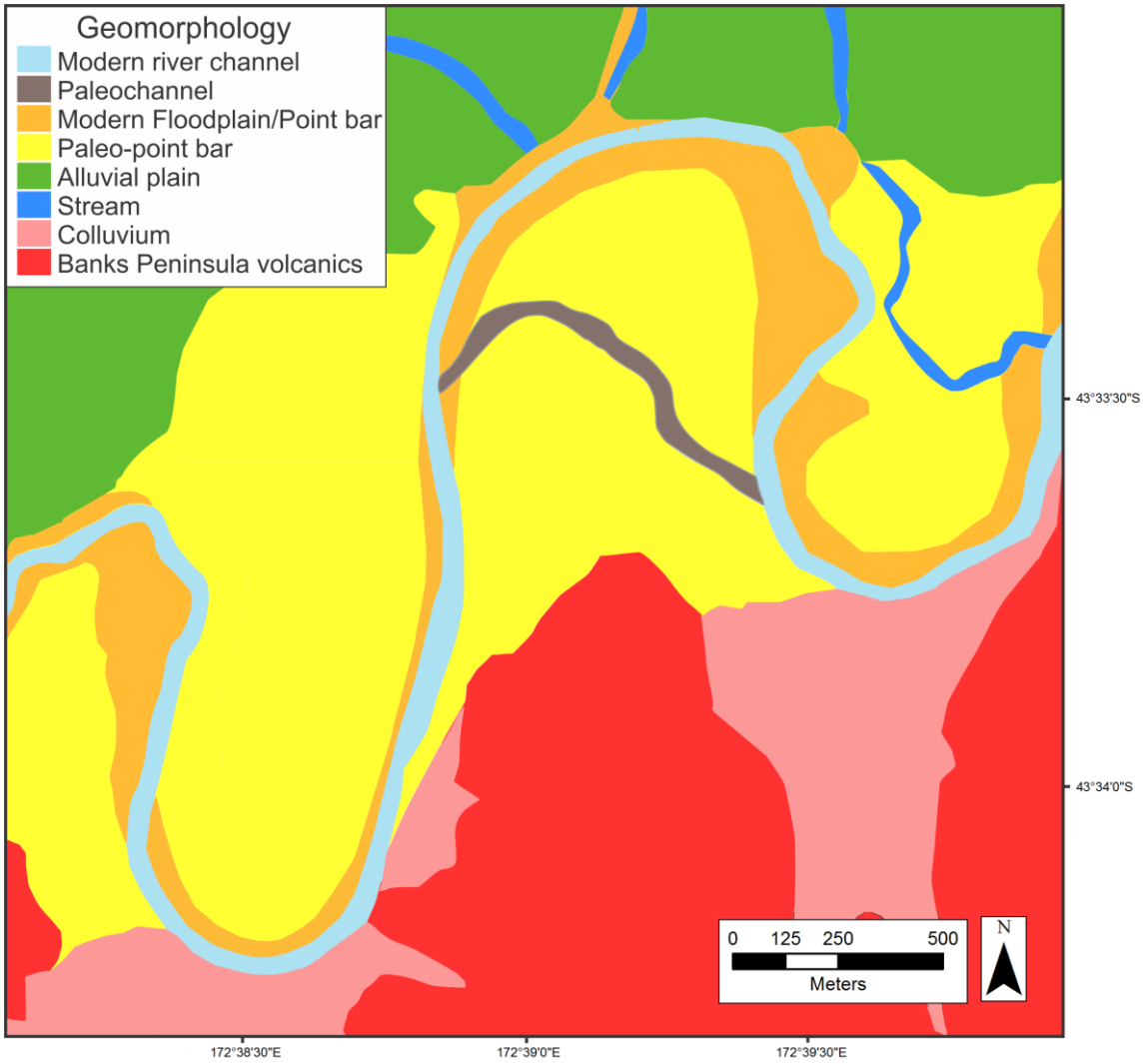

Figure 3.15: New geomorphic map of the study area based on LiDAR data and post-CES surface observations including the location of the paleochannel within the interior of St Martins.

Local residents recall the inner bank of the paleochannel being much steeper preceding modification and the building of Cresselly Place prior to the 1960s, and during flooding events the low-lying channel would consistently flood (P. Greening, pers comm, 2015). A historic photo taken from Murray Aynsley Hill in 1890 overlooking St Martins shows the Heathcote River during flood conditions (Fig. 3.16). Surface water can be seen in the location of the paleochannel (arrow on photo) indicating the lowest topography of the point bar surface (Fig. 3.16).

Figure 3.16: Historic photograph of St Martins looking northwest from Murray Aynsley Hill in 1890 overlooking the Centaurus Road - Wilsons Road intersection and Christchurch City in the distance. The Heathcote River can be seen overflowing its banks in the foreground. Surface water is visible across the area coinciding with the location of the paleochannel as marked by the arrow, with the heavily vegetated Heathcote River banks in the background. From Ogilvie, (1991).

The distribution of liquefaction features (Fig. 3.11) and ground deformation patterns (Fig. 3.13) in Beckenham suggest the point bar contains material more resistant to liquefaction, and has not evolved similarly to St Martins. The expansion of the southward meander loop in Beckenham has likely been constrained by the Miocene volcanics of Banks Peninsula, inhibiting channel migration. Lateral confinement has limited the sinuosity of the meander bend and therefore the ability of the river to develop a paleochannel. Initially the Beckenham point bar would have migrated toward the south. However, channel expansion was abruptly interrupted when the bend apex reached the erosion resistant valley flank of Banks Peninsula. The onset of downstream accretion was further limited by Huntsbury Hill confining the downstream translation of the river reach adjacent to Centaurus Road (Fig. 3.15). The notable steep valley walls adjacent to the eastern limb of the Beckenham may represent erosion from the confined channel (Fig. 3.8).

Channel confinement would have facilitated the overbank flow of floodwater before incision in order to maintain the river's hydraulic efficiency (Ghinassi et al., 2013). Sediment entrained within floodwater would have surmounted the elevated point bar surface promoting the accumulation of stratigraphy containing predominantly finer sediment. The lower lying area in eastern Beckenham contains considerable clay material from standing water. Channel evolution in Beckenham would have preserved successions of finer material resistant to liquefaction. The sandy channel bedforms contained within the Beckenham point bar are therefore inherently older and are capped by thicker flood deposits as the valley margins have limited the capacity for lateral channel adjustments. The silty stratigraphy on the elevated surface and at depth will pass progressively to finer clayey materials in the low-lying area that once contained standing water (Fig. 3.7).

The planview evolution of the study area is therefore strongly controlled by the surrounding morphological constraints (Fig. 3.15). This differing sensitivity to meander migration between St Martins and Beckenham is related to varying influences of bend morphology and material properties which are discussed in more detail in Chapter 4.

3.6.2 Liquefaction distribution and facies control

Liquefaction distributions observed across the study area show distinct differences between the two suburbs (Fig. 3.11). The distribution of liquefied sand bodies in St Martins are believed to be predominantly sourced from sandy point bar deposits preserved within the point bar succession. The variability of surface liquefaction features between largely undisturbed areas indicates the presence of heterolithic bedforms, deposited as the Heathcote River channel migrated (Fig. 3.4). Thicker sand deposits would have supplied the extensive surface manifestations of ejecta while the undisturbed areas are possibly underlain by thinner sandy units, or have been buried by thicker overbank and back swamp deposits in response to bend expansion and downstream translation.

Clustered liquefaction features (Fig. 3.11) in the low-lying area in central St Martins provide further evidence for the presence of the paleochannel. The preserved sandy deposits at low elevations likely enabled the deformation of preserved channel sediments promoting the ejection of large quantities of material. The observed liquefaction distributions correspond well with Brown and Weebers (1992) liquefaction susceptibility map indicating the central St Martins area would be most prone to liquefaction as it lies in a zone consisting of silt

underlain by sand and/or peat with no gravels and a high water table (Fig. 1.8). Investigations by Wotherspoon et al. (2012) revealed similar liquefaction distributions in Kaiapoi north of Christchurch where the most persistent and severe sand boils developed in areas consisting of old river channels (Fig. 1.16).

The inability of Beckenham to expand likely formed a thicker stratigraphy, given the higher elevation of the point bar, consisting of predominantly finer material overlying the channel deposits. Liquefaction within the soil profile may have possibly occurred at depth, however, the surface manifestations of liquefied sand appear to have been inhibited within the Beckenham stratum. The absence of severe liquefaction in Beckenham also corresponds well with Brown and Weebers (1992) liquefaction susceptibility map which indicates the Beckenham point bar would be less prone to liquefaction as it lies in a zone consisting of silt underlain by <10 m thick gravel, loess and loess colluvium overlying volcanic rock (Fig. 1.8)

3.6.3 Subsidence distribution and facies control

The most severe subsidence in St Martins, exceeding 0.5 m, resulted from deformation concentrated at the location of the low-lying paleochannel containing highly susceptible channel sands. In other areas, lesser amounts of subsidence (0 to 0.5 m) reflect the deformation of deposits at variable depths reflecting the former thalweg topography of the channel.

A representative dataset of liquefaction-induced ground movements was formed to identify subsidence patterns at various distances from the modern river channel by creating transects across the point bars at the study area (Fig. 3.17). A transect across the suburb of Avondale, adjacent to the Avon River in eastern Christchurch, was also included for comparison. Within each grid a ground movement value was assigned to reflect the mean of each individual 5 m DEM point from the CES elevation differentials from pre-September 2010 to post-December 2011 (Fig. 3.16).

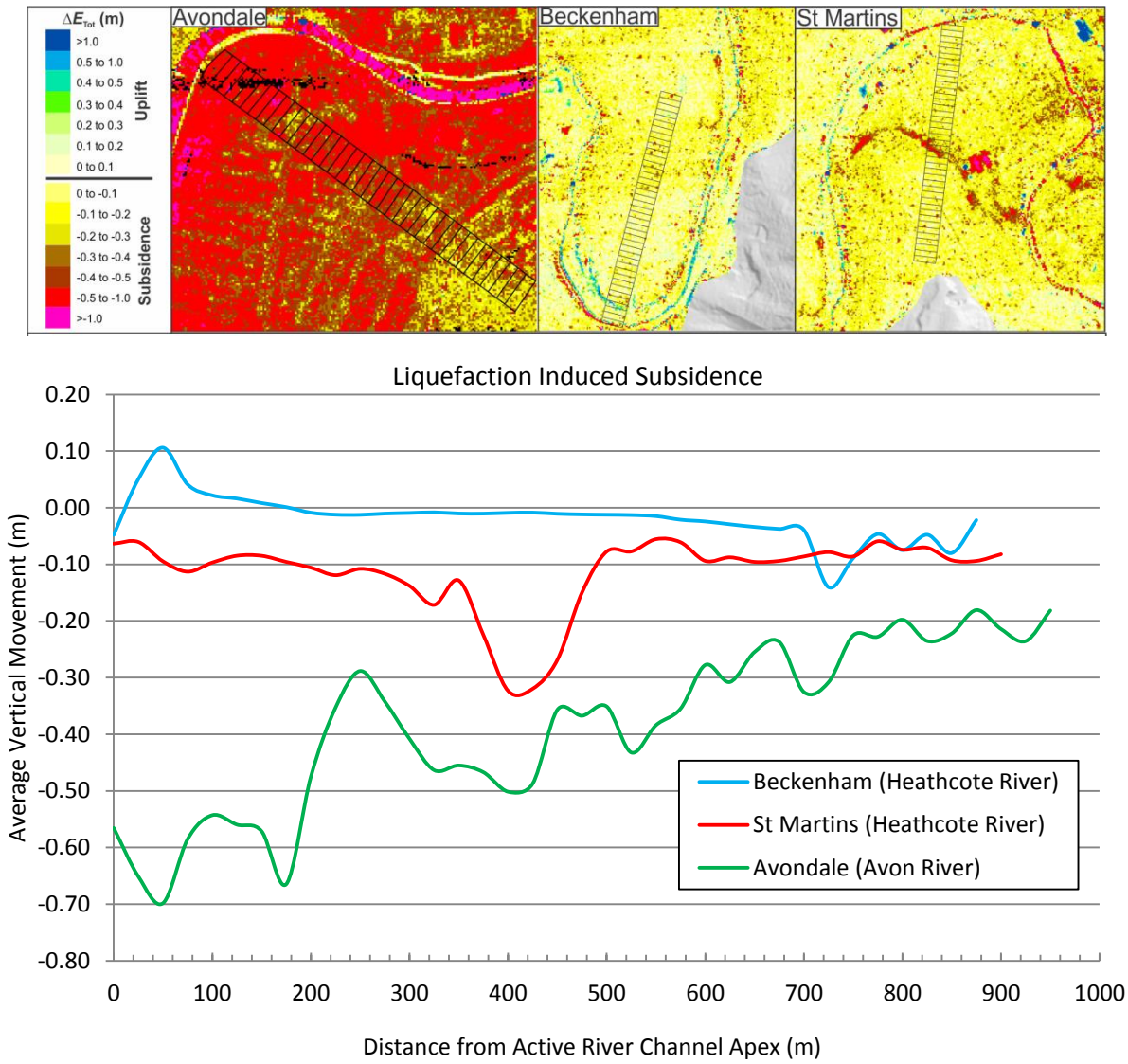

Figure 3.17: Transect locations and CES liquefaction-induced subsidence plots from pre-September 2010 to post-December 2011 for St Martins, Beckenham and Avondale.

The plot shows small amounts of uplift (~0.1 m) occurred closest to the channel in Beckenham, possibly as a result of horizontal translation of the steep topography toward the river (Fig. 3.17). From ~100 m distance, subsidence is clearly absent with only minor subsidence (~0.1 m) occurring at ~700 m from the channel bend apex. In St Martins, relatively small amounts of subsidence occurred closest to the river channel (Fig. 3.17) with the maximum amount of subsidence focused ~380 m from the free face of the modern river channel, corresponding with the location of the paleochannel. The amount of settlement remains constant toward the back of the point bar. This indicates the most severe liquefaction-induced damage occurred away from the free-face during the CES, and the point bar elevation exerted a weak control on the severity of vertical subsidence in St Martins.

The maximum amount of subsidence in Avondale occurred closest to the river channel (~0.7 m) (Fig. 3.17) with ground displacement gradually reducing with greater distance from the Avon River. Here, subsidence appears to be driven predominantly by free face effects, with little effect from inland topography. Conversely, subsidence distributions across the study area in southern Christchurch show no clear pattern, suggesting the ground deformation adjacent to the Heathcote River is not directly affected by the distance to the free face of the river channel.

Historical accounts following the 1869 M_w 4.7-4.9 Christchurch earthquake (Downes and Yetton, 2012) may suggest the suburbs adjacent to the Heathcote River have experienced liquefaction-induced ground deformations previously. The 1869 event generated MMI 7 shaking in the Christchurch CBD causing damage to unreinforced masonry (Quigley et al., in review). While no surface ejecta was observed, it was reported by the Weekly News (26 June, 1869) that '[after the earthquake] *the tide runs higher up the Heathcote River than formerly'* (Downes and Yetton, 2012) indicating this earthquake may have caused subsidence of the study area, consistent with CES observations.

As a result of the subsidence plots, the variables which influenced the distribution and severity of subsidence adjacent to the Heathcote River appear to be more relevant to the location of geomorphic features (paleochannel), and were not directly affected by the distance to the free face of the river channel, unlike the suburb of Avondale. Other effects influencing the distribution of liquefaction-induced subsidence, including geotechnical properties (sediment density), and earthquake characteristics (PGA, M_w, distance from seismic source) are investigated in more detail in Chapter 4.

3.6.4 Lateral spreading distribution and facies control

Both St Martins and Beckenham had minimal to no lateral spreading during the CES with only small amounts of spreading (0 to 0.5 m) closest to the river channel (Fig. 3.18A). The horizontal movement vectors in St Martins are directed toward the east, away from the channel bend apex. Similarly, the vectors in Beckenham are directed toward the east, and not toward the modern channel bend apex of the river. In Avonside, the maximum amount of lateral spreading (> 1 m) occurred closest to the river channel with ground movement mainly directed toward the channel bend apex (Fig. 3.18B).

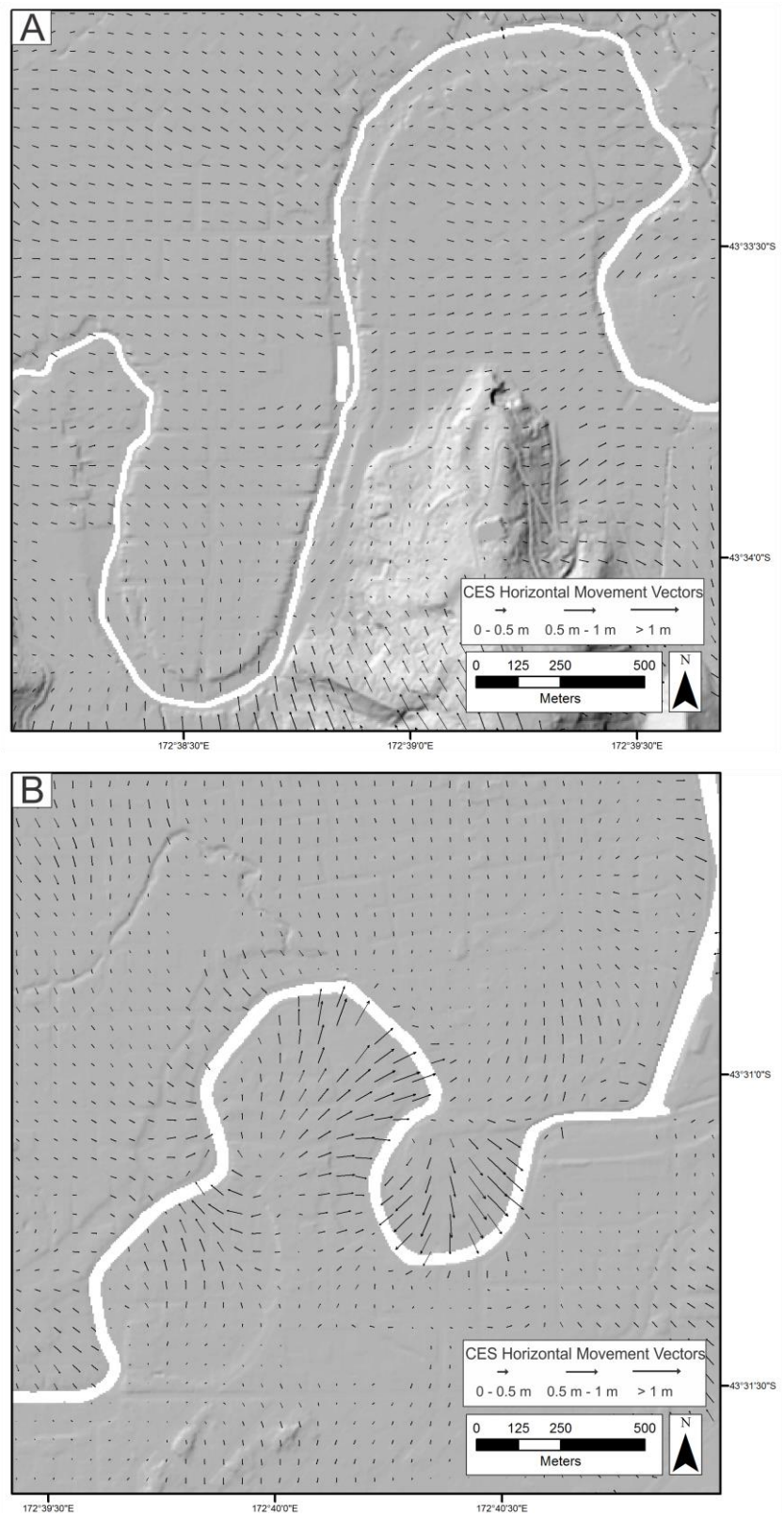

Figure 3.18: Horizontal movement vectors scaled for displacement recording cumulative liquefaction related movements along the Heathcote River (A) and the Avon River (B). Movement vectors from Beavan et al. (2012).

The horizontal movement vectors across the study area suggest lateral spreading adjacent to the Heathcote River is not directly affected by the distance to the free face of the river channel. The vectors in St Martins reveal that the majority of the displacement was directed toward the low-lying eastern area, and the lateral spreading direction of a point bar is not always directed towards the most proximal reach of the modern river channel, unlike Avonside. Similarly, the displacement vectors in central Beckenham are directed eastward indicating the lateral movement of the higher elevated surface toward the lower lying area (Fig. 3.18A). The lateral ground movements appear to be predominantly driven by inland topography, with the effects of free face proximity less apparent when compared to Avonside (Fig. 3.18B).

3.7 SUMMARY

Topographic variations and liquefaction distributions suggest St Martins has undergone recent lateral migration. The majority of liquefaction surface ejecta and liquefaction-induced settlement across the study area was focused at the interior of St Martins reflecting the location of a low-lying paleochannel, a previous course of the Heathcote River. The extensive liquefaction and subsidence indicates the presence of highly susceptible sandy channel deposits, from the migrating meander, separated by undisturbed areas possibly underlain by smaller sand bodies or overlain by thicker overbank or back swamp deposits inhibiting surface liquefaction. Lateral confinement of the Beckenham meander loop by Banks Peninsula has controlled the distribution of CES liquefaction. Limited bend expansion and downstream migration likely enabled the accumulation and preservation of fine grained deposits across the point bar more resistant to liquefaction.

Unique distributions of liquefaction reflect the heterogeneous nature of the study area soils and the influence topographical features have on the displacement patterns and extent of liquefaction. The changes in morphology has shown that meandering rivers exhibit dynamic influences on the sedimentary characteristics of point bar deposits through migration, illustrated by the unique distribution of liquefaction features observed across the study area during the CES. The distribution of heterogeneous material with variable resistances to liquefaction, related to a combination of bend morphology and material properties, is explored in more detail on the following chapter.

CHAPTER 4 SUBSURFACE INVESTIGATIONS

4.1 INTRODUCTION

Chapter 4 presents the findings from subsurface investigations and examines the results from sediment analysis of collected samples. Analyses of the point bar deposits allow the identification of the material properties that effected liquefaction distributions, and the examination and interpretation of the stratigraphy, structural characteristics and formation processes of fluvial sequences. Detailed field investigations are combined with geotechnical data (CPT) to produce plots of the subsurface material properties to identify the liquefiable source sediments. By interpreting the sediment sequences preserved in the point bars, the evolutionary stages resulting from channel adjustments and depositional events can be considered. Spatial relationships between sediment stratigraphy and liquefaction features provide a basis for interpreting liquefaction susceptibility at a given site.

4.2 SUBSURFACE INVESTIGATIONS IN ST MARTINS

Two sites in St Martins were chosen for trenching to document the morphology of CES liquefaction features and subsurface fluvial strata, to investigate the spatial relationships between liquefaction severity and material properties in relation to the location of geomorphic features (i.e. current river channel, paleochannel) (Fig. 4.1). St Martins Park (Site 1) was selected based on the identification of CES surface liquefaction from aerial photographs, the preservation of sand boils in the park (four years after ejection), and the lack of near-surface anthropogenic influence on the distribution of liquefaction (Fig. 4.1). The site was also selected as it is located ~100 m from the previously identified paleochannel. The former site of a residential property at 68a St Martins Road (Site 2) was selected because it was subjected to severe surface liquefaction and ground deformation (>0.5 m subsidence) during the CES. The site was also selected because it is located within the spatial extent of the paleochannel (Fig. 4.1). Comparing liquefaction features between the trenches allows the liquefaction triggering resistances of the sites to be determined, and the effects proximity to the paleochannel had on the deformation of fluvial stratigraphy.

Figure 4.1: Aerial photograph of central St Martins and the locations of Site 1 and 2 (Yellow outline), paleochannel outline from LiDAR and geomorphic mapping (red dashed lines), main roads and the Heathcote River (blue).

4.3 TRENCH SITE 1: ST MARTINS PARK

St Martins Park is located centrally within St Martins, approximately 250 m from the Heathcote River channel (Fig. 4.2). The park has flat topography with elevations of 6.2 - 6.5 m above sea level, ~4 m above the most proximal reach of the Heathcote River. Analysis of post-CES aerial photography indicates minor sand blows across the site following the 22 February 2011 M_w 6.2 and the M_w 6.0 13 June 2011 earthquakes. A 7 m long and ~1.6 m deep trench was excavated in the northern corner of the park, perpendicular to a recognisable bulge in the ground surface signifying the location of an identified sand boil from aerial photography. The trench was also orientated perpendicular to the maximum horizontal movement vectors identified across the park (Fig. 3.18). Deeper strata was sampled in the trench by two hand augers drilled to a depth of 3.5 m, and a 0.5 m deep pit was dug inside the northern end of the trench. The trench and auger logs are presented in Figure 4.3 and selected field photographs are presented in Figure 4.4.

Figure 4.2: Aerial photograph of the Site 1 taken on 24 February 2011 and the location of the trench (Red)

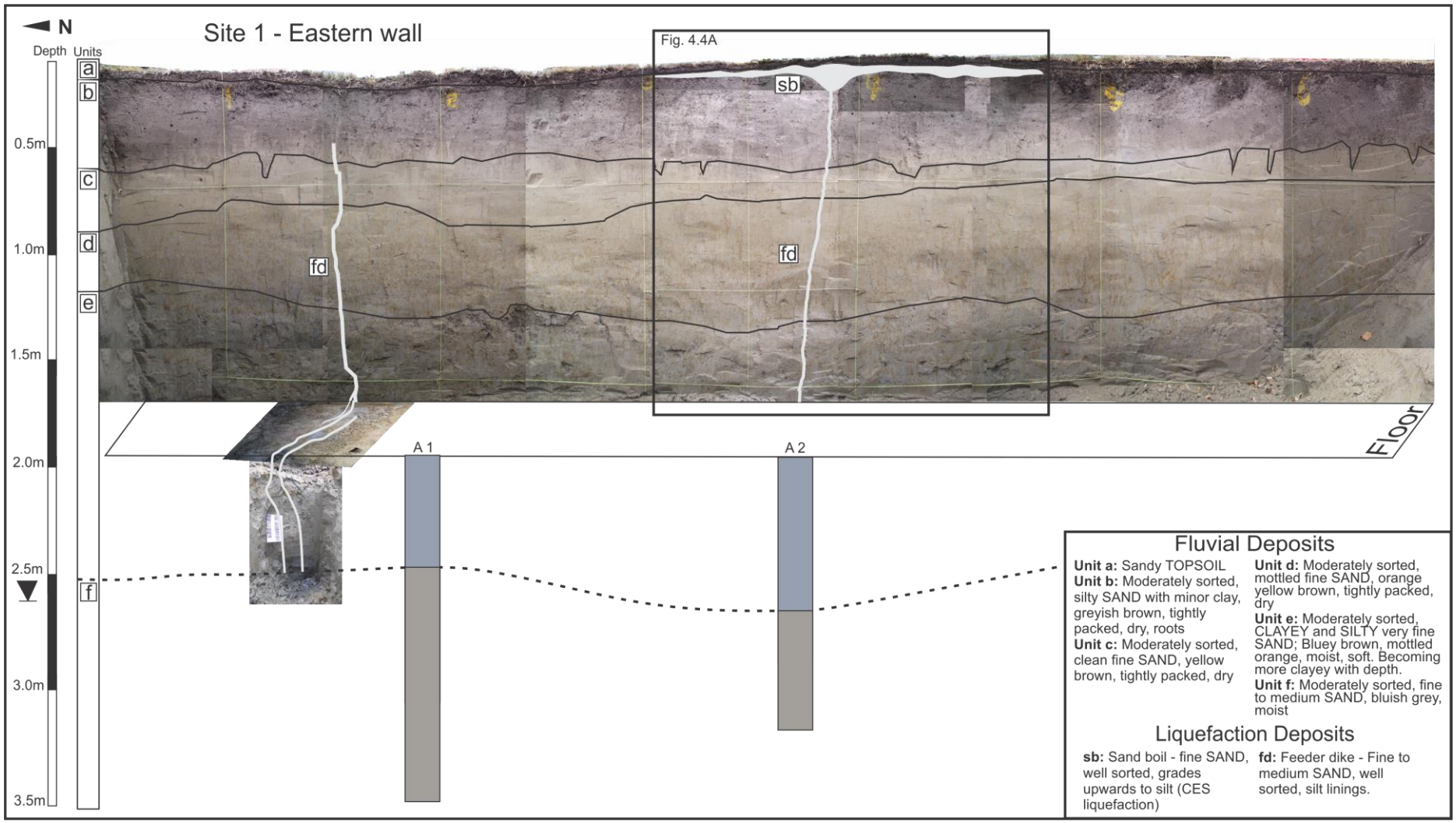

Figure 4.3: Detailed trench log and unit descriptions of the east wall and floor of Site 1. The CES liquefaction feeder dikes (fd) and sand boil (sb) shown in grey cross-cut the fluvial units (a–f) and stratigraphic contacts (black lines) and inferred contacts (dashed lines). Location of auger 1 and 2 (A1–A2) are also indicated.

4.3.1 Trench stratigraphy

The trench at Site 1 exposed stratigraphy composed of a silty very fine sand (Unit e) overlain by a mottled bed of fine sand (Unit d) that grades into a clean fine sand (Unit c) (Fig. 4.3). This unit has an undulating, heavily bioturbated, and gradational contact with an overlying silty sand bed (Unit b). The stratigraphy is capped by ~5–7 cm of topsoil (Unit a). Hand auger sampling (A1–A2) indicated that the silty very fine sand (Unit e) is underlain by fine to medium sand (Unit f) at ~2.5 m depth (Fig. 4.3). The boundary between Unit (e) and (f) was observed in the pit dug at the northern end of the trench (Fig. 4.3). There is a notable absence of interbedding, dipping beds and gravel deposits with most units easily identifiable by colour changes and bioturbation. No datable organic samples were recovered during trenching at Site 1 to yield ages of deposition.

The fine to medium sand bed (Unit f) is coarser than the overlying strata and is consistent with modern channel deposits of the Heathcote River. Unit (f) is therefore interpreted to represent a channel bed or lateral accretion deposit formed during pre-historic channel migration of the Heathcote River. The overlying clayey silt (Unit e) was likely deposited within standing water before overbank deposits accumulated forming upward grading to silty very fine sand. The overlying fine sand and silty sand beds of Units of (d), (c) and (b) are interpreted as further overbank flood deposits from the nearby Heathcote River. The fluvial stratigraphy shows that the channel location has been shifting, forming the changes in grain sizes correlating with channel and overbank deposits. The stratigraphy is consistent with pre-European land categories indicating the low-lying areas adjacent to the Heathcote River consisted of raupo swamp and marshes (Black Maps, 1856). Historical reports of periodic flooding indicate the Heathcote River has the ability to inundate suburbs adjacent to the river (Cowie, 1957).

4.3.2 Liquefaction features

The trench at Site 1 intersected a ~1.6 m wide sand boil that had been subsequently preserved below topsoil following the CES, forming the bulging surface topography and indicating the pre-CES ground surface (Fig. 4.4A). The sand boil contained well-sorted fine sand grading to very fine sand with >5 internal silt laminations and a maximum thickness of 5 cm, pinching out laterally (Fig. 4.4B).

The sand boil was fed by a 0.3–2 cm wide subvertical planar feeder dike that cross-cuts the fluvial stratigraphy to feed into the round sand boil (Fig. 4.4A). The dike, containing well-sorted fine sand, decreases in width and fines upward toward the surface. The dike aligns with a subvertical planar dike on the west wall that did not reach the surface, however the dike could not be traced across the trench floor.

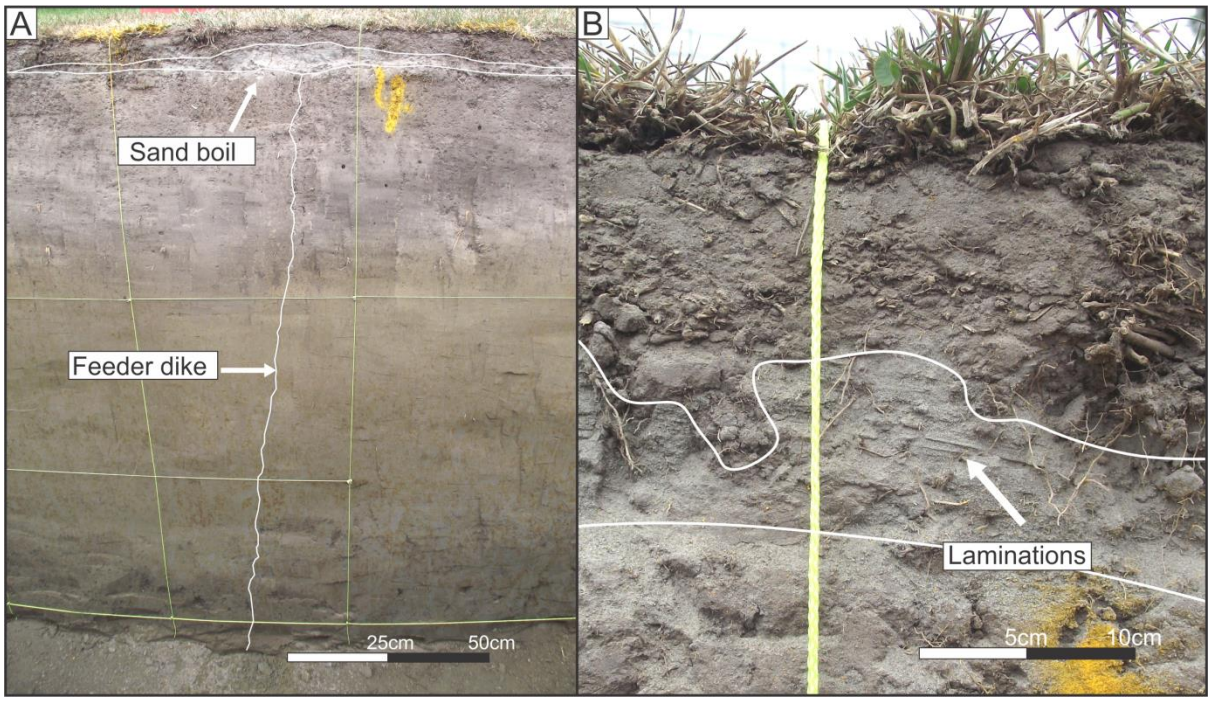

Figure 4.4: (A) Photograph of the east wall showing the subvertical planar dike and preserved sand boil below the surface bulge. (B) Sand boil deposit (white outline) containing down dropped topsoil clasts and subhorizontal silt laminations.

Another subvertical planar dike containing well-sorted fine sand occurs at the northern end of the trench (Fig. 4.5). It is < 1 cm wide and cross-cuts the stratigraphy from the trench floor to ~0.3 m depth where it pinches out. Silt linings ~1–2 mm thick mark the dike margins (Fig. 4.5). Within the trench floor the dike also contains two textures, where medium sand has been deposited next to finer sand (Fig. 4.5).

Four smaller dikes (<5 mm wide) observed in the trench originate from the trench floor on the west wall and terminate ~1 m below the surface. These smaller dikes are composed of fine sand. No evidence of pre-CES liquefaction was identified in the trench.

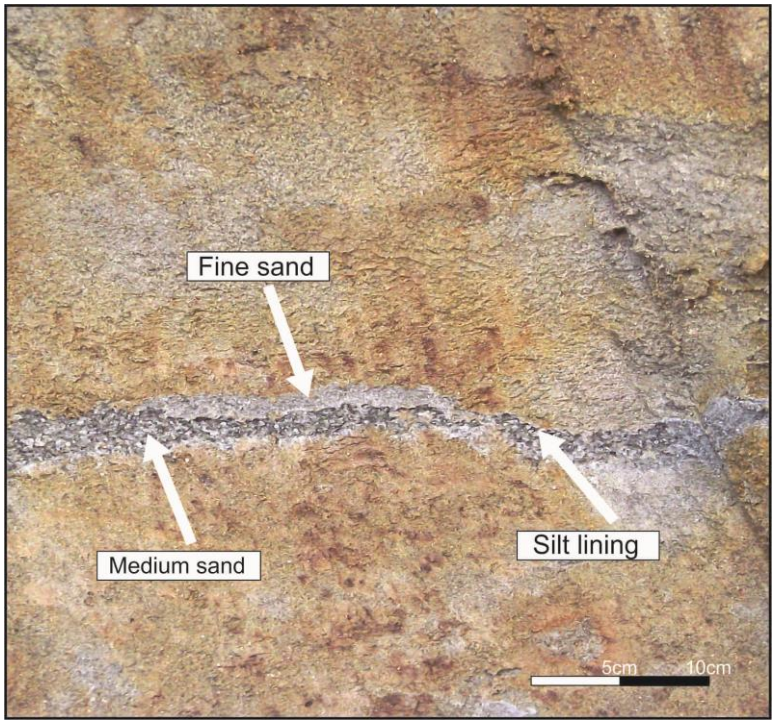

Figure 4.5: The thin dike within the trench floor containing both fine and medium sand.

The dike extending from the trench floor to the surface feeds the CES sand boil, confirming it formed during the Canterbury earthquake sequence. The dikes that cross-cut the fluvial stratigraphy from the trench floor to within ~0.3 m of the surface indicate that their formation post-dated deposition of the lower trench strata. The morphology, composition, and lack of mottling and oxidation of the dikes that pinch out beneath the surface indicate that they also formed during the CES (e.g. Bastin et al., 2015).

A CPT carried out near the site was used to evaluate the strata prone to liquefaction (Fig. 4.6). The likelihood that a soil will liquefy is expressed as a factor of safety against liquefaction (FS), where FS < 1 is considered potentially liquefiable. The results of the CPT indicate that the stratum from ~2.4 to 2.65 m was potentially liquefiable (FS < 1) under ground accelerations generated by the 2011 Christchurch earthquake (Fig. 4.6). The grey, well-sorted, fine to medium sand comprising the dikes is consistent with the fine to medium sand of Unit (f), suggesting the liquefied sediment may be sourced from this unit at a depth of ~2.5 m. Therefore the CPT supports the interpretation that the thin dikes and sand blow at Site 1 were sourced from Unit (f). The sediment from ~4.1 to 4.35 m depth was also potentially liquefiable (FS < 1) (Fig. 4.6).

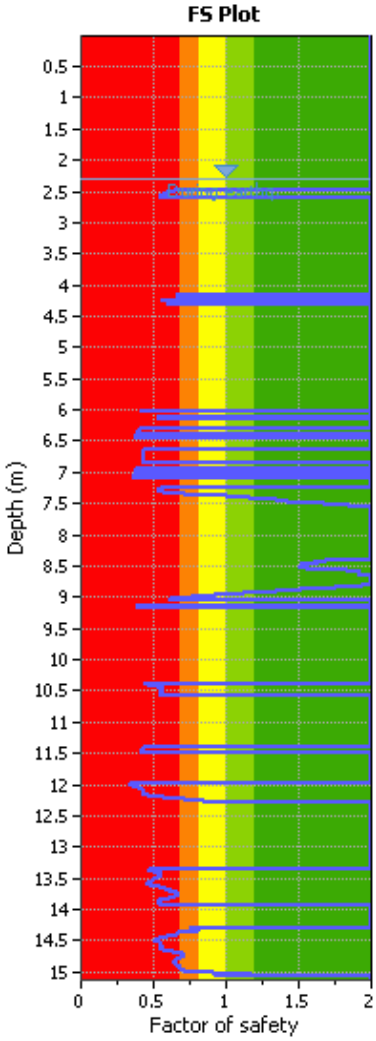

Figure 4.6: The Factor of Safety against liquefaction plot for the CPT test conducted near to Site 1 indicating sediment from ~2.4 to 2.65 m depth was potentially liquefiable (FS < 1) under ground PGAs generated by the 2011 February earthquake (Canterbury Geotechnical Database, 2015).

The upward-fining nature of the medium to fine, sand to silt dikes, indicates sediment sorting occurred during ejection, which may reflect fluid pressure dissipation decreasing flow velocity as the fluids escape, resulting in decreased grain sizes entrained within the flow. The sediment sorting is consistent with the Hjulström curve, in which very fine sand has the lowest critical velocity required to entrain particles and thus is mobilised first (Hjulström, 1939). Flow velocities within the dikes were also likely lower at the dike margins, as suggested by the dike-parallel silt linings (Fig. 4.5). Lateral differences in propagation heights within the trench indicate that flow rates varied laterally within the dikes during ejection. This difference may reflect obstruction of flow (e.g. competent sediment layers) or

differing source volumes, resulting in the formation of both surface sand ejection and dikes pinching out below the surface (Quigley et al., 2013; Bastin et al., 2015).

Subsequent liquefaction initiated during the 13 June 2011 events utilised previous fractures in the host sediment, as shown by the preservation of multiple grain sizes and the ejection of sediment from the same 22 February 2011 sand boil (Fig. 4.5). The permeable pathway created by the initial earthquake was reused to expel liquefied sediment through conduit reactivation. Investigations by Quigley et al. (2013) revealed similar persistent reactivation along distinctive vents, including a small borehole (~10 cm diameter) used as a repetitive source conduit for liquefied sediments during CES aftershocks. The preservation of conduit reactivations shows multiple liquefaction episodes preserved within a dike, reflecting liquefaction in successive earthquake events, as identified at Site 1.

As surface liquefaction at the site was only observed during the M_w 6.2 February and M_w 6.0 June 2011 earthquakes, liquefaction initiated during the September 2010 event was either non-existent or the dikes did not propagate to the surface. This indicates that the higher shaking intensities during the February 2011 event (PGA 0.37g) at the site permitted the propagation of dikes and the formation of the sand boil by more severe liquefaction than the September event.

4.3.3 Grain size analysis

Probabilistic grain size distribution curves of the sediments at Site 1 shows Unit (f), interpreted to be the source of the liquefied sediment, is coarser than the overlying fluvial sediments (Fig. 4.7A). Unit (c) and (d) share similar grain size distributions while Unit (e) overlying the coarser material is finer than the other units with a fines content (< 63 μm) of >85 %. The sand boil and feeder dike have a similar grain size distribution to Unit (f) with a fines content less than 25 % further suggesting Unit (f) was the source of liquefaction (Fig. 4.7B). The slight reduction of coarser material at ~60 μm within the liquefaction features when compared to Unit (f) may be attributed to sediment sorting during ejection, as the fluid pressure dissipates and the critical velocity required to entrain coarser particles decreases.

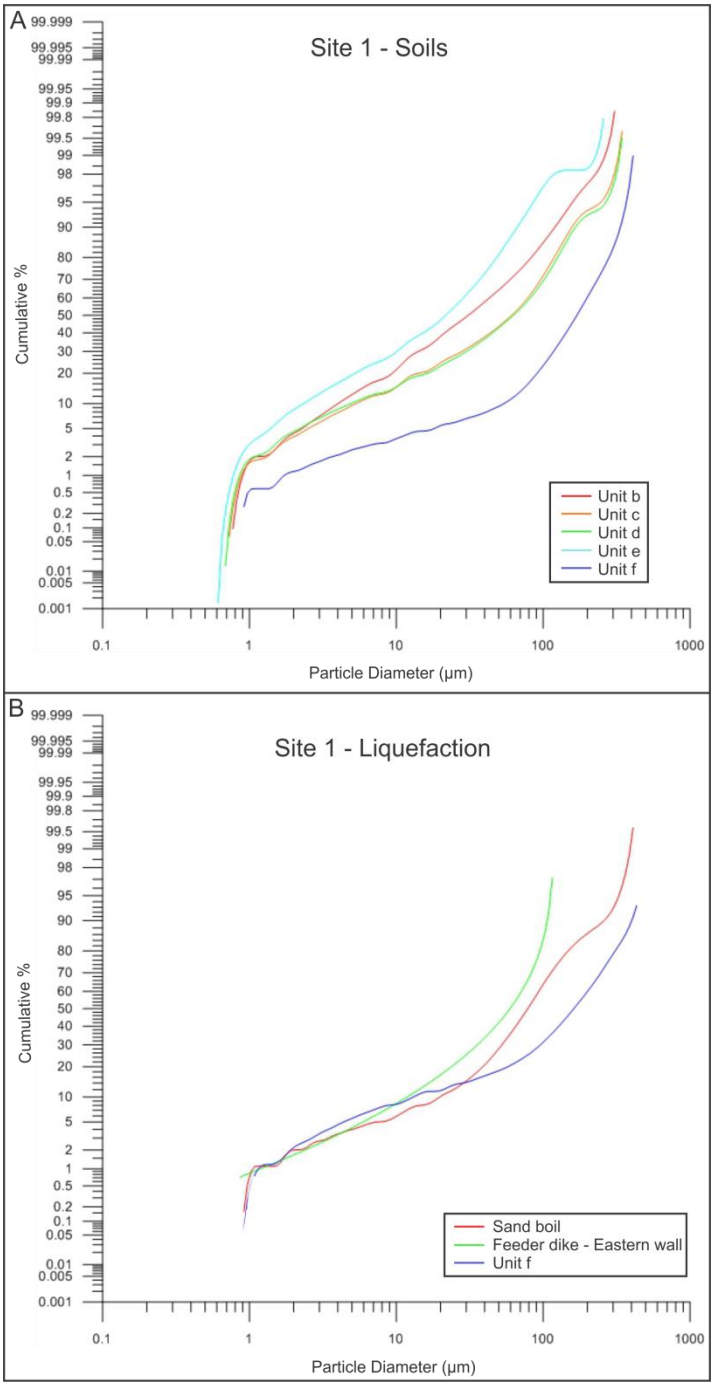

Figure 4.7: Comparison of probabilistic grain size distribution curves of the fluvial stratigraphy (A) and CES liquefaction features (B) identified at Site 1 in St Martins.

4.4 TRENCH SITE 2: 68A ST MARTINS ROAD

The former site of a residential property at 68a St Martins Road is located in central St Martins approximately 290 m from the Heathcote River channel (Fig. 4.1). The property has gently undulating topography with elevations of 5.2 - 6.0 m above sea level, ~3 m above the most proximal reach of the Heathcote River. The low-lying undulating nature of the property

reflects the topography of the ~25 m wide paleochannel (Fig. 4.1). Analysis of post-CES aerial photography and LiDAR differencing indicates the property experienced severe surface liquefaction and subsidence following the 22 February 2011, 13 June 2011 and 23 December 2011 earthquakes (Fig. 3.11; 3.13). The house on the site that was erected in 1965 was severely damaged and subsequently demolished as a result of substantial land deformation from the CES (P. Greening, pers comm, 2015). The residential dwellings adjacent to the property (68b, 68c, 62 St Martins Road) located within the paleochannel were also demolished as a result of severe land damage.

A trench was excavated (10 m long, ~1.5 m deep) in the south-eastern corner of the property (Fig. 4.8), perpendicular to the alignment of sand boils, as identified from aerial photography, and the maximum horizontal movement vectors (Fig. 3.18). The depth of the trench was limited by the water table, which was encountered at ~1.5 m during excavation on 1 April 2015. Two hand-augered holes were excavated in the trench to a depth of 3.5 m. The trench log is presented in Figure 4.9.

Figure 4.8: Aerial photograph of the Site 2 taken on 24 February 2011 and the location of the trench (Red).

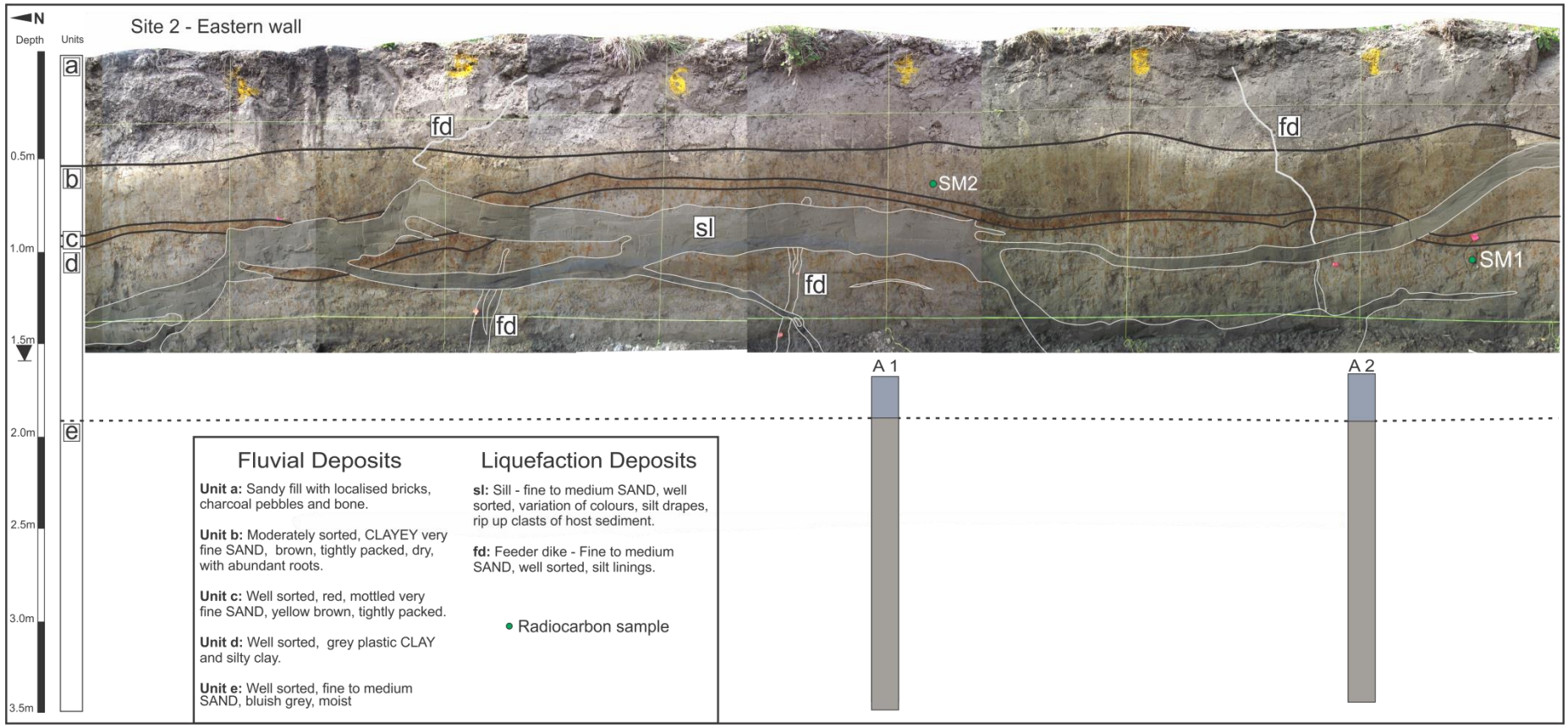

Figure 4.9: Detailed trench log and unit descriptions of the east wall at Site 2. The CES liquefaction feeder dikes (fd) and sills (sl) outlined in grey cross-cut the fluvial units (a–e) and stratigraphic contacts (black lines) and inferred contacts (dashed lines). Location of auger 1 and 2 (A1–A2).

4.4.1 Trench stratigraphy

The trench at Site 2 exposed stratigraphy composed of a plastic silty clay (Unit d) overlain by a thin heavily-oxidised bed of very fine sand (Unit c), and a bioturbated very fine sand (Unit b) (Fig. 4.9). This unit has a sharp contact with a continuous anthropogenic layer of dense sandy fill (Unit a) containing fragments of brick, glass, pebbles and bone overlain with liquefaction ejecta. The hand augers (A1–A2) indicate the silty clay (Unit d) is underlain by fine to medium sand (Unit e) at ~1.9 m depth (Fig. 4.9).

The fine to medium sand bed (Unit e) is coarser than the overlying strata, and is interpreted as a channel bed or lateral accretion deposit formed during pre-historic channel migration of the Heathcote River. The overlying plastic silty clay (Unit d) was likely deposited as channel abandonment fill as the channel avulsed. The overlying very fine sand beds of units (c) and (b) are interpreted as overbank flood deposits from the nearby Heathcote River, and the ground surface prior to anthropogenic influences, indicating the area was periodically flooded. Unit (a) contains flood deposits reworked from historic land use.

Radiocarbon dating of a charcoal fragment obtained from Unit (b) at a depth of 0.7 m yielded an age of 161 years B.P. ± 20 (SM4 - Table 4.1). Radiocarbon dating of a charcoal fragment obtained from Unit (d) at a depth of 1.2 m yielded an age of 2254 years B.P. ± 22 (SM3 - Table 4.1). The results from two wood fragments (SM1, SM2) yielded modern age dates and therefore are excluded from further discussions. These ^{14}C ages indicate that the trench stratigraphy was deposited over a maximum period from 261 - 217 BC to 1834 - 1874 AD.

Table 4.1: Radiocarbon AMS results. See Appendix A for laboratory reports.

Sample no.	Unit	Depth (m)	Sample Material	Conventional Radiocarbon Age (Years BP)	Conventional Radiocarbon Age (Calendar Years BP)
SM1	Unit d	1.1	Wood	Modern	Modern
SM2	Unit b	0.7	Wood	Modern	Modern
SM3	Unit d	1.2	Charcoal	2254 ± 22	261 - 217 BC
SM4	Unit b	0.7	Charcoal	161 ± 20	1834 - 1874 AD

The fluvial stratigraphy exposed in the trench at Site 2 is cross-cut by multiple anthropogenic pits and is overlain by fill material to a depth of ~0.5 m (Unit a). A pit at the southern end of the western wall cuts into Unit (d) to a depth of ~1.5 m and contains the oxidised remains of

an iron drum installed as a soak pit for drainage (Fig. 4.10A). A pit containing brick fragments is exposed in the western wall that cuts into Unit (b) (Fig. 4.10B).

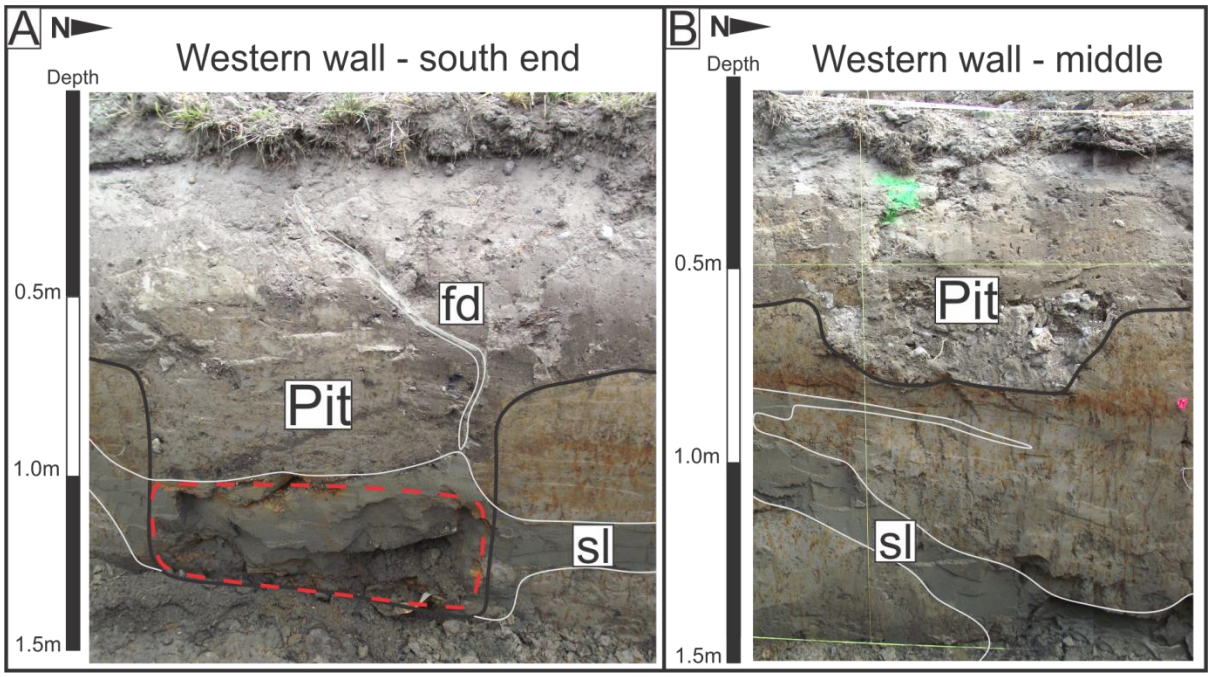

Figure 4.10: Trench logs of anthropogenic pits cross-cutting fluvial stratigraphy. (A) Pit and iron barrel (red outline) cross-cutting western wall fluvial stratigraphy. (B) A pit cross-cutting western wall fluvial stratigraphy. Boundary between fill and natural deposits (black line) and feeder dikes (fd) and sills (sl) outlined by grey lines.

A 130 cm wide pit was excavated for the installation of a sewer pipe in 1965 that cuts into Unit (b) and (c) from ~0.5 m to ~0.9 m depth at the northern end of the trench (Fig. 4.11) (P. Greening, pers comm, 2015).

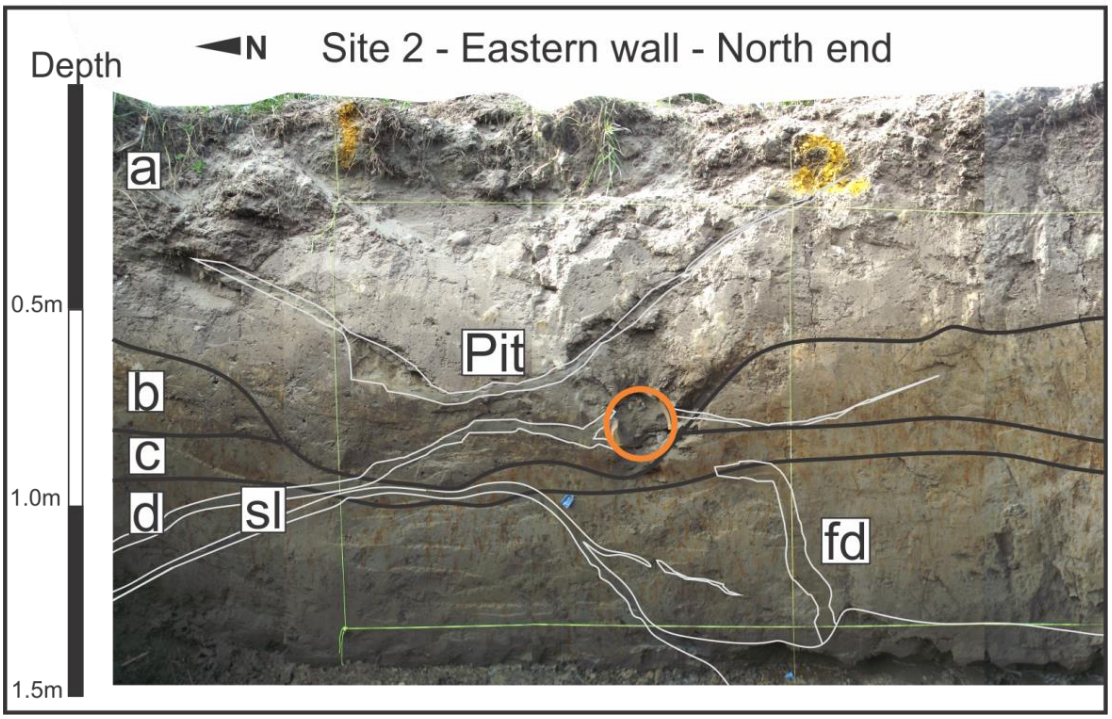

Figure 4.11: Trench log of anthropogenic pit and 1965 sewer pipe (orange circle) cross-cutting eastern wall fluvial stratigraphy. Multiple CES liquefaction sills (sl) cross-cut the pit. Unit boundaries (black line) and feeder dikes (fd) and sills (sl) outlined by grey lines.

4.4.2 Liquefaction features

The trench at Site 2 intersects numerous (~10 - 30 cm thick) subhorizontal liquefaction sills along both walls of the trench from 0.5 m depth to the trench floor (Fig. 4.12A). The sills contain well-sorted, unmottled fine to medium sand and offset the host sediment stratigraphy by up to ~30 cm (Fig. 4.12B). Four sills ~10 cm thick intrude the fluvial stratigraphy from the trench floor and become increasingly horizontal. The sills become thicker (~30 cm) at ~1 m depth and extend laterally through Unit (c) and (d). One sill reaches the surface at the southern end of the trench and small feeder dikes (~1 - 5 cm wide) propagate from the top of the sills to the surface in localised areas.

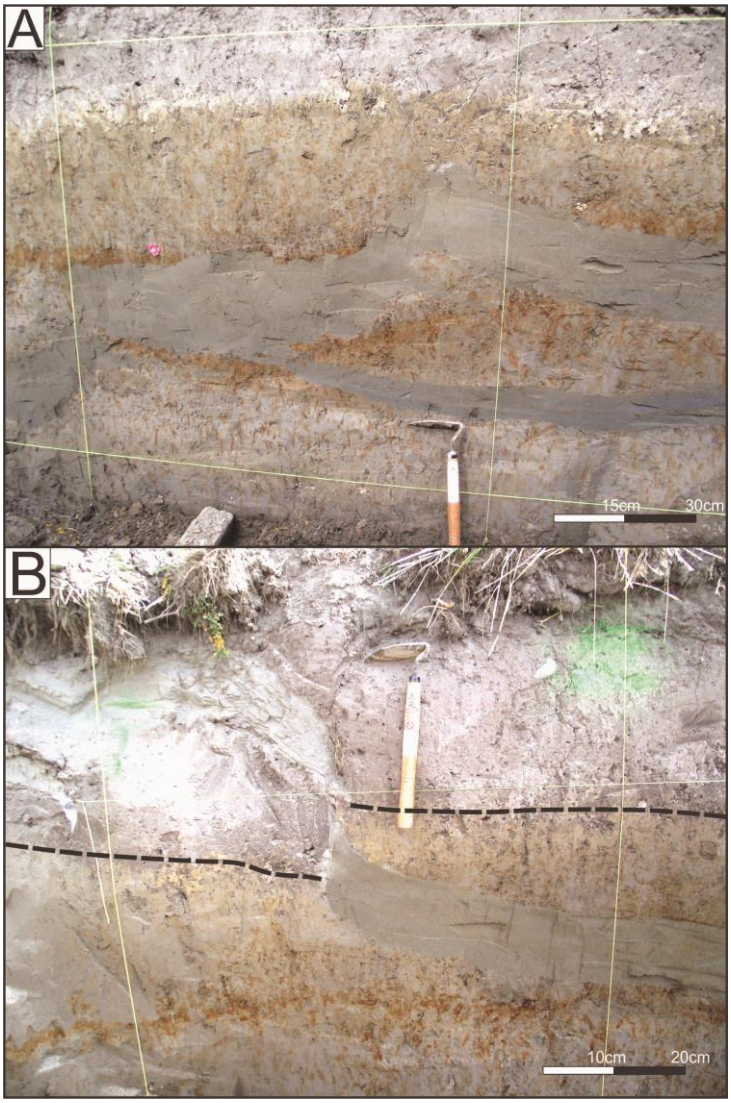

Figure 4.12: (A) Propagation of the liquefaction sill in the eastern wall offsetting Unit (c) (red colour). (B) Offset contact (dashed line) between Unit (a) and (b) from the injection of a sill.

The thickest sills contain two distinct grain sizes of well-sorted brown (5Y 4/3) medium sand and well-sorted blue (Gley 2 4/10b) fine sand. The different grain sizes are notably separated by silt linings and rip up clasts of the silty or clayey sidewall material (Fig. 4.13A). The sills predominantly consist of the medium sand typically twice the thickness of the fine sand (Fig. 4.13B).

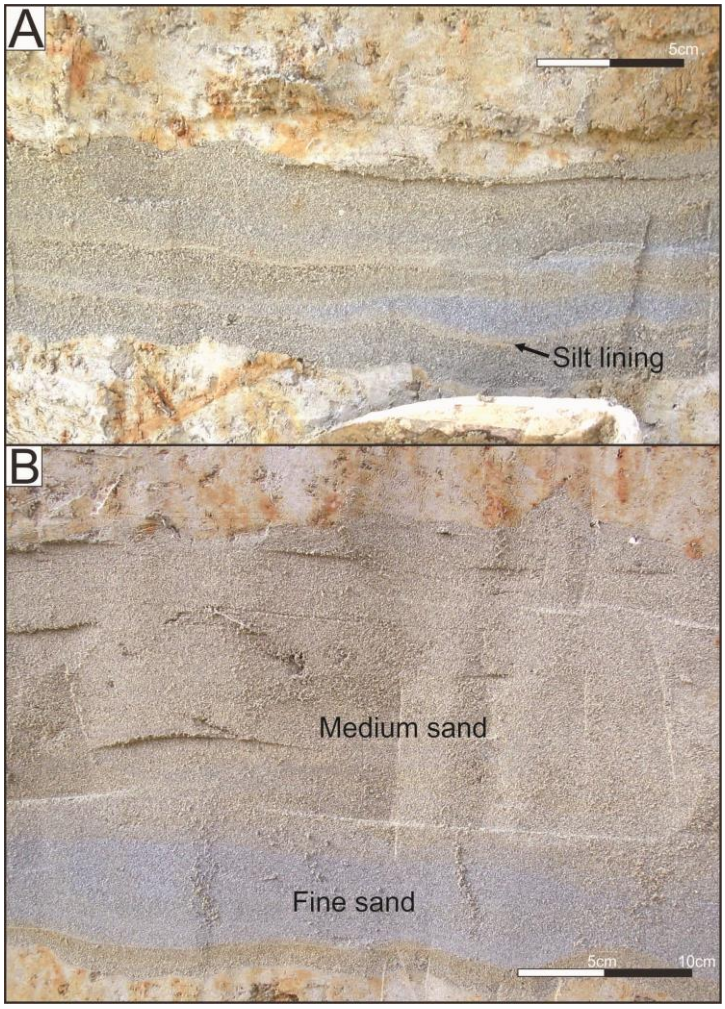

Figure 4.13: (A) Liquefaction sill between the host fluvial sediments containing medium sand (brown colour) and fine sand (blue colour) with silt linings. (B) ~30 cm thick sill composing 1/3 blue and 2/3 brown sand. Note the wavy basal contact of the sill.

The extensive sills also cross-cut two subvertical planar dikes (~5 to 10 cm thick) containing well-sorted brown-grey (Gley 4/10y) fine to medium sand (Fig. 4.14). The dikes propagate from the trench floor and pinch out at ~0.6 m depth below the surface. The truncated dikes are traced across the trench floor and align on the opposing wall (Fig. 4.14). The increasing width of the dikes with depth suggests they formed by the upward injection of sediment.

Figure 4.14: Liquefaction sill truncating a subvertical planar dike (outlined in grey). The dike is traceable across the trench floor.

The liquefied sediments are also found in open cavities of anthropogenic structures (i.e. sewer pipe, soak pit) (Fig. 4.15). The open cavities provided openings for pressurised water containing liquefied sediments to flow through.

Figure 4.15: Liquefaction-filled clay sewer pipe in the northern end of the trench.

Fine to medium sand comprising the dikes and sills is consistent with the fine to medium sand of Unit (e), suggesting the liquefied sediment is sourced from this unit at a depth of ~1.9 m (Fig. 4.9). A CPT carried out at the site indicates that the stratum from ~1.9 to 3.0 m was potentially liquefiable (FS < 1) under ground accelerations generated by the September 2010 earthquake and the February 2011 earthquake (Fig. 4.16). Therefore the CPT supports the interpretation that the dikes and sills at Site 2 were sourced from Unit (e).

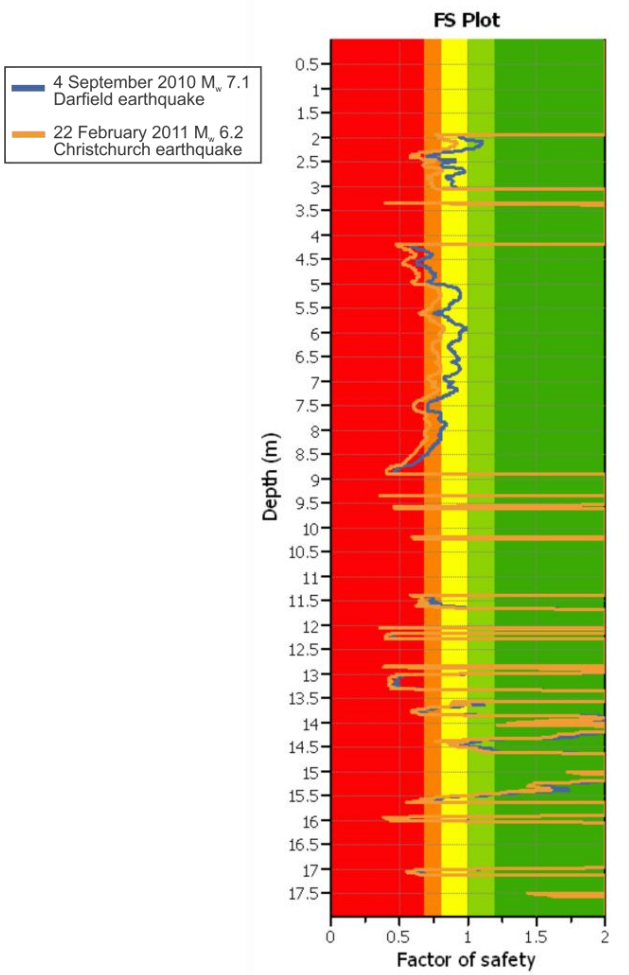

Figure 4.16: The Factor of Safety against liquefaction plot for the CPT test conducted at Site 2 indicating sediment from ~1.9 to 3.0 m depth was potentially liquefiable under PGAs generated by the September 2010 and 2011 February earthquakes. The sediment from ~4.2 to 8.9 m depth was also potentially liquefiable (FS < 1) (Canterbury Geotechnical Database, 2015).

Cross-cutting relationships between the sills and dikes suggest that the truncated subvertical planar dikes were emplaced during the September 2010 earthquake (Fig. 4.14), consistent with surface observations of the site where no surface ejecta was identified at the location of the trench following the initial M_w 7.1 event (P. Greening, pers comm, 2015).

The extensive subhorizontal sills are therefore interpreted to have formed during the 22 February 2011 earthquake under more intensive vertical ground motion. Formation of the sills may be caused by the injection of liquefied sediment into a weaker material layer, the liquefied sediment then propagated laterally during earthquake shaking. Conversely, the cross-cut subvertical planar dikes interpreted to have formed during the September 2010 event did not become deflected by a weaker layer and remained relatively vertical (Fig. 4.14). An alternate primary injection mechanism for the extensive sills could be the fluvial strata delaminating under intense ground motion, breaking apart the soil structure under high vertical accelerations (PGA_v 0.85g, Bradley and Cubrinovski, 2011), allowing the liquefied material to be injected into the openings. The epicentre of the M_w 6.2 earthquake was less than 4 km from St Martins and the steeply dipping nature and up-dip component of slip contributed to the large vertical ground accelerations that would have assisted with sill emplacement (Bradley and Cubrinovski, 2011). The lack of lateral spreading in St Martins may have also facilitated sill emplacement as the liquefied sediment could not be ejected through vertical surface cracks generated by spreading, as was observed in Avonside (Cubrinovski et al., 2012; Robinson et al., 2012; Bastin et al, 2015).

Colouration differences of the sands identified within the sills is interpreted to reflect differing oxidation stages (Fig. 4.13). Silt linings surrounding the different coloured liquefaction deposits also suggest the injection of different flows at different stages (e.g. Quigley et al., 2013). The different colours may reflect individual earthquake events where the liquefied material is reactivating the sills emplacing a younger, less oxidised material of a different grain size. The colour difference may also indicate separate pulses of liquefaction during one event where differently oxidised parts of the liquefiable source are being tapped. Inspection of the sills reveals the finer less-oxidised material (blue) is typically ~1/3 of the total thickness of the sills (Fig. 4.13B). A review of the aerial photography following the 22 February 2011, 13 June 2011 and 23 December 2011 earthquakes allowed the spatial extent of recurrent liquefaction ejecta following the major events to be identified (Fig. 4.17). A new map of recurrent surface liquefaction shows the 13 June 2011 and 23 December 2011 deposited much less sediment at the ground surface (~2/3 less), compared to the 22 February 2011 (Fig. 4.17). The finer less oxidised sand is therefore interpreted to represent liquefaction caused by a later earthquake (13 June 2011 or 23 December 2011), while the coarser browner sand that makes up the majority of the sill volume is inferred to have been emplaced during the 22 February 2011 earthquake.

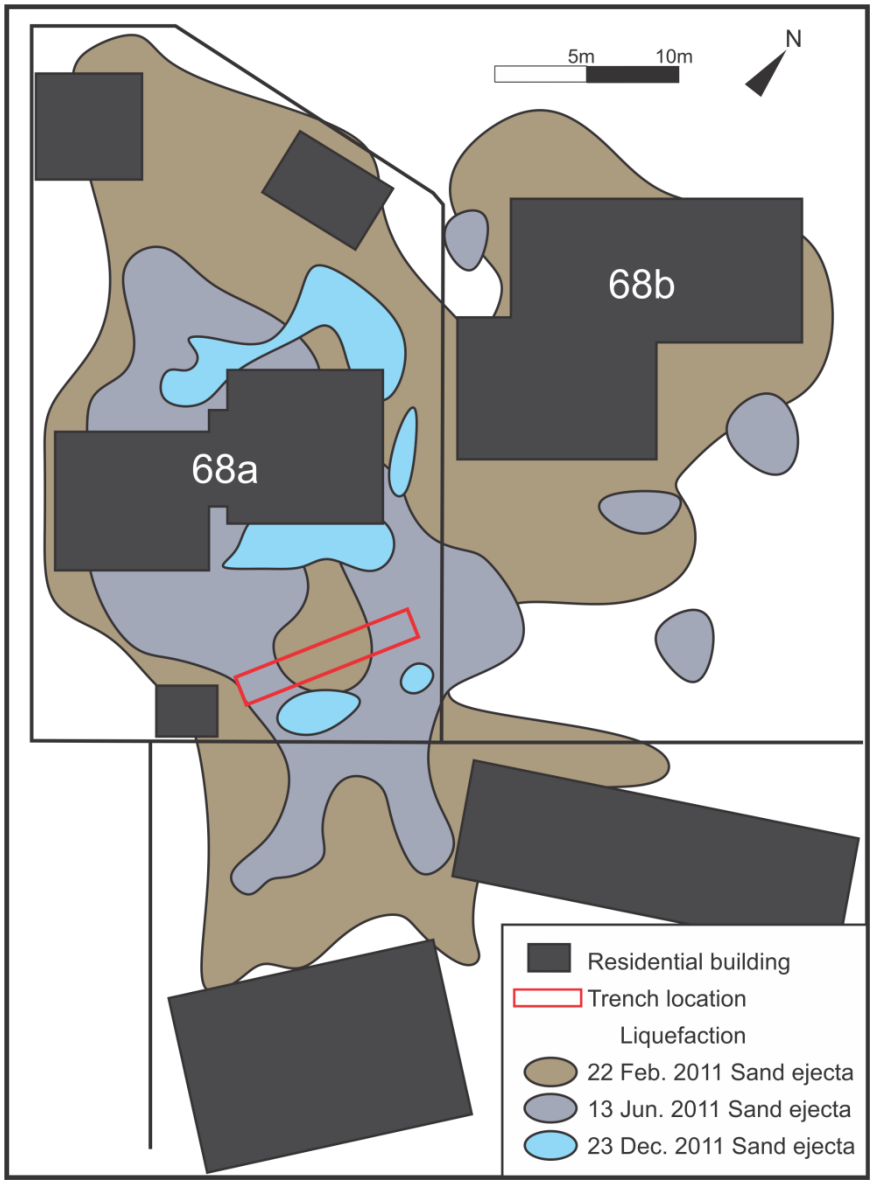

Figure 4.17: Plan-view of Site 2 and surrounding properties showing the mapped spatial distribution of recurrent liquefaction manifestations throughout the 22 February 2011, 13 June 2011 and 23 December 2011 earthquakes.

The liquefaction features indicate at least two generations of CES liquefaction are preserved within the sills, and at least three generations of liquefaction preserved within the trench, including the 4 September vertical dikes. Any additional ground surface manifestations caused by the subsequent 22 February aftershocks could not be distinguished from the liquefaction caused by the initial earthquakes due to the relatively short time span between events and aerial photography taken days following multiple liquefaction-inducting events.

LiDAR differencing shows ground deformations at the site generated surface subsidence of ~0.5 m from the ejection of sediment and post-liquefaction volumetric densification of

underlying material (Fig. 3.13). The subhorizontal morphology of the sills and different thickness of injected material indicate different amounts of subsurface deformation has occurred across the site. In some areas of the trench the sills propagate to the surface, while in other areas the sills become thinner and eventually pinch out (Fig. 4.9). Various sill thicknesses would exacerbate the formation of differential subsidence at the surface promoting greater damage to properties. The amount of property damage expected to occur in a paleochannel would likely be greater where the emplacement of extensive liquefaction sills are prevalent.

4.4.3 Pre-CES liquefaction features

A pre–CES liquefaction dike was identified in the trench at Site 2 based on its structural and material similarities and cross-cutting relationships with CES liquefaction features and fluvial stratigraphy (Fig. 4.18). A CES sill on the western wall at the northern end of the trench at Site 2 cross-cuts a subvertical dike of oxidized and mottled (10YR 4/6), well-sorted, fine to medium sand with irregular and bioturbated contacts containing eroded clasts of the clayey non-liquefiable sidewall material (Fig. 4.19). The dike ranges from ~1 to 3 cm in width and exhibits a subvertical, planar geometry similar to the other CES dikes at Site 2 (Fig. 4.14). The dike cross-cuts the fluvial stratigraphy from the trench floor to ~1 m depth where it is truncated by the 1965 sewer pit. Excavation around the pre-CES liquefaction feature revealed the dike has consistent grain size and sorting. Near the base of the pit the dike in places becomes horizontal, exhibiting the morphology of a sill (Fig. 4.18). Excavation below the trench floor was limited by the height of the water table.

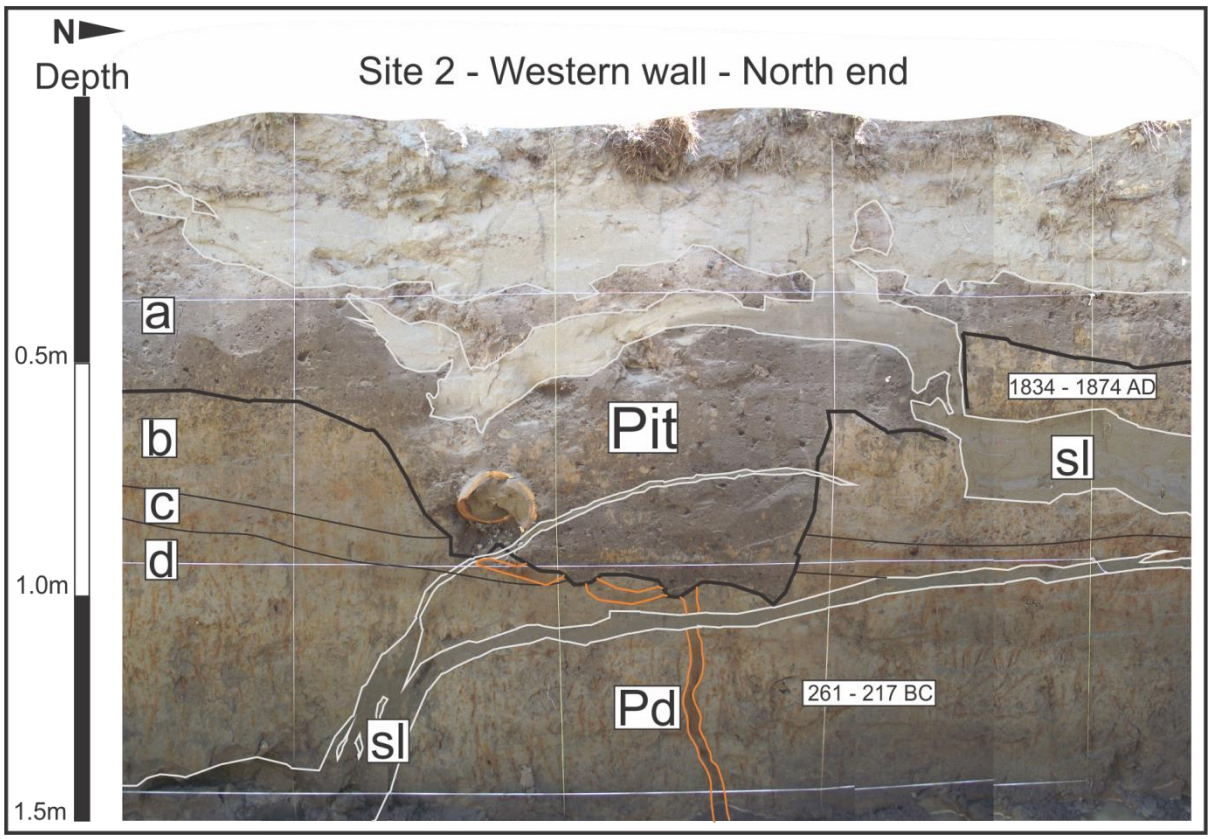

Figure 4.18: Trench log of the northern end of the western wall at Site 2. The CES sills (sl) cross-cut and offset the fluvial stratigraphy (a-d), and the pre-CES liquefaction dike (Pd). The overlying pit truncates the highest extent of the pre-CES liquefaction feature at ~1m depth.

The oxidised dike beneath the sewer pit formed by upward subvertical injection of liquefied sediment. Subvertical planar geometry and texture of well-sorted sands, similar to the adjacent CES dikes, indicates that the oxidized feature was seismically triggered. The oxidation and mottling within this feature indicate that it has been subjected to prolonged fluctuations in water table height, suggesting it predates the CES (Fig. 4.19). The feature is cross-cut by a CES injection sill that also cross-cuts the 1965 sewer pit above, indicating its emplacement prior to the development of the site. The deflection of the subvertical dike into a sill may suggest the fluvial stratum at ~1 m depth is more competent than the underlying units. A modern CES sill also becomes more horizontal at a similar elevation and suggests the competency of Unit (d) changes, promoting the horizontal propagation of the upward-injecting liquefaction (Fig. 4.18). Excavation of the sewer pit to a depth of ~1 m also suggests the sediment at the top of Unit (d) is more competent as the pit was unable to be dug deeper once the resistant layer was reached.

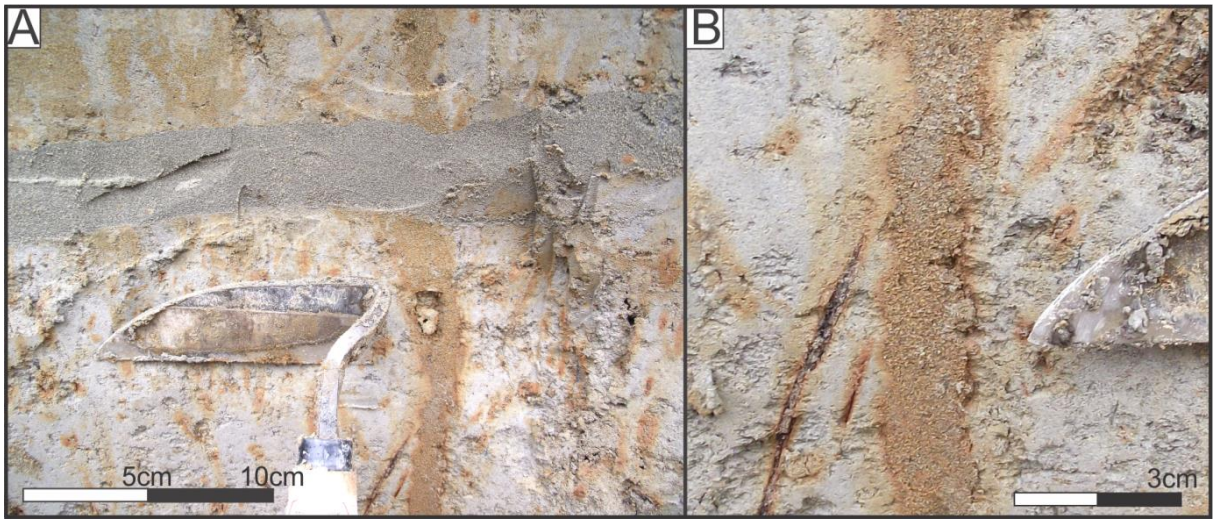

Figure 4.19: (A) CES sill cross-cutting the pre-CES liquefaction dike with eroded clasts of the clayey non-liquefiable sidewall material. (B) Close up of the pre-CES liquefaction dike showing the oxidized and mottled, well-sorted fine to medium sand with irregular and bioturbated contacts.

The results of ^{14}C analyses, and characterisation of anthropogenic stratigraphy, provide some constraint on the timing of the pre-CES liquefaction event. The pre–CES liquefaction feature cross-cuts the fluvial silty clay of Unit (d) from the trench floor to ~1 m depth where it is truncated by the sewer pit. This indicates that this liquefaction feature formed in an event that post-dated deposition of the Unit (d) (261 - 217 BC calibrated ^{14}C age) and predates the excavation of the 1965 sewer pit (Fig. 4.18). The pre-CES liquefaction feature indicates that the causative earthquake triggered liquefaction likely within Unit (e), however, it did not generate the shaking intensities required to form extensive sills from the deformation of the fluvial stratigraphy. It is possible that localised ejecta did form at other locations across the site but were not exposed within the trench or have been subsequently modified by anthropogenic processes. The maximum width of feeder dikes and sills formed during the CES earthquakes exceeds that of the identified paleoliquefaction dike, suggesting that the liquefaction in these events and earthquake shaking intensities in southern Christchurch were more severe in the recent CES earthquakes. This hypothesis is consistent with subsurface investigations of susceptible Late Holocene sediments with low liquefaction triggering resistances in eastern Christchurch where liquefaction features were most prominent from the recent CES events (e.g. Bastin et al., 2015).

4.4.4 Grain size analysis

The probabilistic grain size distribution curves of the soils at Site 2 shows Unit (e), interpreted as the source of the liquefied sediment, is coarser than the overlying fluvial sediments (Units a-d) (Fig. 4.21A). The multiple liquefaction deposits identified within the trench at Site 2 are displayed in Figure 4.20 and the grain sizes are compared in Figure 4.21B. Liquefaction features from individual events have a similar grain size distribution to Unit (e), with a fines content less than 25 %, further suggesting Unit (e) was the source of liquefaction at Site 2 (Fig. 4.21B). Coarser material observed within Unit (e) when compared to the liquefaction features may be attributed to sediment sorting during ejection as the fluid pressure dissipates and the critical velocity required to entrain coarser particles decreases. The grain size distribution of the pre-CES liquefaction dike (paleoliquefaction) is similar to the CES liquefaction, supporting the interpretation of a liquefaction-inducing paleoearthquake event prior to the CES (Fig. 4.21B).

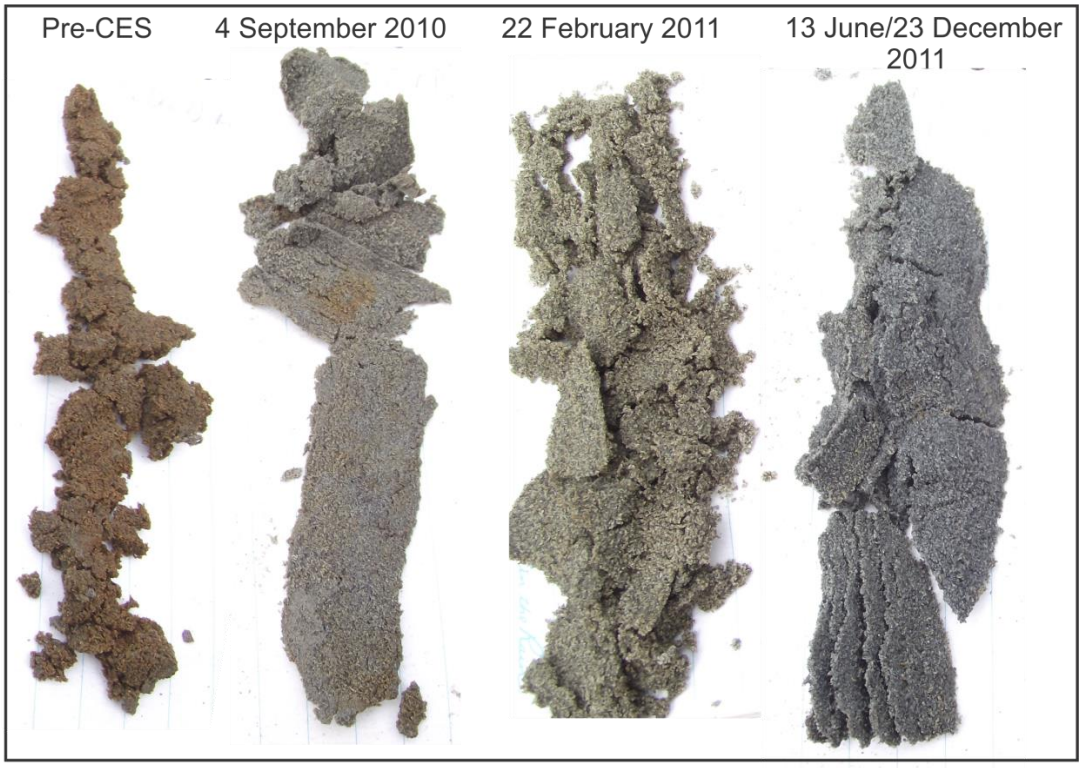

Figure 4.20: Liquefaction deposits collected from Site 2 showing the oxidation and textural differenced of the sediment from individual earthquake events.

The grain size differences between Unit (e) and the liquefaction features may also represent different provenance during the each earthquake event. The grain size distribution of both the 4 September 2010 and paleoliquefaction features display slightly finer material that may have

been sourced from a shallower zone of the liquefiable sediment (Fig. 4.21B). The coarser grain sizes of the 22 February 2011 and 13 June 2011 liquefaction may therefore represent genesis from lower in the liquefiable body initiated from higher ground accelerations experienced in Christchurch during these events.

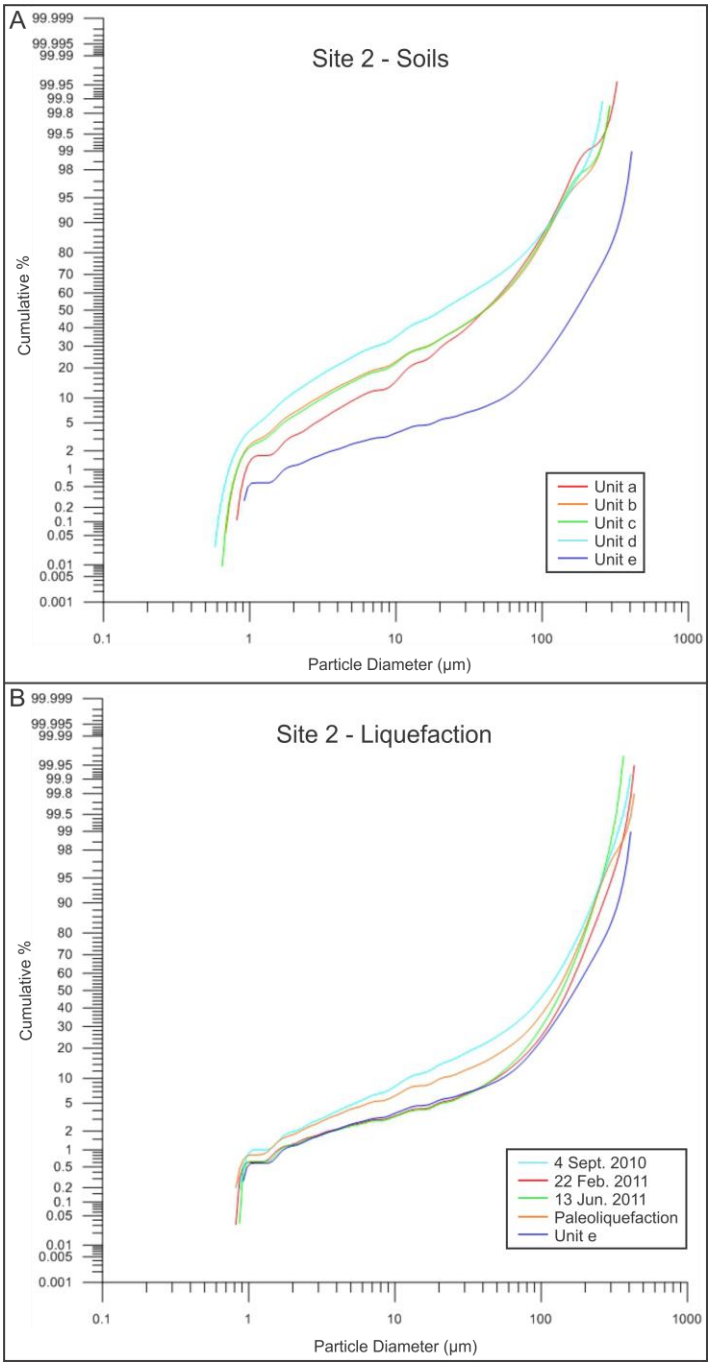

Figure 4.21: Comparison of probabilistic grain sizes distribution curves of the fluvial stratigraphy (A) and interpreted CES liquefaction and pre-CES liquefaction features (B) identified at Site 2 in St Martins.

4.5 SUBSURFACE INVESTIGATIONS IN BECKENHAM

Three sampling locations in Beckenham where selected along the inner meander loop to the channel apex for hand auger excavation (Fig. 4.22). The sites were chosen to document the subsurface fluvial stratigraphy and investigate the material properties of the soils in relation to the current location of the river and the evolution of the point bar.

Beckenham Park (Aug 1) was selected based on the lack of near-surface anthropogenic structures. The site was also selected as it is located >100 m away from the Heathcote River channel in the low-lying area (Fig. 3.7). The residential property at 70 Corson Ave (Aug 2) was selected because it is located centrally within the inner meander loop and the intersection of Waimea Tce and Eastern Tce (Aug 3) was selected to compare the subsurface fluvial stratigraphy between the inner meander loop and the modern flood plain (Fig. 3.15).

Figure 4.22: Aerial photograph of Beckenham, the locations of the auger sites and the Heathcote River (blue).

4.5.1 Beckenham Park: Auger 1

Beckenham Park is located in northwest Beckenham approximately 100 to 300 m from the Heathcote River channel (Fig. 4.22). The park has flat topography with elevations of 5.9 - 6.5

m above sea level, ~4 m above the most proximal reach of the Heathcote River. Analysis of post-CES aerial photography indicates minor sand blows formed across the eastern side of the park closest to the Heathcote River following the 22 February 2011 M_w 6.2 earthquake and the 13 June 2011 earthquakes. A hand auger was drilled to 2 m depth in the western corner of the park where no liquefaction was observed during the CES to identify the subsurface fluvial stratigraphy (Fig. 4.23).

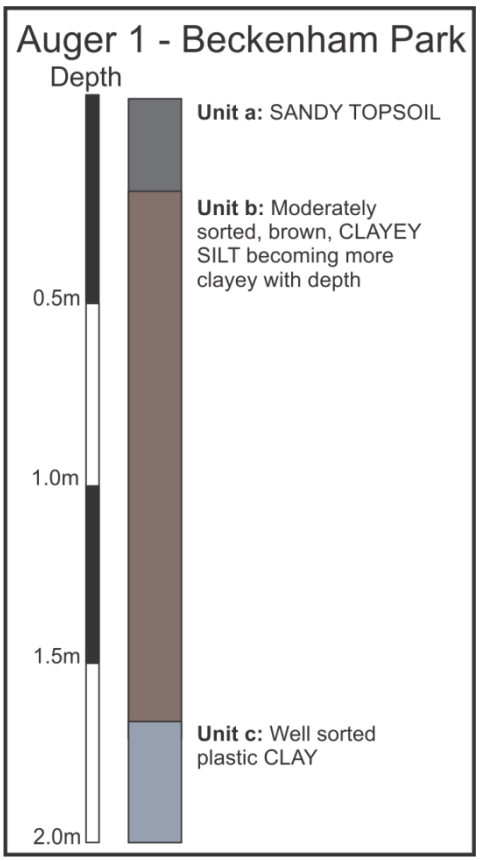

Figure 4.23: Soil profile from Beckenham Park.

The auger shows the stratigraphy consists of ~20 cm of sandy topsoil overlying a ~1.5 m thick unit of moderately sorted clayey silt (Fig. 4.23). The unit becomes more clayey with depth before a sharp transition to a well-sorted plastic clay unit at ~1.7 m depth. The plastic clay at ~1.7 m depth indicates deposition in standing water. The lack of roots and soil horizons also suggests the area had constant standing water out of the flood plain and did not dry out often enough to develop plants with roots. The overlying clayey silt indicates the increasing presence of flood waters. This suggests that Beckenham Park and the lower lying area of Beckenham was inundated with floodwaters of the Heathcote River prior to down-cutting of the river forming the terrace and modern flood plain (Fig. 3.15). The overlying

sandy topsoil layers may represent periodic flooding from large storm events (e.g. Cowie, 1957)

A CPT carried out near the site was used to evaluate the sediments prone to liquefaction (Fig. 4.24). The CPT indicates that a thin unit at ~4.6 m was potentially liquefiable (FS < 1) under ground accelerations generated by the 22 February 2011 Christchurch earthquake. The sediment from ~7.1 to 7.6 m depth was also potentially liquefiable (FS < 1) (Fig. 4.24). The CPT analysis for the site shows the subsurface fluvial stratigraphy was not particularly liquefiable under the shaking conditions experienced with few zones where the sediments show FS < 1 between thicker stratum (~3 m) of resistant material.

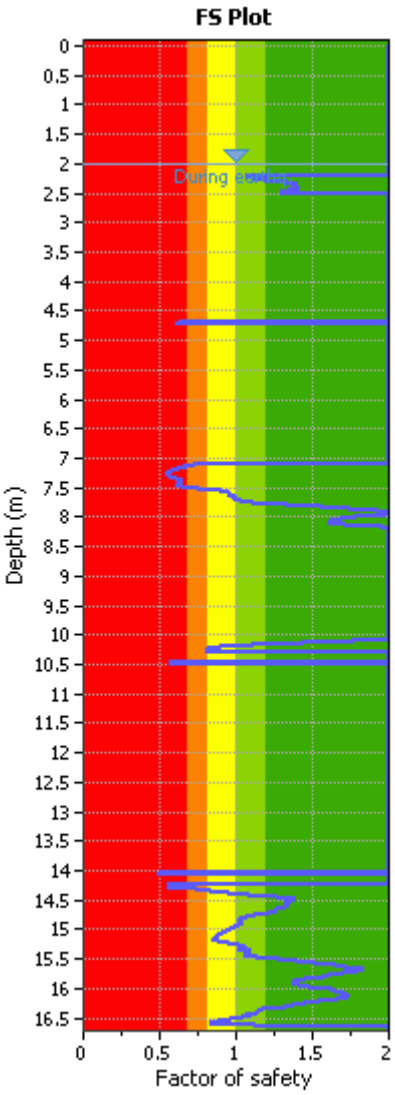

Figure 4.24: The Factor of Safety against liquefaction plot for the 22 February earthquake from a CPT conducted near Beckenham Park. The results indicate the majority of the stratum was not particularly liquefiable (FS >1) under the earthquake conditions. (Canterbury Geotechnical Database, 2015).

4.5.2 70 Corson Ave: Auger 2

The residential property at 70 Corson Ave is located in central Beckenham approximately 150 m from the Heathcote River channel (Fig. 4.22). The property has flat topography ~6 m above sea level, ~4 m above the most proximal reach of the Heathcote River. Analysis of post-CES aerial photography indicates no liquefaction occurred at the property. A hand auger was drilled to 1 m depth in the northern corner of the property (Fig. 4.25).

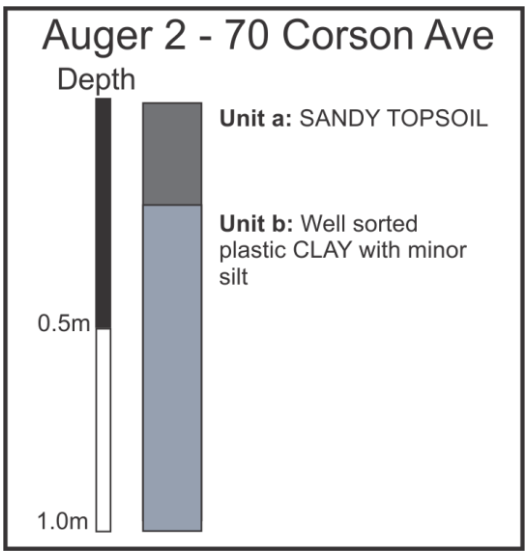

Figure 4.25: Soil profile from 70 Corson Ave.

The auger shows the stratigraphy consists of ~20 cm of sandy topsoil overlying a well-sorted plastic clay unit to 1 m depth (Fig. 4.25). The presence of clay below ~0.2 m depth indicates the area contained standing water and flood waters containing coarser sediments were unable to inundate the location. The lack of roots and soil horizons suggests the clays formed in an area with consistent standing water.

A CPT carried out near the site was used to evaluate the sediments prone to liquefaction (Fig. 4.26). The CPT indicates that thin units at ~6.4 m and ~8.0 m depth were potentially liquefiable under ground accelerations generated by the 22 Feb. 2011 Christchurch earthquake (FS < 1) (Fig. 4.26). The CPT analysis shows the subsurface fluvial stratigraphy was not particularly liquefiable under the shaking conditions experienced, with the thin zones of susceptible material separated between resistant strata >1 m thick.

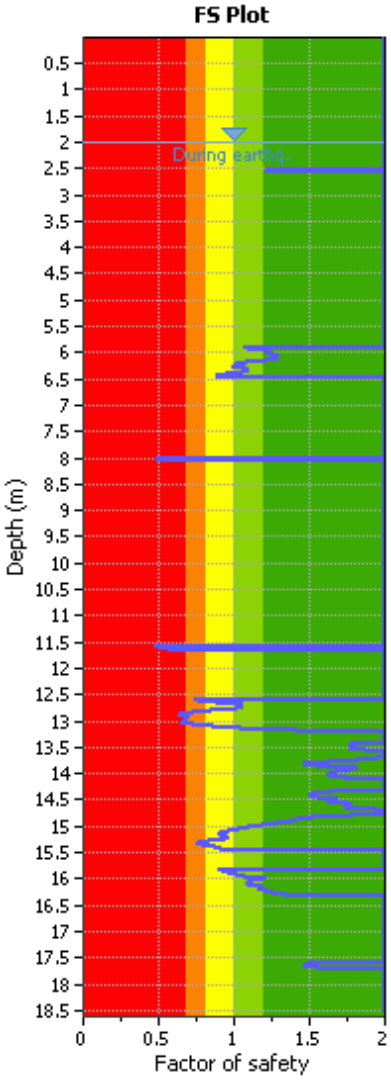

Figure 4.26: The Factor of Safety against liquefaction plot for the 22 February earthquake from a CPT conducted near 70 Corson Ave. The results indicate the majority of the stratum was not particularly liquefiable (FS >1) under the shaking conditions experienced. (Canterbury Geotechnical Database, 2015).

4.5.3 Intersection of Waimea Tce and Eastern Tce: Auger 3

The intersection of Waimea Tce and Eastern Tce is located in southern Beckenham adjacent to the Heathcote River channel on the flood plain at ~3.6 m above sea level (Fig. 4.22). Analysis of post-CES aerial photography indicates minor cracks formed across the flood plain along Eastern Tce following the 22 Feb. 2011 M_w 6.2 earthquake. A hand auger was drilled to 1.5 m depth on the river bank (Fig. 4.27).

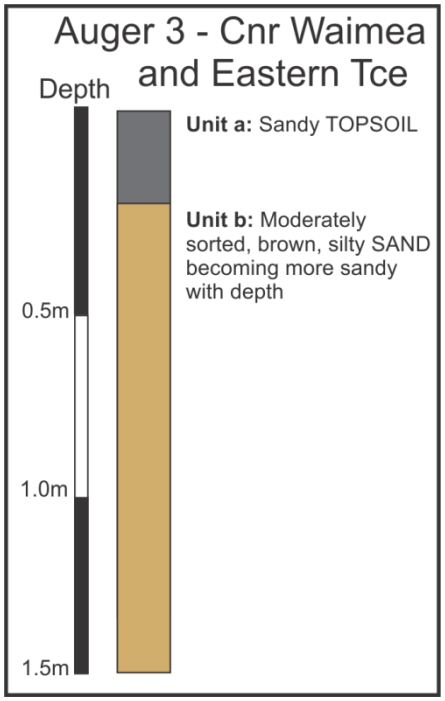

Figure 4.27: Soil profile from the intersection of Waimea Tce and Eastern Tce.

The auger shows the stratigraphy consists of ~20 cm of sandy topsoil overlying a ~1.3 m thick unit of moderately sorted silty sand (Fig. 4.27). The unit becomes sandier to a depth of 1.5 m. The sandy sediments in southern bank of the Heathcote River channel are interpreted to represent modern flood and lateral accretion deposits at the convex bank. Recent channel adjustments along the modern flood plain have preserved the sandy sediments within the river banks.

4.5.4 Grain size analysis

The probabilistic grain size distribution curves of the sediments collected from Beckenham Park (Unit c) and 70 Corson Ave (Unit b) shows the soils have a fines content (< 63 µm) of >99 % (Fig. 4.28). This suggests the deposits formed in a previous swampy area containing standing water. The area around Beckenham Park and Corson Ave would have been lower than the surrounding topography allowing the clay-rich strata to develop. Subsequent incision of the Heathcote River, forming the terrace riser between inner meander loop and modern floodplain, has preserved the clayey stratum in central Beckenham. The soil collected from the intersection of Waimea Tce and Eastern Tce contain sandy lateral accretion deposits from recent channel migration and flood plain deposition at the river's current level.

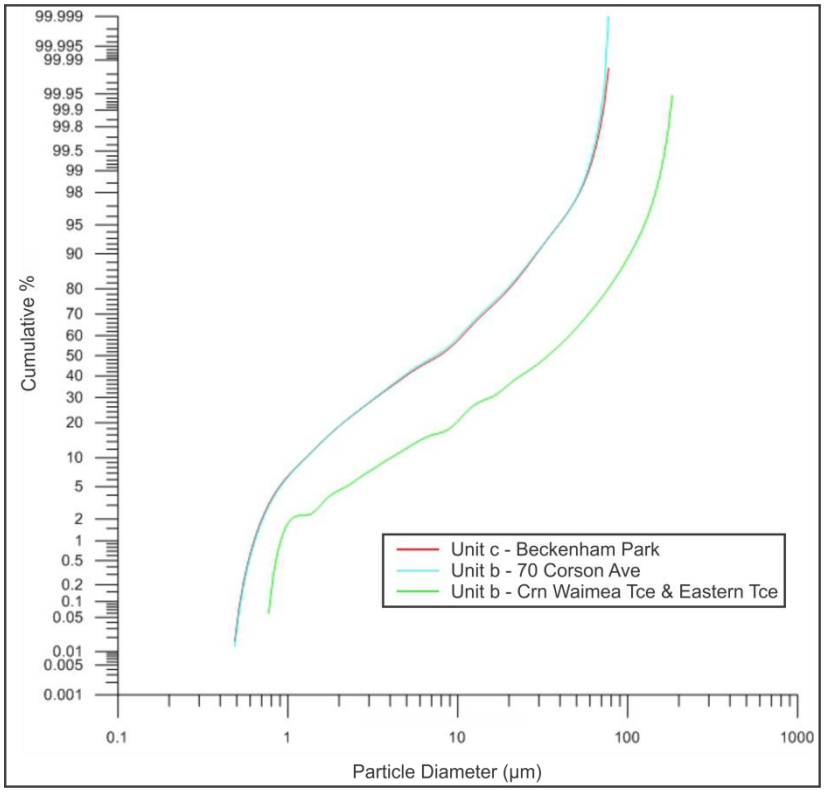

Figure 4.28: Comparison of probabilistic grain sizes distribution curves of the samples collected across Beckenham.

4.6 CLAY ANALYSIS

Eight samples were analysed using the methods outlined in Chapter 2 to calibrate the total proportion of clay within selected sediments from the study locations. Two samples from previous subsurface investigations in Avonside were also included in the analysis to compare the clay contents of inner meander loop deposits between the Heathcote and Avon Rivers. The results from the clay analysis are presented in Table 4.1.

Table 4.1: Total percentages of clay from pipette analysis

Location	Sample Name	Depth (m)	Sediment description	Clay % (<9Φ)	CES liquefaction at site
Site 1 - St Martins	Unit d	1.0	Silty sand	5.5	Yes
	Unit e	1.5	Silty sand	5.1	
Site 2 - St Martins	Unit d	1.55	Silty clay	14.5	Yes
	Unit e	1.95	Fine sand	8.8	
Auger 1 - Beckenham	Unit c	2.0	Plastic clay	26.4	No
Auger 2 - Beckenham	Unit b	1.0	Plastic clay	21.3	
Sullivan Park Avonside	SP_T6_S3	1.0	Fine sand	2.7	Yes
Bracken St Avonside	BS_T4_S9	0.6	Sandy silt	6.4	

The results from the clay analysis show Units (d) and (e) collected from Site 1 in St Martins have a clay content of ~5 %. The sediment collected from Units (d) and (e) within the trench at Site 2 in St Martins have a clay content of 14.5 % and 8.8 % respectively. The sediment samples collected from the hand augers in Beckenham (Unit c - Beckenham Park, Unit b - 70 Corson Ave) both have a clay content of >20 %. The samples collected from subsurface investigation in Sullivan Park and Bracken St in Avonside have clay contents of 2.7 % and 6.4 %.

The quantity of clay within the fluvial strata, combined with the inferred liquefiable sources and liquefaction features identified across the study area, suggests that the proportion of clay within the subsurface sediments heavily influences the surface manifestations of liquefaction in an earthquake. Samples collected in Beckenham, where no surface manifestations of liquefaction were observed, contain the highest clay contents of the samples analysed (>20 %). The clay percentages indicate that fluvial deposits containing plastic clays >~20 % likely influence soil behaviour and inhibit surface ejection of liquefied sediment during earthquake shaking. The clay-rich units identified from Auger 1 and Auger 2 are also relatively thick (>~1 m) compared to the units overlying the liquefiable sources identified in the trenches at St Martins (Fig. 4.3; 4.9). Liquefaction within the soil profile may have still occurred at depth in Beckenham, however surface manifestations of sand boils appear to have been subdued by thicker units containing high clay contents.

The samples from St Martins generally contain less than 10 % clay, with the exception of Unit (d) at Site 2. The higher clay content identified in Unit (d) at Site 2 (14.5 %) may have initially inhibited the ejection of liquefied sediments during the February 2011 earthquake, allowing greater pore pressures to be generated in the subsurface. Subsequent deformation of the overlying strata under higher pore pressures may have assisted the propagation of the extensive liquefaction sills observed in the trench and the wide distributions of surface ejecta across the property and surrounding area (Fig. 4.12). The samples from Site 1 contained less than ~5.5 % clay where less extensive liquefaction was observed. Lower clay contents within the fluvial stratigraphy overlying the liquefiable source at Site 1 may have inhibited the generation of higher pore pressures, leading to the formation of relatively smaller liquefaction features (thin dikes < 2 cm wide) and isolated sand boils (Fig. 4.3). The lower clay content of the overlying fluvial stratigraphy, and the relatively shallow depth of liquefiable sediment

identified from CPT plots, when compared with Beckenham, appears to have greatly influenced the manifestation of liquefaction between the two suburbs.

The results from the analysis therefore suggest that the presence of clay in the overlying fluvial stratigraphy appears necessary to generate excess pore pressures adequate to facilitate the liquefaction of sandy sediments. However, if the clay content in the overlying sediments is >20 %, and the thickness of the confining resistant layers are >1 m, the surface manifestation of liquefied sediments are likely subdued and ground deformation inhibited, as observed in Beckenham.

Various amounts of clay contained within the fluvial strata, influencing the manifestation of liquefaction, is directly related to the sediment source and geomorphology in which the fluvial deposits were formed. Clay introduced into the Heathcote River system, sourced from the Port Hills, would have been concentrated in areas containing standing water across the depositional setting. Accumulation of clay-rich sediments within the Beckenham meander loop has likely produced strata sufficient to confine units susceptible to liquefaction, preventing the widespread ejection of liquefied sand during the CES. The ability of the St Martins meander to migrate allowed the formation of overbank deposits, but the point bar lacked thick clay units as the channel moved laterally. The higher clay content of Unit (d) overlying the sandy channel deposit of Unit (e) at Site 2, likely reflects the presence of standing water contained within the low-lying paleochannel following channel abandonment (Fig. 3.15). Clay-rich deposits in St Martins were therefore concentrated in the paleochannel, but the absence of thicker strata containing >20 % clay likely permitted the widespread ejection of the underlying liquefied sediment.

Although St Martins, Beckenham, and Avonside share similar inner meander loop geometries, severe lateral spreading observed adjacent to the Avon River, following the February 2011 earthquake, suggests the strata in eastern Christchurch is different to that of the study area (e.g. Orense et al., 2011). The preservation of clay material adjacent to the Heathcote River system may have inhibited the formation of lateral spreading. The resistant layers in Avonside, however, were possibly too thin to suppress liquefaction but competent enough to generate excess pore pressures to facilitate rafting of the overlying crust by up to several meters toward the free face of the river channel causing the extensive proberty damage during the CES (Fig. 1.13) (Robinson et al., 2012).

4.7 DISCUSSION

4.7.1 Geologic evolution of the study area

The provenance of modern fluvial sediments in Christchurch is much different than previous Holocene depositional environments. The majority of the Christchurch urban area, including the study area in southern Christchurch, was underwater at ~6.5 ka (Fig. 1.4) and the majority of finer sediments would have been transported out to sea (Brown and Weeber, 1992). Following the mid-Holocene highstand, coastline progradation toward the east would have allowed the fine-grained sediments, including clays from the Port Hills, to accumulate and become mixed with greywacke-derived sediments sourced from the avulsing Waimakariri River (Brown and Weeber, 1992). Deposition of gravels, attributed to incursions from the Waimakariri River that intermittently avulsed across Christchurch, ceased once the river became established to the north of the city, allowing the accumulation of resistant stratum in southern Christchurch.

4.7.2 Liquefaction expressions and site characteristics

The trench at Site 2, shown in Figure 4.9, shows significantly larger ground deformations than Site 1, including the injection of lateral sills within the near-subsurface from the volumetric densification and expulsion of excess groundwater. The extensive planar sills offset the fluvial stratigraphy, causing significant changes in the surface topography that led to the devastation of the building on the property. Recent geotechnical data indicate an important difference in soil conditions between Site 1 and Site 2. Data from Site 1 indicates potentially liquefiable material (FS < 1) occurring at a depth of ~2.4 m to 2.65 m (Fig. 4.6) whereas a CPT located at Site 2 shows potentiality liquefiable material from ~1.9 m to 3 m, with a thicker susceptible body extending from ~4 m to a depth of 9 m (Fig. 4.16). The shallower and thicker zone of potentially liquefiable material at Site 2 likely represents the deposits of the paleochannel that led to significant ground deformation at the site. Preferential manifestation of liquefaction would therefore have been focused in the paleochannel deposit of loosely consolidated sands of lower resistance at shallow depths, overlain by a slightly stronger cap (Unit d), compared to the surrounding silty units. The paleochannel underlies the regions which experienced severe (>0.5 m) subsidence across St Martins forming the spatial variability of severe liquefaction (Fig. 3.13).

In Beckenham, the centre of the meander loop is capped by thick (>1 m) non-liquefying strata containing clay-rich material (>20 %), likely remnant swamp deposits, that inhibited liquefied sediment injections from reaching the surface. CPT data from Beckenham (Fig. 4.24; 4.26) show the liquefying soil layers were isolated and interbedded between the thicker layers resistant to liquefaction. The isolated pockets in the subsurface that were potentially liquefiable were suppressed by the resistive fluvial strata. Orense et al. (2011) similarly concluded that the presence of abundant clay (>20 %) within the soil in southern Christchurch was a major reason why liquefaction was less extensive around the Heathcote River compared to the suburbs adjacent to the Avon River.

The results of subsurface sediment analysis of liquefaction in the layered soil profiles demonstrate that surficial manifestations of liquefaction depend on the depth of susceptible sand bodies and the overlying soil material. Site-specific variations of liquefaction manifestations are consistent with the liquefaction triggering mechanisms defined by Idriss and Boulanger (2008) and ground conditions described in Brown and Weeber (1992). The cross-cutting relationships of the modern and paleoliquefaction features at shallow depths suggest the ejection of well-sorted sands in unconsolidated facies is a common occurrence, and conduits for the pervasive liquefied sediments (dikes and sills) feature throughout the Holocene strata in Christchurch.

4.7.3 Seismologic triggering thresholds of CES liquefaction features

Seismic shaking thresholds for liquefaction manifestations across the study area varied widely due to the variations in the site-specific geotechnical properties and the geomorphic characteristics of the site. Calibration of the occurrence and non-occurrence of observed liquefaction from aerial photography with nearby accelerometer measurements of PGA versus M_w enabled the liquefaction triggering thresholds for each site to be established (Fig. 5.1).

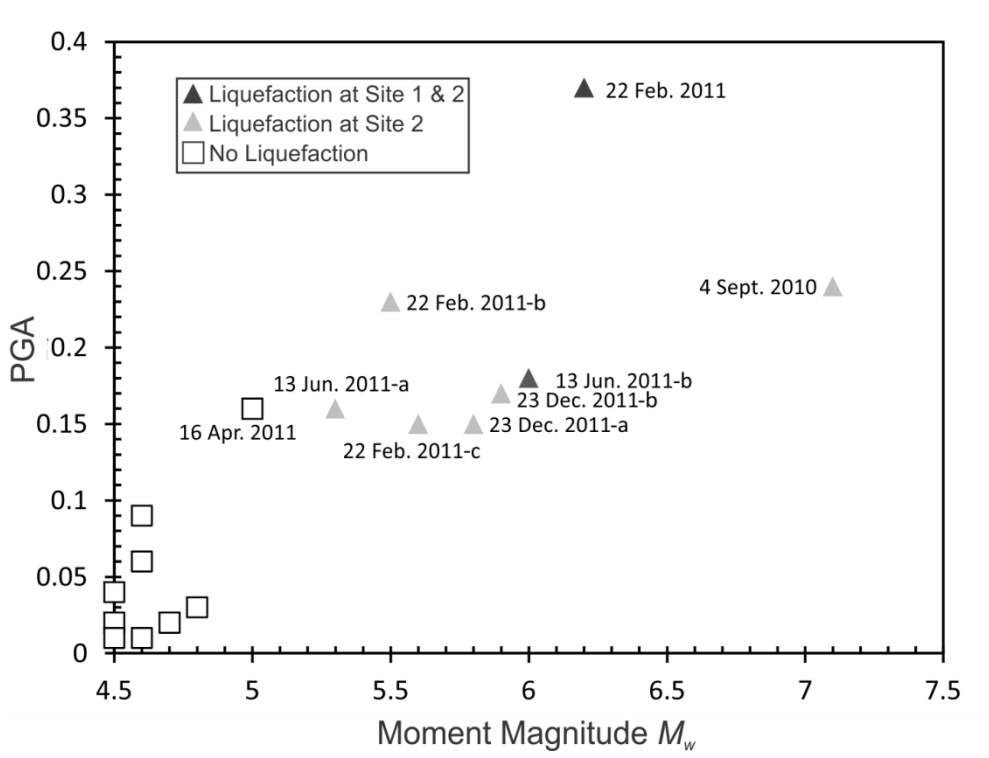

Figure 4.29: PGA vs. M_w of major CES events showing the occurrence and non-occurrence of liquefaction determined from aerial photography at the investigated sites in St Martins.

The distribution of liquefaction in St Martins varied with measures of earthquake magnitude and shaking intensity. The 4 September 2010 M_w 7.1 earthquake, interpreted to have formed the subvertical planar dikes observed in the trench at Site 2 (Fig. 4. 14) from PGAs of 0.24g, caused only minor surface manifestations locally in St Martins with no liquefaction observed at Site 1. Liquefaction was induced within the thicker susceptible sediments in the paleochannel at Site 2 (Fig. 4.16) in earthquakes with PGA ≥ 0.15g. Thinner units susceptible to liquefaction at Site 1 (Fig. 4.6) did not liquefy as frequently and required higher shaking intensities to induce surface manifestations (≥ 0.18g). The combination of emplaced liquefaction features and fractured crusts created preferential pathways for liquefied material in subsequent earthquakes.

Surface liquefaction manifested at both sites in the M_w 6.2 22 February earthquake as identified from aerial photography. The PGA experienced in the study area is estimated to have been ~0.37g (Bradley et al., 2014). The only other event where surface liquefaction occurred at both Site 1 and 2 was the 13 June 2011 M_w 6.0 earthquake, despite lower PGA values than the M_w 6.2 22 February event (Fig. 5.1). Piezometer measurements following the

initial M_w 5.3 13 June earthquake, ~80 minutes prior to the larger M_w 6.0 earthquake (Table 1.1), show excess pore water pressures were generated in the subsurface which did not fully dissipate before the subsequent event (Fig. 5.2). The elevated pore pressures likely increased the severity of liquefaction for the latter earthquake and the manifestation of a sand boil at the more resistant Site 1 following the M_w 6.0 13 June earthquake.

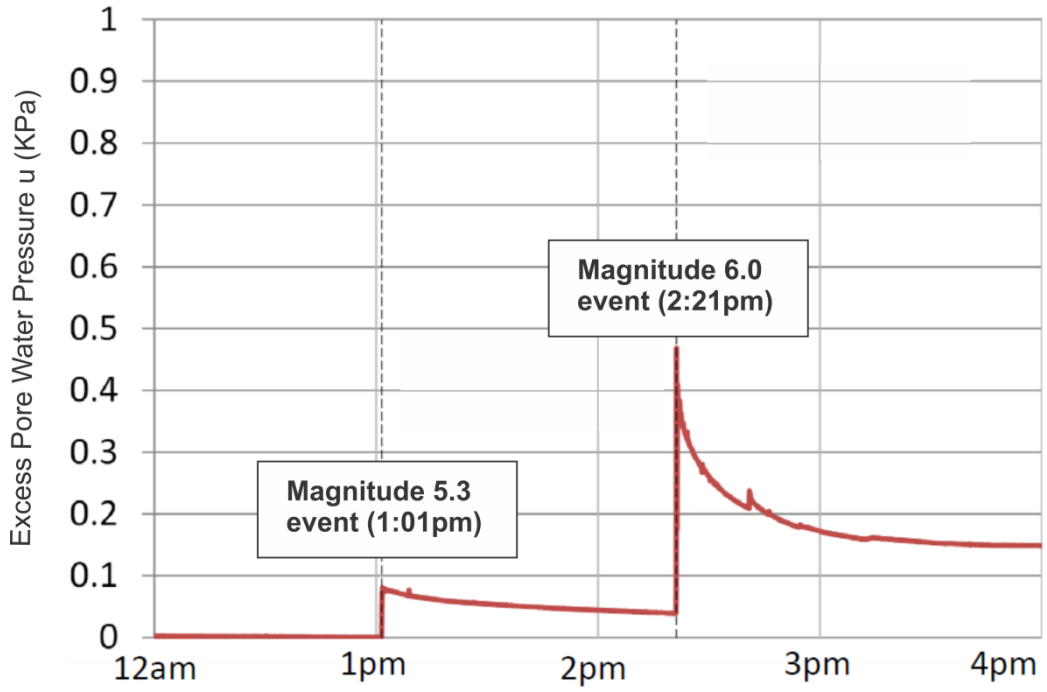

Figure 4.30: Measured water pressures for the 13 June 2011 earthquakes at a depth of 6m from a Pore Pressure Transducer (PPT) in St Martins. The water pressures are expressed as an excess pore pressure ratio (r_u), where a value of zero represents the pre-earthquake steady state water pressure condition at that depth (i.e. zero excess pore water pressure) and a value of one represents a total pore water pressure condition equal to the total stress (i.e. the soil weight) at that depth, resulting in complete loss of strength of the soil and is defined as the point at which the soil has liquefied. From Quigley et al. (in review).

4.7.4 Paleoseismic implications

The pre–CES dike at Site 2 cross-cuts the fluvial stratigraphy and is cross-cut by the younger anthropogenic pit (Fig. 4.18). This indicates that the pre–CES dike postdates the depositional age of 261 - 217 BC for Unit (d) and predates the installation of the sewer pipe in 1965. The preliminary evidence suggests a paleoearthquake occurred between 261 - 217 BC and 1965 with sufficient ground motions to induce liquefaction in southern Christchurch at Site 2 but possibly not Site 1, as no evidence for paleoliquefaction was obtained from the latter.

Evidence for paleoliquefaction was documented at several sites in eastern Christchurch adjacent to the Avon River where CES liquefaction occurred (e.g. Quigley et al., 2013; Bastin et al., 2015). Paleoliquefaction features including feeder dikes, sills, bulbous intrusions, lateral spreading cracks, and subsurface sand blows analogous to CES features have been observed within trenches at ~1-2 m depth (Bastin et al., 2015). The paleo-feeder dikes observed to cross-cut mid to late Holocene sediments have been heavily mottled by oxidation and reactivated or cross-cut by CES liquefaction features. A combination of radiocarbon dating, optically stimulated luminescence (OSL) dating and cross-cutting relationships with anthropogenic pits suggests liquefaction-inducing paleoearthquakes occurred in Christchurch between 1660 to 1800 AD and before ca. 1905 (Bastin et al., 2015).

The morphology of the paleoliquefaction dike, combined with the cross-cutting relationships of fluvial and anthropogenic deposits at Site 2 in St Martins, suggests that the pre-CES liquefaction feature formed in an event prior to 1965. It is possible that this feature formed during a large, far-field earthquake such as the ~M_w 7.9 ± 0.3 1717 Alpine fault event, which postdates the depositional age of 261 - 217 BC for Unit (d) (Sutherland et al., 2007) (Fig. 4.18). If the pre-CES liquefaction features cross-cut Unit (b), the liquefaction-inducing earthquake would have occurred after 1834 - 1874 AD, indicating liquefaction was initiated at the site likely during the 1869 M_w 4.7-4.9 Christchurch earthquake or the 1901 M_w 6.9 Cheviot earthquake. The dike however is truncated by the sewer pit and is not observed to intrude onto Unit (b). The pre-CES liquefaction feature is therefore interpreted to have formed in an earthquake during the last ~2000 years, likely during a proximal earthquake in the last ~300 years in accordance with the findings of Bastin et al. (2015).

The preserved paleoliquefaction feature may provide information about relative site-specific shaking intensities and liquefaction triggering resistances from the liquefaction-inducing paleoearthquake (Quigley et al., 2013). Lunina and Gladkov (2015) discuss how liquefaction-induced dikes can be applied as indicators of paleoseismic shaking and earthquake magnitude from a bounding relationship between the earthquake magnitude and the maximum width, maximum visible height and intensity of discernible dikes. They cautioned however that this approach results in a lower bound evaluation of seismological parameters and does not account for geotechnical conditions where less optimal liquefaction conditions (lower water tables, interbedded strata) will result in less prominent features (Lunina and Gladkov, 2015). This is apparent when comparing the liquefaction features observed at Site 1 and Site 2 and

also with studies conducted in eastern Christchurch (e.g. Bastin et al., 2015). Smaller liquefaction features and less surface deformation at Site 1 suggest that these deposits have a higher triggering resistance when compared with the extensive liquefaction and paleoliquefaction features at Site 2. The distributions of the surface ejecta across St Martins suggests the evolution of meander loops, and the presence of highly susceptible paleochannel deposits, directly influences the distribution and severity of damaging liquefaction (e.g. Tuttle, 2001).

4.7.5 CPT data

CPT profiles can be complicated by soil heterogeneity as shown by post-earthquake CPT data obtained from St Martins (Fig. 4.6; 4.16). Variability of the CPT tip resistances illustrates the stratification of coarser-and finer-grained soils in the point bar deposits. While it may be straightforward for engineers to categorise the vulnerability of a site from in situ geotechnical investigations, the sharp transitions in observed CES liquefaction distributions reflecting the heterogeneous nature of the fluvial deposits makes clear that significantly diverse sediments have accumulated adjacent to the Heathcote River as a direct result of the geomorphic setting. The majority of liquefaction-induced subsidence across the study area was focused in a narrow corridor reflecting the location of a low-lying paleochannel in St Martins (Fig. 3.13; 3.15), unlike the widespread deformation experienced across Avonside. Thus, representative CPTs may not accurately describe the stratigraphic character of an entire site, which is likely the case in much of Christchurch where widespread fluvial sediments, deposited by migrating rivers, are found.

In a study on the ability of CPT-based liquefaction triggering methods, Van T Veen (2015) found that large amounts of liquefaction and settlement that were estimated by CPT in Christchurch only sustained small amounts of liquefaction during the CES; the soil behaviour types defined by CPT do not always appear to match soil classification found by other means (logging, laboratory testing). The study suggested the reason for these issues is likely due to the CPT soil behaviour types used for liquefaction susceptibility analysis are calibrated mostly for clean sands, soils which are very different from those in some areas of Christchurch, which predominantly include silts, clayey silts, and silty clays (e.g. Beckenham) (Van T Veen, 2015). This suggests that liquefaction hazard assessments are less accurate at sites having soils with high fines content (Maurer et al., 2014b). Site vulnerability classification therefore requires knowledge of the spatial variability of fluvial deposits. As a

result, consideration must be given to whether spatial heterogeneities are random or have systematic variations that produce different layers that can control the manifestation of liquefaction (Idriss and Boulanger, 2008). The recognition of subsurface heterogeneity thus has implications for geotechnical investigations and building foundation design, as the scale of possible liquefiable layers and total ground subsidence indicated from CPT data may not reflect the true liquefaction potential of a site, particularly in the suburbs of Christchurch.

4.7.6 Liquefaction characteristics as proxies for channel location

The morphology and cross-cutting relationships of modern and paleoliquefaction features may be related to the floodplain evolution which has a dynamic influence on the susceptibility of the fluvial deposits. Because the pre-CES dike identified at Site 2 (Fig. 4.18) displayed a similar morphology to the subvertical planar dikes interpreted to have formed during the 4 September 2010 earthquake (Fig. 4.14), the ground motions experienced in St Martins during the September event (M_w 7.1, PGA 0.24g) are possibly similar to the liquefaction-inducing paleoearthquake event. This interpretation however must also consider the channel location at the time of the paleo-event, as dynamic morphological properties would have influenced the extent of paleoliquefaction features, and the causative earthquake properties.

The active channel may have been closer to the location of the trench at Site 2 at the time of the paleoearthquake event. The smaller distance to the river could have possibly promoted more extensive soil deformation and therefore facilitated the ejection of liquefied sediments during the paleoearthquake, allowing the emplacement of the paleodike during smaller shaking intensities compared to the September 2010 event. Subsequent channel migration has possibly inhibited the propagation of soil fractures, reducing the efficiency of ejection pathways for liquefaction during more recent earthquakes. Channel migration could have therefore inhibited evidence of liquefaction-inducing paleoearthquakes.

4.8 SUMMARY

The extent, range and variation of liquefaction features identified within the study area illustrate the complex influence of various factors affecting manifestation. CES liquefaction features were recognised in the subsurface by their correlation with observed surface sand boils and their cross-cutting relationships with fluvial and anthropogenic stratigraphy. The observed liquefaction features were documented in detail to record the morphologies of

subsurface liquefaction, identify the influences liquefaction has on the extent of surface deformations, and assist with the identification of pre–CES liquefaction features. Linking sediment sequences and liquefaction features to their chronology is vital in determining phases of seismic activity. Subsurface liquefaction features included well-sorted fine to medium sand dikes, sills and sand boils, which fractured the fluvial stratigraphy interpreted to be less than a few thousand years old. Liquefaction was most prevalent in Late Holocene fluvial fine to medium sand deposits at depths of >1.9 m.

In St Martins, liquefaction was very pronounced and of large magnitude in the trench and surroundings at Site 2, but much smaller at Site 1. A pre-CES liquefaction dike observed in the trench at Site 2 is interpreted to have formed in an earthquake during the last ~2000 years. Differences in surficial liquefaction distributions, ground deformations and shallow subsurface intrusions between the two selected sites occurred as a result of host sediment heterogeneity, intrinsic site characteristics, proximity to the paleochannel, and anthropogenic soil modifications. The intensity of subsurface liquefaction features and surface deformation suggests Site 2 has a lower liquefaction triggering resistance than Site 1, and would be prone to severe liquefaction-induced deformation in future earthquakes.

The results of subsurface sediment analysis of the layered soil profiles demonstrate that the surface manifestation of liquefaction depends on the depth of susceptible sand bodies, the overlying soil material properties, and sediment source. The ejection of liquefied sediment in Beckenham was inhibited by widespread units of thick non-liquefying, plastic clay-rich strata effectively acting as a seal on potentially liquefiable sediments.

CHAPTER 5 CONCLUSIONS

5.1 INTRODUCTION

Liquefaction features observed in southern Christchurch provide a record of the spatial variability of point bar deposits and associated facies changes from Late Quaternary meander loop migration of the Heathcote River. The objectives of this thesis were to build an understanding of river migration processes and the susceptibility of different areas to liquefaction dependent on the evolution of sedimentary facies and geomorphic controls. Digital elevation models, new geomorphic and topographic maps, detailed subsurface investigations, grain size analysis and ^{14}C dating of organic material were employed to determine why major differences in liquefaction distributions and severity of damage occurred in the suburbs of St Martins and Beckenham, adjacent to the Heathcote River. Below, the key findings of this thesis are summarised and future implications and recommendations for liquefaction susceptibility analysis are presented.

5.2 KEY FINDINGS

5.2.1 The influence of meander migration on liquefaction susceptibility

River migration has formed sand-dominant facies at shallow depths across Christchurch producing a substrate susceptible to ground deformation and the formation of liquefaction dikes, sills and sand boils. Susceptible fluvial sediments of dominantly saturated Late Holocene fine to medium sands at depths of < 5 m adjacent to the city's urban rivers caused the most extensive damage during the 2010 – 2011 earthquakes (Cubrinovski et al., 2012; Wotherspoon et al., 2012; Quigley et al., 2013). The geologic variability of the CES region comprising Late Holocene alluvial sediments with active and abandoned river channels contributed to the diversity of observed damages.

Migrating rivers inherently promote the formation of point bars which preserve unique successions of fluvial stratigraphy that reflect the flow regime, sediment sources and geologic setting of the river system (Willis and Tang, 2010; Fryirs and Brierley, 2012; Ghinassi et al., 2013). Preservation of these fluvial deposits, which are typically young, at low elevations and in proximity to a water body, subsequently make point bars in migrating fluvial systems susceptible to liquefaction (Makaske and Weerts, 2005). As the CES has illustrated, the severity of liquefaction manifestations and the distributions of subsidence across the study

area were directly influenced by the spatial and geologic variability of geomorphic features formed by the migration of the Heathcote River channel.

5.2.2 Comparison of St Martins and Beckenham meander loops

The majority of liquefaction surface ejecta and liquefaction-induced settlement across the study area was focused in the interior of St Martins, primarily within a paleochannel. The extensive liquefaction and subsidence indicates the presence of shallow, unconsolidated and saturated sands deposited and preserved by the migration of the Heathcote River. Targeted trenching, hand augers and interpretation of post-earthquake CPT data across this area shows severe liquefaction coincided with sand bodies close to the surface (< 5 m depth). The liquefaction was sourced from deposits of fine to medium sand of the pre-existing channel found at variable depths (Site 1: 2.5 m; Site 2: 1.9 m), reflecting the former thalweg topography during the active expanding stage of the meander, likely ~2000 – 3000 years ago based on the radiocarbon dates of overlying strata (Table 4.1). Subsequent overbank flood deposits of typically finer sediment have preserved the sandy channel deposits creating a crustal material which possibly promoted the ejection of liquefaction. CPT data show a shallower and thicker stratum of potentially liquefiable material at Site 2, signifying the location of the paleochannel that led to significant ground deformation (>0.5 m) of central St Martins.

Liquefaction was initiated at Site 2 during the 4 September 2010 earthquake but the dikes were unable to reach the surface. Intense vertical shaking and volumetric densification of the paleochannel sands led to the delamination of the overlying fluvial stratigraphy, favouring the formation of extensive sills (~30 cm thick) during the 22 February 2011 earthquake. The strong ground accelerations caused widespread surface ejection of liquefied sands and extensive property damage. Reactivation of the liquefaction features and ejection of liquefied sand in subsequent earthquakes was facilitated by the reuse of permeable pathways created in the prior events. The surface effects of liquefaction at Site 1 were less damaging with only localised sand boils fed by thin dikes (< 2 cm) and minor ground deformation initiated during the 22 February and 13 June 2011 earthquakes. Greater depths to the water table and deeper and thinner susceptible units likely contributed to the smaller liquefaction features and localised ejecta at Site 1.

In Beckenham, lateral confinement by Banks Peninsula forced the point bar to become immobile, promoting the deposition of thick clayey overbank and back swamp sediments which produced a stratigraphy sufficient to confine units susceptible to liquefaction. The inability of the point bar to migrate, and formation of resistant stratigraphy, prevented the widespread ejection of liquefied sands and severe subsidence observed in St Martins. Sediment collected from the auger sites in Beckenham contained the highest clay contents of the samples analysed (>20 %), suggesting that the proportion of plastic clay within the crustal sediments, likely sourced from the Port Hills, subdued the surface manifestations of liquefaction. Future geochemical analysis of the clay material is recommended to prove the source of these sediments. The capacity of plastic soils to inhibit liquefaction manifestation by affecting pore pressure development and surface ejecta should be further evaluated (Maurer et al., 2014b).

5.2.3 Comparison of the Heathcote River with the Avon River

Extensive liquefaction and lateral spreading that occurred in eastern Christchurch adjacent to the Avon River suggests the depositional system is very different from the studied modern Heathcote River, despite similarities in sinuosity, greater epicentral distances, and lower PGAs. The accumulated sediments in the Avon River system lack sufficient clay contents to resist the effects of liquefaction. The damage observed along the Avon River suggests severe liquefaction-induced ground deformations are more prominent in unconfined river systems where the ability of the channel to migrate is controlled only by the confining flood plain sediments, and abundant clay deposits are absent. Extensive lateral spreading that occurred around the Avon River fractured the overlying non-liquefying soil producing permeable pathways for excess water to be ejected which facilitated greater liquefaction manifestation in eastern Christchurch (Quigley et al., 2013; Bastin et al., 2015). The differences in liquefaction severity between the Avon and Heathcote rivers were influenced by the inability of the Heathcote River to freely migrate forming a fluvial stratigraphy containing more resistant material.

5.3 FUTURE IMPLICATIONS

5.3.1 Landform controls on liquefaction

The degree to which the geomorphic setting controlled the extent and severity of liquefaction, as opposed to other mechanisms such as sediment consolidation, is an important issue for

identifying liquefaction susceptibilities elsewhere. Noticeable spatial differences between the point bar deposits are observed when comparing the surface topography, liquefaction distributions and subsidence patterns across the study area. Clear differences reflect the heterogeneity of fluvial deposits within the subsurface, controlled by evolution of the geologic setting. The most distinctive information indicating migration of the Heathcote River comes from the topographic DEMs (Fig. 3.7; 3.8), showing the St Martins point bar has migrated by lateral expansion and downstream translation, creating a complex setting of stratigraphic heterogeneities containing liquefiable and non-liquefiable facies.

The low-lying topography of a paleochannel and ability to preserve sandy deposits during abandonment phases makes former river channels highly susceptible to liquefaction. The liquefaction distributions observed at the study area and in other case histories (e.g. Ishihara, 1993; Wotherspoon et al., 2012) highlight the fact that areas in former river channels and abandoned meanders are prone to extensive liquefaction and subsidence. In the case of Kaiapoi, where the liquefaction distributions correlated with the former location of the Waimakariri River, the river channels were only recently abandoned and reclaimed (late 1800s) (Wotherspoon et al., 2012). Widespread liquefaction-induced ground deformation was also observed in Horseshoe Lake, a paleochannel of the Avon River in eastern Christchurch that was likely abandoned >2000 years ago (van Ballegooy et al., 2014). This suggests the majority of abandoned Holocene channels containing sand deposits are prone to severe liquefaction.

Recognition of geomorphic features through GIS data and the ability to predict facies associations and bedform morphology in sinuous river systems, combined with established geotechnical methods, can be beneficial for interpreting the susceptibility of an area to liquefaction. The likelihood a site will experience liquefaction and lateral spreading must therefore acknowledge variations in soil stratigraphy, geomorphic features and material origins which, as observed adjacent to the Heathcote River, can exert a strong influence on liquefaction manifestation patterns.

5.3.2 Geotechnical Investigations

Analytical procedures for assessing liquefaction triggering have relied on empirical data from various in situ test indices to identify site-specific liquefaction susceptibility (Idriss and Boulanger, 2008). These analytical procedures also need to consider the morphology and

origin of the soils by identifying the nature of the surface material and underlying geologic properties to identify local-scale differences that affect susceptibility. In Christchurch, the river reaches most affected by severe liquefaction-induced subsidence are in zones of tidal-fluvial transitions. Modern site investigations in coastal settings generally do not take into account tidal influences, or the depositional effects of tidal-fluvial transitions. The combination of empirical data with geomorphic interpretations and source material can be beneficial for identifying fluvial stratigraphy, and therefore liquefaction susceptibility analysis.

Combining geomorphic mapping with geotechnical subsurface data to assess liquefaction potential will assist engineers to make better-informed decisions when designing suitable foundations for new buildings. A key challenge is to structure liquefaction triggering analysis in ways that appropriately consider a site's stratigraphy (e.g. primary strata and spatial heterogeneity) and the potential consequences of liquefaction (liquefaction of isolated pockets versus continuous layers and the influence of previous liquefaction features) (Idriss and Boulanger, 2008). Consideration of river migration processes and the geomorphology of an area will therefore allow a greater understanding of facies distributions and the stratigraphy of subsurface material adjacent to river systems, and the susceptibility of a site to of liquefaction-induced ground deformation. The damages sustained from liquefaction during the CES emphasises the importance of a good understanding of the fluvial evolution of a region. Recognising the geomorphology of an area can aid predictions of the magnitudes of earthquake-induced surface deformations a site will likely experience. Combining geomorphic interpretations with geotechnical data can be applied elsewhere to improve existing liquefaction susceptibility datasets.

5.3.3 Land classification and building guidelines

The inaccuracy of CPTs from geotechnical investigations, in areas consisting of heterogeneous soils which over-estimate the potential for liquefaction and vertical settlement, may influence the economic recoverability of a property or the possible development of a site (Van T Veen, 2015). Overestimating the liquefaction potential is potentially causing those using the information for foundation design and land remediation to invest much larger sums of money into projects than may be necessary (Maurer et al., 2014b). Caution should therefore be exercised when extrapolating CPT correlations for construction purposes adjacent to meandering fluvial systems containing heterogeneous deposits of sands, silts and

clays (Robertson and Wride, 1998). Additionally, simple and economic trenching investigations may be warranted to assess the vulnerability of a site based on the occurrence or non-occurrence of paleoliquefaction. Liquefaction across the study area was most prominent during the CES at Site 2, which has experienced liquefaction prior to the recent events. The abundance of subsurface liquefaction features in the near subsurface (<1.5 m), identified from the two trenches, suggests recognising if a site has been subjected to liquefaction in the past may be an applicable method of assessing the susceptibility of a site to liquefaction in the future.

Current land classifications and foundation guidelines for rebuilding damaged houses should also consider the possible effects CES liquefaction will have on the future vulnerability of a site. Preceding earthquakes are likely to have increased the susceptibility of many areas to liquefaction and ground deformations. Subsidence from preceding earthquakes would have decreased relative water table depths, and fissuring and cracking of soil crusts would provide more efficient ejecta pathways, likely increasing the severity of liquefaction in subsequent earthquakes. The TC1, TC2, and TC3 areas outlined by the MBIE provide guidelines on the foundation solutions appropriate for rebuilding based on the level of damage sustained by the existing buildings and land (van Ballegooy et al., 2014). Properties located within the most susceptible areas (paleochannels) may require more enhanced structural foundation systems or ground improvement, in conjunction with TC3 foundation systems, to reduce the liquefaction related damage to buildings in future earthquake events.

The extensive sills consisting of fine to medium sand identified in the subsurface at Site 2 (Fig. 4.9) may influence the response of the site in future earthquake events. The laterally extensive sills will likely promote shallower water tables from the fracturing and emplacement of permeable sediments, and assist the flow of liquefied sediments as identified by the reactivation of the CES dikes and sills during multiple earthquakes (Fig. 4.13). Land technical categories and associated foundation requirements should consider the implications previous earthquake effects will have on the nature and extent of damage likely to be experienced in future earthquakes.

5.3.4 Liquefaction susceptibility mapping

Surficial liquefaction distributions and localised ground deformations due to earthquake-induced shaking are difficult to quantitatively predict due to the heterogeneity of geologic

deposits, sporadic formation of cracks and sand boils, and uncertainty in seismic shaking intensity and duration (Idriss and Boulanger, 2008). The damage patterns observed in Christchurch shows the importance of knowledge of fluvial history, and the high liquefaction susceptibility of abandoned and reclaimed river channels (Wotherspoon et al., 2012; Robinson et al. 2012; Cubrinovski et al., 2014; Bastin et al., 2015b). Currently, liquefaction hazard maps are developed by incorporating subsurface geotechnical investigations with surficial geology. However, in some areas detailed geologic investigations and abundant geotechnical data may be unavailable, or may be relatively expensive to obtain. In this instance, liquefaction hazard mapping is dependent on the characteristics of surficial geology. Additionally, the current methods of liquefaction assessments use the surficial geology to classify regions into qualitative susceptibility categories that are not related to liquefaction triggering resistances or specific earthquake event parameters (Daley, 2012). There is therefore a need to develop liquefaction hazard mapping methods based on geomorphic interpretations by utilising broadly available geospatial data, as utilised in this thesis, which can be used to assess the vulnerability of an area to liquefaction. Knowledge of depositional systems, in conjunction with geospatial data, can be used to estimate the geotechnical and geologic data necessary for evaluating the liquefaction potential of soils. For example, geomorphic data identified from surface topography, elevation changes, ground slope and water table elevations can be calculated from DEMs. The use of such geospatial layers that estimate soil properties will allow for improved liquefaction hazard mapping in regions where geotechnical data are limited.

Predictive stratigraphic models are needed based on detailed studies of fluvial depositional systems accessible to the concerning parties (e.g. engineers, urban planners). In this way, it is possible to build a composite knowledge base that includes the key characteristics of the basic lithofacies texture and composition, the lithofacies assemblages and patterns, the connectivity between sand bodies, and the character of the significant correlative surfaces (sandy channel bedforms). Being able to distinguish between these landform variations, and to define specific depositional facies in the subsurface, is key to providing high-quality liquefaction susceptibility models for urban areas.

These new approaches make use of readily-available digital map-based topographic and hydrologic information that will aid liquefaction hazard categorisation and effective land use planning. The development of liquefaction hazard assessments based on geomorphic

interpretations allows for land susceptibility classification that is not dependent on site-specific data, and can therefore be implemented across wider areas. This method would be most economic for councils or governments, identifying the subsurface properties and liquefaction susceptibility of a region, as they would not have to undertake costly subsurface geotechnical investigations. The liquefaction hazard assessments would however need collation with adequate subsurface geotechnical investigation to be assessable for engineers designing site-specific foundations. Having more than two trenches collated with CPT investigations in this study would have helped to validate the proposed methodology and refine it further due to more variation within the fluvial stratigraphy. Additional work is warranted to refine the applicability of geomorphic interpretations and evaluate the effectiveness of capturing liquefaction-induced land damages in other seismically active regions consisting of Late Holocene alluvial strata, with particular attention to the source materials, river geometries and paleoliquefaction features. When used appropriately, these geomorphic understandings would provide a proactive platform for land management applications.

5.4 RESEARCH SUMMARY

This thesis has presented newly acquired geospatial data, geotechnical reports and eye-witness discussions to provide a detailed account of the liquefaction distributions in southern Christchurch throughout the CES. LiDAR data and aerial photography reveal the location and magnitude of recurrent liquefaction and subsidence distribution across the adjacent suburbs of Beckenham and St Martins. The majority of severe liquefaction and subsidence was concentrated within the spatial extent of a paleochannel, a remnant river channel from the Holocene migration of the meander in St Martins. Subsurface investigations and sediment analysis in the fluvial strata demonstrate that liquefaction occurrence is largely dependent on the proximity to geomorphic features (paleochannels), the redistribution of stratum from previous earthquakes (reactivation through permeable pathways), the lateral confinement of migrating point bars forming resistant deposits (St Martins vs. Beckenham) along with the source origin of fluvial sediments (Heathcote River versus Avon River) and therefore not uniquely related to pre-earthquake soil properties or hydrogeology alone.

As the CES has illustrated, there is a critical need to predict the occurrence and severity of soil liquefaction for engineering design, hazard mapping, urban planning, and regulatory

purposes (Maurer et al., 2014). Surface ejecta and subsurface evidence from St Martins and Beckenham, and the compilation of pre-existing vulnerability studies, indicates that predicting liquefaction susceptibility is not straightforward in a migrating river system. The liquefaction distributions highlight small-scale heterogeneity of sedimentary deposits within fluvial depositional systems, and the potential limitations of site-specific geotechnical testing in determining subsurface sediment type and the overall liquefaction potential of a given area. While CPT-based liquefaction vulnerability assessments are the preferred methods used for assessing the susceptibility of a site to liquefaction (Maurer et al., 2015), the assessments are subject to a range of uncertainties including spatial geologic variability, soil profile and ground water complexities, and earthquake ground motion characteristics. The analytical procedures for assessing liquefaction susceptibility should consider land surface properties to categorise local scale differences (Idriss and Boulanger, 2008). The locations of geomorphic features, including subtle topographic lows across point bars reflecting previous channel locations, should be considered when undertaking geotechnical investigations and developing liquefaction susceptibility estimates.

Geomorphic interpretations may prove to be a useful supplement in predicting regional liquefaction susceptibilities and earthquake damage. LiDAR data combined with river morphology enables interpretations of geologic and geomorphic variability. Comparison of the liquefaction distributions with near-surface properties highlights the potential application of geomorphic mapping to determine the likely distribution of potentially liquefiable sediments within fluvial settings. Understanding how liquefaction-induced damage varies within fluvial settings (i.e. point bars deposited in migrating river systems) may be most useful for future building design and hazard management applications.

References

Akin, M., Ozvan, A., Akin, M. K., & Topal, T. (2013). Evaluation of liquefaction in Karasu River floodplain after the October 23, 2011, Van (Turkey) earthquake. *Natural hazards*, *69*(3), 1551-1575.

Asahi, K., Shimizu, Y., Nelson, J., & Parker, G. (2013). Numerical simulation of river meandering with self-evolving banks. *Journal of Geophysical Research: Earth Surface*, *118*(4), 2208-2229.

Bannister, S., & Gledhill, K. (2012). Evolution of the 2010–2012 Canterbury earthquake sequence. *New Zealand Journal of Geology and Geophysics*, *55*(3), 295-304.

Bardet, J. P., Seed, R. B., Cetin, K. O., Lettis, W., Rathje, E., Rau, G., R. B. Seed, D. Ural, M. B. Baturay, R. W. Boulanger, J. D. Bray, D. Erten, D. Frost, & Kaya, A. (2000). Soil liquefaction, landslides, and subsidences. *Earthquake Spectra*, *16*(1), 141-162.

Bastin, S., Reid, C.M., Quigley, M.C. and Bassett, K.N. (2013). Earthquake Impacts on Soft Sediments in Eastern Christchurch. In: Reid, C.M. & Hampton, S.J. (compilers). Field Trip Guides, Geosciences 2013 Conference, Christchurch, New Zealand. Geoscience Society of New Zealand Miscellaneous Publication 136B, 21 p.

Bastin, S. H., Quigley, M. C., & Bassett, K.N. (2015). Paleoliquefaction in Christchurch, New Zealand. *Geological Society of America Bulletin*, B31174-1.

Bastin, S. H., Quigley, M. C., & Bassett, K. (2015b). Comparison of liquefaction-induced land damage and geomorphic variability in Avonside, New Zealand. Retrieved from http://www.drquigs.com/wp-content/uploads/2015/07/Revised_Bastin_etal2.pdf

Beavan, J., Motagh, M., Fielding, E. J., Donnelly, N., & Collett, D. (2012). Fault slip models of the 2010–2011 Canterbury, New Zealand, earthquakes from geodetic data and observations of postseismic ground deformation. *New Zealand Journal of Geology and Geophysics*, *55*(3), 207-221.

Bell, D. H., & Trangmar, B. B. (1987). Regolith materials and erosion processes on the Port Hills, Christchurch, New Zealand. In *Fifth International Conference and Field Workshop on Landslides*, 93-105.

Berrill, J.B., Mulqueen, P., & Ooi, E. (1994). Liquefaction at Kaiapoi in the 1901 Cheviot, New Zealand Earthquake. *Bulletin of the New Zealand Society for Earthquake Engineering 27(1)*, 178-189.

Black Maps (1856). Christchurch Waterways, Swamps and Vegetation Cover. Retrieved from the Christchurch City Council http://resources.ccc.govt.nz/files/blackmap-environmentecology.pdf

Bowen, H. J., Jacka, M. E., Van Ballegooy, S., Sinclair, T. J. E., & Cowan, H. (2012). Lateral spreading in the Canterbury earthquakes–Observations and empirical prediction methods. In *Proceedings, 15th World Conference on Earthquake Engineering*.

Brackley, H. L. (compiler). (2012). Review of liquefaction hazard information in eastern Canterbury, including Christchurch City and parts of Selwyn, Waimakariri and Hurunui Districts, *GNS Science Consultancy Report* 2012/218. 99 p.

Bradley, B. A., & Cubrinovski, M. (2011). Near-source strong ground motions observed in the 22 February 2011 Christchurch earthquake. *Seismological Research Letters*, *82*(6), 853-865.

Bradley, B. A., & Hughes, M. (2013). Spatially-Distributed Ground Motion Intensity Maps: Application for Site-Specific Liquefaction Evaluations in Christchurch. In *2013 NZSEE Conference*.

Bradley, B. A., Quigley, M. C., Van Dissen, R. J., & Litchfield, N. J. (2014). Ground motion and seismic source aspects of the Canterbury earthquake sequence. *Earthquake Spectra*, *30*(1), 1-15.

Bridge, J. S. (1992). A revised model for water flow, sediment transport, bed topography and grain size sorting in natural river bends. *Water Resources Research*, *28*(4), 999-1013.

Bridge, J. S., Alexander, J., Collier, R. E., Gawthorpe, R. L., & Jarvis, J. (1995). Ground-penetrating radar and coring used to study the large-scale structure of point-bar deposits in three dimensions. *Sedimentology*, *42*(6), 839-852.

Brierley, G. J., & Fryirs, K. A. (2005). Geomorphology and river management: applications of the river styles framework. Blackwell Publishing, Oxford, UK, 398 p.

Brown, L. J. and Weeber, J. H. 1992: *Geology of the Christchurch urban area*. 1:25,000 geological map and booklet. *Institute of Geological and Nuclear Sciences, Wellington*. 104 p. + 1 folded map.

Canterbury Geotechnical Database (2012) "Aerial Photography", Map Layer CGD0100 - 1 June 2012, retrieved 1/4/2015 from https://canterburygeotechnicaldatabase.projectorbit.com/

Canterbury Geotechnical Database (2012) "Observed Ground Crack Locations", Map Layer CGD0400 - 23 July 2012, retrieved 1/4/2015 from https://canterburygeotechnicaldatabase.projectorbit.com/

Canterbury Geotechnical Database (2013) "Liquefaction Interpreted from Aerial Photography", Map Layer CGD0200 - 11 Feb 2013, retrieved 1/4/2015 from https://canterburygeotechnicaldatabase.projectorbit.com/

Canterbury Geotechnical Database (2015) "Liquefaction evaluation of CPT investigations", Map Layer CGD0050, retrieved 1/4/2015 from https://canterburygeotechnicaldatabase.projectorbit.com/

Christchurch Engineering Lifelines Group 1997: Risks and Realities: A Multi-disciplinary Approach to the Vulnerability of Lifelines to Natural Hazards. Report of the Christchurch Engineering Lifelines Group. *Centre for Advanced Engineering*, Christchurch.

Chu, D. B., Stewart, J. P., Lee, S., Tsai, J. S., Lin, P. S., Chu, B. L., Seed, R. B., Hsu, S. C., Yu, M. S. & Wang, M. C. (2004). Documentation of soil conditions at liquefaction and non-liquefaction sites from 1999 Chi–Chi (Taiwan) earthquake. *Soil Dynamics and Earthquake Engineering*, *24*(9), 647-657.

Clough, B. (2005). Christchurch Liquefaction Study: Stage IV (addendum report). *Environment Canterbury report* U04/25/2. Beca, Carter, Hollings and Ferner Ltd, Christchurch.

Cowan, H. A. (1991). The North Canterbury earthquake of September 1, 1888. *Journal of the Royal Society of New Zealand*, *21*(1), 1-12.

Cowie, C. A. (1957). Floods in New Zealand 1920-1953. *The Soil Conservation and Rivers Control Council, Wellington, New Zealand*.

Cox, S. C., Rutter, H. K., Sims, A., Manga, M., Weir, J. J., Ezzy, T., Whitef P.A. Horton, T.W., & Scott, D. (2012). Hydrological effects of the MW 7.1 Darfield (Canterbury) earthquake, 4 September 2010, New Zealand. *New Zealand Journal of Geology and Geophysics*, *55*(3), 231-247.

Cubrinovski, M. & Green, R. A. (2010). Geotechnical reconnaissance of the 2010 Darfield (Canterbury) earthquake. *Bulletin of the New Zealand Society for Earthquake Engineering, 43*(4), 243-320.

Cubrinovski, M., Bray, J. D., Taylor, M., Giorgini, S., Bradley, B., Wotherspoon, L., & Zupan, J. (2011). Soil liquefaction effects in the central business district during the February 2011 Christchurch earthquake. *Seismological Research Letters*, *82*(6), 893-904.

Cubrinovski, M., Robinson, K., Taylor, M., Hughes, M., & Orense, R. (2012). Lateral spreading and its impacts in urban areas in the 2010–2011 Christchurch earthquakes. *New Zealand Journal of Geology and Geophysics*, *55*(3), 255-269.

Cubrinovski, M., Winkley, A., Haskell, J., Palermo, A., Wotherspoon, L., Robinson, K., Bradley, B., Brabhaharan, P. and Hughes, M. (2014). Spreading-induced damage to short-span bridges in Christchurch, New Zealand. *Earthquake Spectra* , 30(1), 57-83.

Daley, D. J. (2012). *A Geospatial Liquefaction Model* (Doctoral dissertation, TUFTS University). Retrieved from http://gradworks.umi.com/15/12/1512876.html

Dalrymple, R. W., & Choi, K. (2007). Morphologic and facies trends through the fluvial–marine transition in tide-dominated depositional systems: a schematic framework for environmental and sequence-stratigraphic interpretation. *Earth-Science Reviews*, *81*(3), 135-174.

Downes, G., & Yetton, M. (2012). Pre-2010 historical seismicity near Christchurch, New Zealand: the 1869 Mw 4.7–4.9 Christchurch and 1870 Mw 5.6–5.8 Lake Ellesmere earthquakes. *New Zealand Journal of Geology and Geophysics*, *55*(3), 199-205.

Duffy, B., Quigley, M., Barrell, D. J., Van Dissen, R., Stahl, T., Leprince, S., McInnes, C. & Bilderback, E. (2013). Fault kinematics and surface deformation across a releasing bend during the 2010 MW 7.1 Darfield, New Zealand, earthquake revealed by differential LiDAR and cadastral surveying. *Geological Society of America Bulletin*, *125*(3-4), 420-431.

Elder, D. M. G., McCahon, I. F. & Yetton, M. D. (1991). The Earthquake Hazard in Christchurch: A Detailed Evaluation. Soils & Foundations Ltd, Christchurch. Report funded by the Earthquake Commission.

Elder, D. M., McCahon, I. F., & Yetton, M. (1991). The earthquake hazard in Christchurch: a detailed evaluation. *EQC Report, available at http://www. eqc. govt.nz/home/research/researchpapers. aspx*.

Forsyth, P. J., Jongens, R., & Barrell, D. J. A. (2008). *Geology of the Christchurch area*. Lower Hutt: GNS Science.

Fryirs, K. A., & Brierley, G. J. (2012). Geomorphic analysis of river systems: an approach to reading the landscape. John Wiley & Sons.

Ghinassi, M., Billi, P., Libsekal, Y., Papini, M., & Rook, L. (2013). Inferring fluvial morphodynamics and overbank flow control from 3D outcrop sections of a Pleistocene point bar, Dandiero Basin, Eritrea. *Journal of Sedimentary Research*, *83*(12), 1066-1084.

Gledhill, K., Ristau, J., Reyners, M., Fry, B., & Holden, C. (2011). The Darfield (Canterbury, New Zealand) Mw 7.1 earthquake of September 2010: A preliminary seismological report. *Seismological Research Letters*, *82*(3), 378-386.

Green, R. A., Obermeier, S. F., & Olson, S. M. (2005). Engineering geologic and geotechnical analysis of paleoseismic shaking using liquefaction effects: field examples. *Engineering Geology*, *76*(3), 263-293.

Green, R. A., Cubrinovski, M., Cox, B., Wood, C., Wotherspoon, L., Bradley, B., & Maurer, B. (2014). Select liquefaction case histories from the 2010-2011 Canterbury earthquake sequence. *Earthquake Spectra*, *30*(1), 131-153.

Hicks. M. (1993). Sedimentation and erosion in the Avon-Heathcote catchment and estuary. Report to the Canterbury regional council and Christchurch City Council. Retrieved from http://docs.niwa.co.nz/library/public/MRFD27.pdf

Hjulström, F. (1939). Transportation of detritus by moving water: Part 1. Transportation.*in* Trask, P.D., ed., Recent Marine Sediments. *American Association of Petroleum Geologists 10*, 5-31.

Hooke, J. M. (2004). Cutoffs galore!: occurrence and causes of multiple cutoffs on a meandering river. *Geomorphology*, *61*(3), 225-238.

Hooke, J. M. (2007). Spatial variability, mechanisms and propagation of change in an active meandering river. *Geomorphology*, *84*(3), 277-296.

Hooke, J. M. (2008). Temporal variations in fluvial processes on an active meandering river over a 20-year period. *Geomorphology*, *100*(1), 3-13.

Hornblow, S., Quigley, M., Nicol, A., Van Dissen, R., & Wang, N. (2014). Paleoseismology of the 2010 M w 7.1 Darfield (Canterbury) earthquake source, Greendale Fault, New Zealand. *Tectonophysics*, *637*, 178-190.

Howard, M., Nicol, A., Campbell, J., & Pettinga, J. R. (2005). Holocene paleoearthquakes on the strike-slip Porters Pass fault, Canterbury, New Zealand. *New Zealand Journal of Geology and Geophysics*, *48*(1), 59-74.

Hughes, M. W., Quigley, M. C., van Ballegooy, S., Deam, B. L., Bradley, B. A., & Hart, D. E. (2015). The sinking city: Earthquakes increase flood hazard in Christchurch, New Zealand. *GSA Today*, *25*(3).

Idriss, I. M., & Boulanger, R. W. (2008). *Soil liquefaction during earthquakes*. Earthquake engineering research institute.

Ishihara, K. (1985). Stability of natural deposits during earthquakes. Proceedings of the 11th International Conference on Soil Mechanics and Foundation Engineering, (1), 321-376.

Ishihara, K., Acacio, A. and Towhata, I. (1993).Liquefaction-induced ground damage in Dagupan in the July 16, 1990 Luzon Earthquake," *Soils and Foundations*, 33 (1), 133-154.

Iwasaki, T., Arakawa, T., & Tokida, K. I. (1984). Simplified procedures for assessing soil liquefaction during earthquakes. *International Journal of Soil Dynamics and Earthquake Engineering*, *3*(1), 49-58.

Iwasaki, T., Tokida, K., Tatsuoka, F., Watanabe, S., Yasuda, S., & Sato, H. (1982). Microzonation for soil liquefaction potential using simplified methods. In *Proceedings of the 3rd international conference on microzonation, Seattle* (3), 1310-1330.

Jacka, M. E., & Murahidy, K. M. (2011). Observation and characterisation of land damage due to liquefaction and lateral spreading. In *Proceedings 9th Pacific Conference on Earthquake Engineering*.

Jongens, R., Barrell, D. J. A., Campbell, J. K., & Pettinga, J. R. (2012). Faulting and folding beneath the Canterbury Plains identified prior to the 2010 emergence of the Greendale Fault. *New Zealand Journal of Geology and Geophysics*, *55*(3), 169-176.

Knudsen, K. L., & Bott, J. D. J. (2011). Geologic and geomorphic evaluation of liquefaction case histories–toward rapid hazard mapping. *Seismological Research Letters*, *82*(2), 334-335.

Labrecque, P. A., Hubbard, S. M., Jensen, J. L., & Nielsen, H. (2011). Sedimentology and stratigraphic architecture of a point bar deposit, Lower Cretaceous McMurray Formation, Alberta, Canada. *Bulletin of Canadian Petroleum Geology*, *59*(2), 147-171.

Lewis, D. W., & McConchie, D. (1994). *Analytical sedimentology*. Springer Science & Business Media.

Litchfield, N., Van Dissen, R., Sutherland, R., Barnes, P., Cox, S., Norris, R., Beavan, R., Langridge, R., Villamor, P., Berryman, K., 2014. (2014). A model of active faulting in New Zealand. *New Zealand Journal of Geology and Geophysics*, *57*(1), 32-56.

Lunina, O. V., & Gladkov, A. S. (2015). Seismically induced clastic dikes as a potential approach for the estimation of the lower-bound magnitude/intensity of paleoearthquakes. *Engineering Geology*, *195*, 206-213.

Makaske, B., & Weerts, H. J. (2005). Muddy lateral accretion and low stream power in a sub-recent confined channel belt, Rhine-Meuse delta, central Netherlands. *Sedimentology*, *52*(3), 651-668.

Maurer, B.W., Green, R.A., Cubrinovski, M., & Bradley, B.A. (2014). Evaluation of the Liquefaction Potential Index for Assessing Liquefaction Hazard in Christchurch, New Zealand. *Journal of Geotechnical and Geoenvironmental Engineering.*

Maurer, B. W., Green, R. A., Cubrinovski, M., & Bradley, B. A. (2014b). Fines-content effects on liquefaction hazard evaluation for infrastructure in Christchurch, New Zealand. *Soil Dynamics and Earthquake Engineering*.

Maurer, B.W., Green, R.A., Cubrinovski, M. & Bradley, B.A. (2015). Assessment of CPT-based methods for liquefaction evaluation in a liquefaction potential index framework. *Geotechnique, 65*(5), 328-336.

Mike, S. (Photographer). (2012, August 20). *Meandering river in the Artic* [digital image]. Retrieved from http://www.flickriver.com/photos/31856336@N03/7831522814/

National Institute of Water and Atmospheric Research, (NIWA). (2013). *Flood modelling of the Heathcote River, Christchurch*. Retrieved from https://www.niwa.co.nz/climate/urban-impacts-toolbox/case-studies/flood-modelling-of-the-heathcote-river-christchurch

Obermeier, S. F. (1996). Use of liquefaction-induced features for paleoseismic analysis-an overview of how seismic liquefaction features can be distinguished from other features and how their regional distribution and properties of source sediment can be used to infer the location and strength of Holocene paleo-earthquakes. *Engineering Geology*, *44*(1), 1-76.

Obermeier, S. F., Olson, S. M., & Green, R. A. (2005). Field occurrences of liquefaction-induced features: a primer for engineering geologic analysis of paleoseismic shaking. *Engineering Geology*, *76*(3), 209-234.

Ogilvie, G. (1991). *The Port Hills of Christchurch*. Phillip King Publications, 246 p.

Orense, R. P., Kiyota, T., Yamada, S., Cubrinovski, M., Hosono, Y., Okamura, M., & Yasuda, S. (2011). Comparison of liquefaction features observed during the 2010 and 2011 Canterbury earthquakes. *Seismological Research Letters*, *82*(6), 905-918.

Peakall, J., Ashworth, P. J., & Best, J. L. (2007). Meander-bend evolution, alluvial architecture, and the role of cohesion in sinuous river channels: a flume study. *Journal of Sedimentary Research*, *77*(3), 197-212.

Pettinga, J. R., Yetton, M. D., Van Dissen, R. J., & Downes, G.(2001). Earthquake source identification and characterisation for the Canterbury region, South Island, New Zealand. *Bulletin of the New Zealand National Society for Earthquake Engineering*, *34*(4), 282-317.

Quigley, M., Van Dissen, R., Villamor, P., Litchfield, N., Barrell, D., Furlong, K., Stahl, T., Duffy, B., Bilderback, E., Noble, D., Townsend, D., Begg, J., Jongens, R., Ries, W., Claridge, J., Klahn, A., Mackenzie, H., Smith, A., Hornblow, S., Nicol, A., Cox, S., Langridge, R., Pedley, K. (2010).

Surface rupture of the Greendale fault during the Darfield (Canterbury) earthquake, New Zealand: initial findings. *Bulletin of the New Zealand Society for Earthquake Engineering*, *43*(4), 236.

Quigley, M., Van Dissen, R., Litchfield, N., Villamor, P., Duffy, B., Barrell, D., Furlong, K., Stahl, T., Bilderback, E., Noble, D. (2012). Surface rupture during the 2010 Mw 7.1 Darfield (Canterbury) earthquake: Implications for fault rupture dynamics and seismic-hazard analysis. *Geology*, *40*(1), 55-58.

Quigley, M. C., Bastin, S., & Bradley, B. A. (2013). Recurrent liquefaction in Christchurch, New Zealand, during the Canterbury earthquake sequence. *Geology*, *41*(4), 419-422.

Quigley, M., Hughes, M., Bradley, B., van Ballegooy, S., Reid, C., Morgrenroth, J., Horton, T., Duffy, B., & Pettinga, J. R. (in review). The 2010-2011 Canterbury Earthquake Sequence: Environmental effects, seismic triggering thresholds and geologic legacy.

Rahman, M. M., & Lo, S. R. (2008). Effect of sand gradation and fines type on the liquefaction behaviour of sand-fines mixtures.

Rauch, A. F. (1997). EPOLLS: an empirical method for prediciting surface displacements due to liquefaction-induced lateral spreading in earthquakes. (Doctoral thesis, Virginia Polytechnic Institute and State University). Retrieved from http://scholar.lib.vt.edu/theses/available/etd-219182249741411/unrestricted/Etd.pdf

Robertson, P. K., & Wride, C. E. (1998). Evaluating cyclic liquefaction potential using the cone penetration test. *Canadian Geotechnical Journal*, *35*(3), 442-459.

Robinson, K., Bradley, B. A., & Cubrinovski, M. (2012). Analysis of liquefaction-induced lateral spreading data from the 2010 Darfield and 2011 Christchurch earthquakes. In *Proceedings of the 2012 NZSEE annual technical conference, Christchurch, New Zealand. Wellington: New Zealand Society for Earthquake Engineering*.

Schumm, S. A., & Lichty, R. W. (1965). Time, space, and causality in geomorphology. *American Journal of Science*, *263*(2), 110-119.

Statistics New Zealand. (2015). *Christchurch population*. Retrieved from http://www.stats.govt.nz/Census/2013-census/profile-and-summary-reports/quickstats-about-a-place.aspx?request_value=14758&tabname=

Sutherland, R., Eberhart-Phillips, D., Harris, R. A., Stern, T., Beavan, J., Ellis, S., Henrys, S., Cox, S., Norris, R. J., Berryman, K. R., Townend, J., Bannister, S., Pettinga, J., Leitner, B., Wallace, L., Little, T. A., Cooper, A. F., Yetton, M. and Stirling, M. (2007). Do Great Earthquakes Occur on the Alpine Fault in Central South Island, New Zealand?, in A Continental Plate Boundary: Tectonics at South Island, New Zealand (eds D. Okaya, T. Stern and F. Davey), American Geophysical Union, Washington, D. C.

Toonen, W. H., Kleinhans, M. G., & Cohen, K. M. (2012). Sedimentary architecture of abandoned channel fills. *Earth surface processes and landforms*, *37*(4), 459-472.

Tuttle, M. P. (2001). The use of liquefaction features in paleoseismology: Lessons learned in the New Madrid seismic zone, central United States. *Journal of Seismology*, *5*(3), 361-380.

van Ballegooy, S., Malan, P., Lacrosse, V., Jacka, M., Cubrinovski, M., Bray, J., O'Rourke, T., Crawford, S., Cowan, H., (2014). Assessment of liquefaction-induced land damage for residential Christchurch. *Earthquake Spectra*, *30*(1), 31-55.

Van T Veen, L. H. (2015). CPT Prediction of Soil Behaviour Type, Liquefaction Potential and Ground Settlement in North-West Christchurch ((Masters thesis, University of Canterbury). Retrieved from http://ir.canterbury.ac.nz/handle/10092/10468

Villamor, P., Litchfield, N., Barrell, D., Van Dissen, R., Hornblow, S., Quigley, M., Levick, S., Ries, W., Duffy, B., Begg, J., Townsend, D., Stahl, T., Bilderback, E., Noble, D., Furlong, K., Grant, H. (2012). Map of the 2010 Greendale Fault surface rupture, Canterbury, New Zealand: application to land use planning. *New Zealand Journal of Geology and Geophysics*, *55*(3), 223-230.

Villemure, M., Wilson, T. M., Bristow, D., Gallagher, M., Giovinazzi, S., & Brown, C. (2012). Liquefaction ejecta clean-up in Christchurch during the 2010-2011 earthquake sequence. *Bulletin of the New Zealand Society for Earthquake Engineering* , 131, 1-11.

Wallace, L. M., Beavan, J., McCaffrey, R., Berryman, K., & Denys, P. (2007). Balancing the plate motion budget in the South Island, New Zealand using GPS, geological and seismological data. *Geophysical Journal International*, *168*(1), 332-352.

Willis, B. J. (1989). Palaeochannel reconstructions from point bar deposits: a three-dimensional perspective. *Sedimentology*, *36*(5), 757-766.

Willis, B. J., & Tang, H. (2010). Three-dimensional connectivity of point-bar deposits. *Journal of Sedimentary Research*, *80*(5), 440-454.

Wotherspoon, L. M., Pender, M. J., & Orense, R. P. (2012). Relationship between observed liquefaction at Kaiapoi following the 2010 Darfield earthquake and former channels of the Waimakariri River. *Engineering Geology*, *125*, 45-55.

Yasuda, S., Ishihara, K., Harada, K., & Shinkawa, N. (1996). Effect of soil improvement on ground subsidence due to liquefaction. *Soils and foundations*, 99-107.

Youd, T. L., & Perkins, D. M. (1978). Mapping liquefaction-induced ground failure potential. *Journal of the Geotechnical Engineering Division*, *104*(4), 433-446.

Youd, T., Idriss, I., Andrus, R.D., Arango, I., Castro, G., Christian, J.T., Dobry, R., Finn, W.L., Harder Jr, L.F., Hynes, M.E., Ishihara, K., Koester, J., Liao, S., Marcuson III, W., Martin, G.R., Mitchell, J.K., Moriwaki, Y., Power, M.S., Robertson, P.K., Seed, R.B., Stokoe, K.H. (2001). Liquefaction resistance of soils: summary report from the 1996 NCEER and 1998 NCEER/NSF workshops on evaluation of liquefaction resistance of soils. *Journal of Geotechnical and Geoenvironmental engineering 127*, 817-833.

Appendix A

Rafter Radiocarbon AMS laboratory reports

Sample no. SM1
Unit d
1.1 m depth
Wood
Conventional Radiocarbon Age (years BP): **Modern**
^{13}C and Source of measurement: **-28.2 ± 0.2**
Fraction modern: **1.4563 ± 0.0033**
^{14}C (‰) and collection date: **444.9 ± 3.3, 5 Apr 2015**

Sample Treatment Details
945.5mg of raw sample was received. Description of sample when received: sample submitted in a plastic bag as a mix of light tan coloured sediment along with some chunks of fragile looking wood coated in the sediment. Broke up sediment clots to be sure no wood was inside. 100.7mg was subsampled and prepared by: Cut/Scrape and picking. Pretreatment description: picked out largest wood pieces, brushed off sediment, removed a root hair then scraped as much sediment from the wood as possible, but as wood was fragile, some sediment remained. Cut wood into pieces for treatment. Chemical pretreatment was by cellulose extraction. Weight obtained after chemical pretreatment was 2.4mg. Carbon dioxide was generated by sealed tube combustion and 0.6mgC was obtained. Sample carbon dioxide was converted to graphite by reduction with hydrogen over iron catalyst.

Sample no. SM2
Unit b
0.7 m depth
Wood
Conventional Radiocarbon Age (years BP): **Modern**
^{13}C and Source of measurement: **-29.3 ± 0.2**
Fraction modern: **1.1894 ± 0.0028**
^{14}C (‰) and collection date: **180 ± 2.8, 5 Apr 2015**

Sample Treatment Details
54008mg of raw sample was received. Description of sample when received: Fragments of plant material with coating of yellowish brown sediment and a lump of dried yellowish brown sediment with plant material embedded within it. Plant material resembles hollow plant stems often with a woody core present. The stem coat is thin and pliable. Micro root hairs growing through some of the pieces. Sample prepared by: Picking and cut/scrape. Pretreatment description: Selected stem like fragments scraped sediment off where possible then sonicated. Collected on sieve. Opened up hollow stems and scraped out any micro root hairs and remaining sediment. Dried in oven. Checked under microscope after drying and removed a fibre. Scraped sediment still remaining off as much a possible. Removed and stored pieces with obvious root hairs remaining. Loaded clean sample into tube for treatment. Chemical pretreatment was by acid, alkali, acid. Weight obtained after chemical pretreatment was 11.4mg. Carbon dioxide was generated by elemental analyser combustion and 1.1mgC was obtained. Sample carbon dioxide was converted to graphite by reduction with hydrogen over iron catalyst.

Sample no. SM3

Unit d

1.2 m depth

Charcoal

Conventional Radiocarbon Age (years BP): **2254 ± 22**

^{13}C and Source of measurement: **-25.5 ± 0.2**

Fraction modern: **0.7554 ± 0.0021**

^{14}C (‰) and collection date: **-250.6 ± 2.1, 5 Apr 2015**

Sample Treatment Details

1393.9mg of raw sample was received. Description of sample when received: Chunk of charcoal approx. 1.5cm square, and some small fragments of charcoal embedded in a lump of yellowish brown sediment. Vascular structure visible. Broke up sediment to extract charcoal but only minor amount present. Outer layers of charcoal brownish colour but inner surfaces are black and glossy. No root hairs or other contaminants present. 249.8mg was subsampled. Sample prepared by: Cut/Scrape. Pretreatment description: Selected large piece of charcoal and scraped sediment off surfaces and crushed up into smaller pieces, loaded into centrifuge tube for chemical treatment. Chemical pretreatment was by acid, alkali, (which was repeated), acid. Weight obtained after chemical pretreatment was 24.8mg. Carbon dioxide was generated by elemental analyser combustion and 0.4mgC was obtained. Sample carbon dioxide was converted to graphite by reduction with hydrogen over iron catalyst.

Sample no. SM4

Unit b

0.7 m depth

Charcoal

Conventional Radiocarbon Age (years BP): **161 ± 20**

^{13}C and Source of measurement: **-25.6 ± 0.2**

Fraction modern: **0.9801 ± 0.0024**

^{14}C (‰) and collection date: **-27.6 ± 2.4, 5 Apr 2015**

Sample Treatment Details

311.4mg of raw sample was received. Description of sample when received: sample submitted in a plastic bag as a piece of dark material coated in sediment and some loose sediment. Selected large piece and scrapped off outer coating with scalpel. 112.1mg was subsampled. Sample prepared by: Cut/Scrape and picking. Pretreatment description: sample under coating was charcoal with a vascular structure. Broke apart a bit to check for root hairs then loaded into centrifuge tube for treatment.Chemical pretreatment was by acid, alkali, (which was repeated), acid. Weight obtained after chemical pretreatment was 54.9mg.Carbon dioxide was generated by elemental analyser combustion and 1mgC was obtained. Sample carbon dioxide was converted to graphite by reduction with hydrogen over iron catalyst.